DOI:10.15774/PPKE.ITK.2016.004

“Development of multimodal diagnostic tools for epilepsy patients implanted with intracranial micro- and macroelectrodes”

Ph.D. Dissertation

Emília Tóth

Roska Tamás Doctoral School of Sciences and Technology
Faculty of Information Technology and Bionics
Pázmány Péter Catholic University

Scientific advisors:
István Ulbert M.Sc., M.D., D.Sc.
Dániel Fabó M.D., Ph.D.

Budapest, 2015

DOI:10.15774/PPKE.ITK.2016.004

Table of Contents

TABLE OF CONTENTS

DOI:10.15774/PPKE.ITK.2016.004

Table of Contents

DOI:10.15774/PPKE.ITK.2016.004

Abbreviations

ABBREVIATIONS

ANOVA	Analysis of Variance
BVT	Brain Visualization Tool
CA 1,2,3	Cornu Ammonis region 1,2,3 of the hippocampus
CCEP	Cortico-Cortical Evoked Potential
CES	Cortical Electrical Stimulation
CHEP	Cortico-hippocampal Evoked Potential
CSD	Current Source Density
CT	Computer Tomography
Ctx	Cortex
DC	Direct Current
DG	Dentate Gyrus
dME	deep multichannel microelectrode array
EC	Entorhinal Cortex
ECG	electrocardiogram
ECoG	Electro-Corticogram
EEG	Electro-Encephalogram
EP	Evoked Potential
ERSP	Event Related Spectral Perturbation
ESM	electrical stimulation mapping
FFT	Fast Fourier Transform
fMRI	functional Magnetic Resonance Imaging
FR	Fast Ripple
GABA	Gamma Amino Butyric Acid
Hc	hippocampus
HcF	Hippocampal formation
HFA	High Frequency Activity
HFO	High-Frequency Oscillation
HS	Hippocampal sclerosis
IIS/IID	Interictal Spike/Interictal Discharge
ILAE	International League Against Epilepsy
LFP, LFPg	Local Field Potential
ME	Microelectrode
MI	Modulation Index
MRI	Magnetic Resonance Imaging
mTLE	mesial Temporal Lobe Epilepsy
MUA	Multiple Unit Activity
NICN	National Institute of Clinical Neurosciences
NP	connection between non-ictal (normal, physiological) and pathological (ictal) areas
NN	connection between non-ictal (normal, physiological) and non-ictal (normal, physiological) areas
Non-REM	non rapid eye movement
NSLIJ	North Shore-LIJ Health System
OKITI	National Institute of Clinical Neurosciences
OPNI †	National Institute of Psychiatry and Neurology
OR	Operating Room
PAC	Phase-amplitude coupling
PN	connection between pathological (ictal) and non-ictal (normal, physiological) areas
PP	connection between pathological (ictal) and pathological (ictal) areas
PR	putative ripple
PreS	Presubiculum
REM	rapid eye movement
RMS	Root Mean Square
RSFC	resting - state functional connectivity
RST	Ripple Selection Tool
SD	standard deviation
SPES	single pulse electrical stimulation
Sub/SUB	subiculum

DOI:10.15774/PPKE.ITK.2016.004

1 INTRODUCTION

Despite the revolutionary improvement of genetics, imaging (MRI, nuclear imaging) and other techniques in the field of medicine, the electro-encephalographic (EEG) methods remained unchanged for many decades. The original approach of Berger's using scalp electrodes [1] had been extended with intraoperative acute and chronic intracranial electrodes in the 1950's. The collected data consisted of spontaneous (interictal and ictal) and train stimulus evoked activities, and the analysis was based mostly on visual inspection of raw data undergone some filtering. The types of the recorded brain activities and the analysis methods used in the clinical work remained relatively stable ever since. The inrush of the digital EEG in the midst of the 1980's brought free digital re-filtering and re-referencing possibilities for the clinicians but did not replace the visual analysis methods. Digital source localizing and frequency analysis methodologies focused on the same brain waves that were the subject of visual inspection as well.

In the last decade a paradigm change has begun to emerge in the field of electrophysiology. New electrophysiological modalities entered the field of epilepsy and clinicians begun to urge neurophysiologists to provide a feasible tool to see these new features. High frequency brain oscillations were detected and proved to be hallmarks of the seizure prone cortex, and new brain stimulation paradigms using single-shock electrical pulses were developed. Although these brain activities are visible on the raw EEG too, the extraction of clinically useful information in everyday work needs new digital algorithms to speed up and clarify the process. Such modalities applied on the data from similar electrodes were followed by new – smaller implanted electrodes (into the brain) with which micro-spikes, microseizures and abnormal unit firing could already be demonstrated in the human epileptic neocortex.

In this work, we have started to develop new electrophysiological tools and methods to link such needs to the concrete possibilities, which would allow researchers and clinicians to read EEG through these new glasses. During this translational research we tried to test and verify results originated from animal research on human data and describe their relevance in pathological conditions. Our major aim was also to develop tools that can handle data from microelectrodes capable of recording activity of small neuronal clusters or even single units.

The human brain is a complex system in which electrical signals emerge as a result of the neuronal co-operation at various micro -, and macroscale. To explore this complexity, we applied multiscale electrophysiological methods including scalp-, and intracranial macro-, and intracerebral microelectrodes in epilepsy patients undergoing multimodal presurgical investigation including high resolution (3T) MRI and fMRI modalities [2-4].

DOI:10.15774/PPKE.ITK.2016.004

In my thesis work I focused on the integrated analysis of these new electrophysiological signals together with MRI brain reconstruction for visualizing macroelectrodes and histological data for microelectrodes. Using this approach we were able to link these modalities and scales in order to help the clinical examination of patients and draw the right scientific conclusions from the results.

1.1 AIMS

My main aims were to develop analysis tools to examine evoked and spontaneous neuronal unit and field activity for research purposes, which may also be applicable to facilitate clinical decision making.

Aim 1: Develop algorithms for cortico-cortical evoked potential (CCEP) detection and analysis.

a) Analyse the effects of single pulse electrical stimulation (SPES) on the neocortex and in the hippocampus recorded with macro- and microelectrodes.

b) Mapping functional and epileptic areas using cortico-cortical evoked potentials (CCEPs).

Aim 2: Develop algorithms for high frequency oscillation (HFO) detection and analysis.

a) Improve tools to detect and validate HFO events.

b) Characterize the overall variability of evoked potentials and evoked high frequency activity (HFA) of hippocampus in anaesthetized condition.

Aim 3: Develop a visualization tool of the biomarkers on the patient's individual 3D brain reconstruction surface.

Aim 1 was successfully realized in Thesis I., I.a, I.b and Aim 2 in Thesis II., II.a, II.b. Despite the fact that Aim 3 has not been actualized as a thesis, I considered it as equally important and complimentary in all of the other two aims.

DOI:10.15774/PPKE.ITK.2016.004

2 BACKGROUND

As our senior neurologist, Professor Péter Halász expressed well, epilepsy is a window to the brain that gives us the opportunity to get closer look at the operation of the human mind. For ease of understanding, we have become acquainted with the basic neuronal functions, the behaviour and cooperation of the neural cells, the anatomy and connections of the brain structures and everything that could affect the nature of epilepsy.

2.1 EPILEPSY

Epilepsy is a generic term for chronic diseases with a common feature of frequent spontaneous seizures. These seizures are associated with transient loss of consciousness, behavioural alterations, involuntary motor actions or convulsions. The patients are usually unemployed and isolated from the society despite the fact that most of them are asymptomatic between the seizures. The unpredictable occurrence of the seizures, the cognitive impairment, the neurological deficits, or the psychiatric symptoms due to the underlying etiological factor or caused by the treatment can all exasperate the decrease in the quality of life of an epileptic patient. Epilepsy occurs in 1% of the population worldwide, children and older people affected more often.

The treatment primarily relies on the use of medical drugs, which induces seizure freedom for only the 60-70% of the patients. The remaining 30-40% can benefit from alternative treating strategies like special diets, neuro-modulation or surgical treatment, but approximately 30% of the patients are resistant to any available therapy [5].

All patients involved in this work were candidates to surgical treatment due to their medically resistant epilepsy. To understand the justification of the surgical treatment, first we have to learn about the different types of epilepsy.

2.1.1 CATEGORIZATION OF EPILEPSIES

The epilepsies were classified by the ILAE (International League Against Epilepsy) in 1989 and 2001 [6, 7] with major changes based on recent results in 2010. Regarding the etiology of epilepsy, there are five main types: 1: genetic, where direct evidence is present for specific chromosomal or gene alterations; 2: structural, that may include various congenital or acquired structural defects of the brain; 3: other epilepsies which are related to metabolic alterations, 4: epilepsies caused by autoimmune or infectious diseases or 5: unknown origin [8, 9]. Another classification exists for the seizures as the major symptom of these epilepsies. The recent classification had two classes for seizures. One is focal, when seizure activity starts from one

DOI:10.15774/PPKE.ITK.2016.004

well-defined area of the brain and the other is generalized, when the seizure activity involves both hemispheres of the brain. Figure 1 illustrates the current seizure classification.

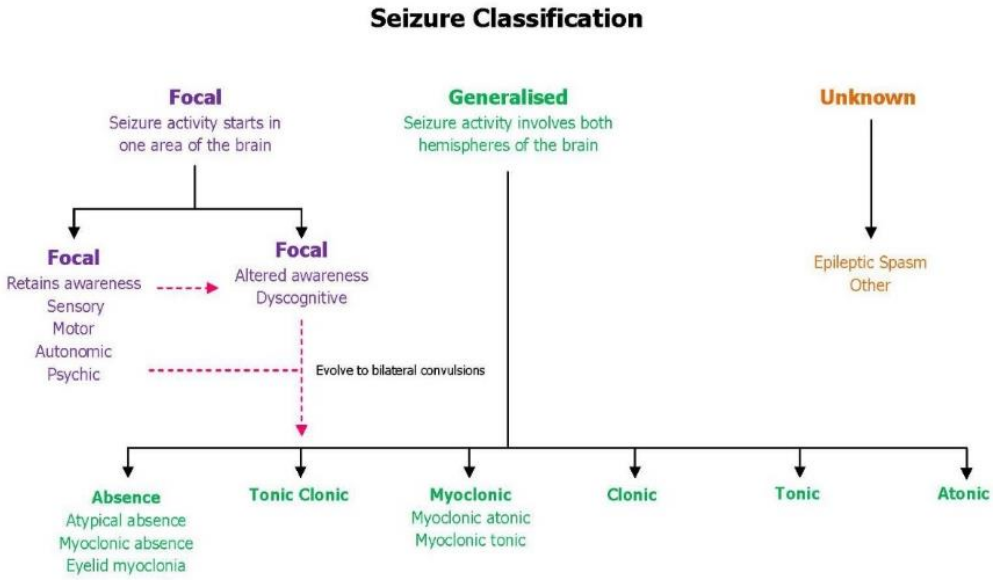

Figure 1. Epilepsy categorization based on seizure spread. The recent classification had two classes for seizures. One is focal, when seizure activity starts from one well-defined area of the brain and the other is generalized, when the seizure activity involves both hemispheres of the brain. This categorization is important in the treatment of the epilepsy. (Source of the picture: * 1)

Bearing in mind that correct classification of patients according to the existing scheme is important in order to achieve better surgical outcome. [10]

2.1.2 Epilepsy Surgery

The patients enter surgical evaluation when their seizures are pharmacoresistant. Such a state is defined by the failure of at least two medical regimes (seizures must interfere with the patients' quality of life and fail to be controlled by at least two first line AEDs trials in monotherapy at the maximum tolerated doses). Usually a minimum of 2 years of medical treatment is carried out in most of the adult cases [11]. The surgical treatment is applied to focal epilepsies where seizures arise from a well circumscribed area in the brain. The goal of the surgery is the removal of the brain area responsible for seizure generation. The process aimed to determine this area is called presurgical evaluation which includes neurological seizure description (seizure semiology), neuropsychology (to define the affected brain functions), non-invasive preoperative imaging techniques like MRI, PET, SPECT, fMRI, CT and invasive or non-invasive interictal and ictal EEG monitoring. The decision of the application of invasive or non-invasive EEG monitoring is based on the convergence of the results as shown on the following flowchart (Figure 2). [12]

DOI:10.15774/PPKE.ITK.2016.004

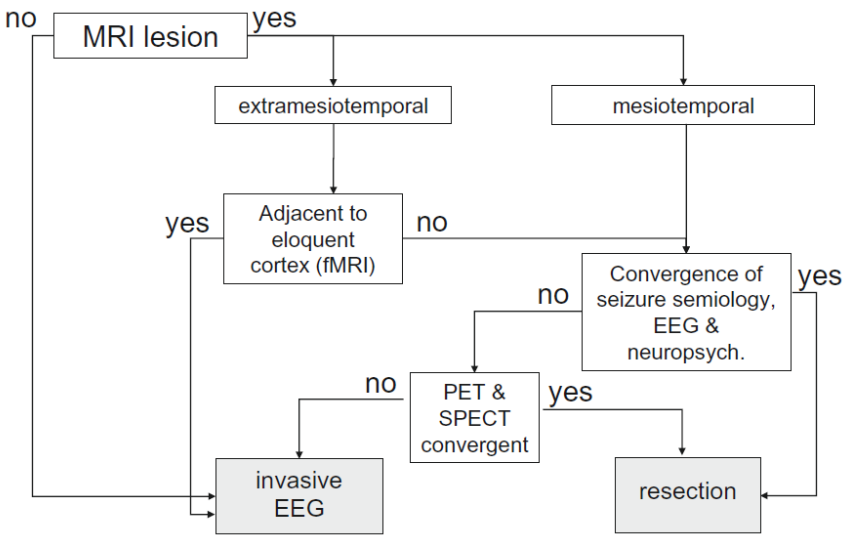

Figure 2. Flowchart of diagnostic evaluation in epilepsy surgery. The decision of the application of invasive or non-invasive EEG monitoring is made based on the convergence of the preceding tests (MRI, fMRI, EEG, neuropsychology, etc.). [12]

As an example to this procedure let's consider mesial temporal lobe epilepsy (mTLE). This syndrome is characterized by seizures with loss of consciousness starting with gastric or olfactory sensation usually appearing first during young adulthood. Usually a specific lesion is present on the MRI located at the mesial (closest to the midline) aspect of one of the temporal lobes, which is most typically hippocampal sclerosis. Interictal EEG shows wide temporal sharp waves, ictal EEG usually shows lateralized theta frequencies upon the temporal structures. On the positron emission tomographic (PET) images, a wide range hypometabolism is detected in the affected temporal lobe. If the results of these modalities converge to the same temporal lobe, no further invasive EEG is required to locate the seizure focus. Otherwise, the patient is a candidate to an operation where electrodes are placed on the surface of the brain (electrocorticography - ECoG) or into the brain (stereo-electro-encephalography - sEEG) to investigate other evidence to lateralize or localize the seizures. In our patients, we mainly registered data from the brain surface with electrocorticography (ECoG), and only occasionally used deep brain electrodes.

To understand the meaning of the invasive EEG recordings, I have to introduce some epileptological definitions. Based on different measures, the brain can be divided into overlapping zones [13].). The irritative zone is the area along the brain surface that gives rise to interictal discharges (IID) or spikes. The seizure onset zone is the area where seizures originate from, and the symptomatic zone is the area where seizures spread and contribute to the clinical signs during it. The existence of these zones is required to define focal epilepsy. The epileptogenic lesion is a visible structural alteration that serves as etiological factor for the seizures. The functional deficit zone is responsible for functional deficits which can also be affected even between seizures. Such dysfunctions may be impaired neuronal functions e.g.

DOI:10.15774/PPKE.ITK.2016.004

memory, language, motor, etc. The last and most enigmatic zone is rather theoretical. The epileptogenic zone is the area we are looking for during the epilepsy surgery investigation, as its resection is necessary and fundamental to eliminate seizures. It can be estimated by the other measurable zones listed above. The uncertainty in defining of the epileptogenic zone underlies the extensive research after more specific biomarkers of epilepsy surgery.

2.1.3 SELECTION OF BIOMARKERS FOR EPILEPSY SURGERY

Biomarkers or surrogate markers are biological signals that can embody complex biological phenomena, and as a measure, make them detectable, and gradable.

Invasive EEG provides very clear and detailed information of the brain, and together with the attached imaging and other clinical data, they form excellent candidates for the biomarker research of the epileptogenic zone. This research can be passive (non-interventional) when the spontaneous states of the patients are examined, and active (interventional) when some intervention is applied.

Under spontaneous states in the behaviour of the patient, interictal (between seizures) and ictal (during seizure) electrical signals can be analysed. Interictal EEG may harbour sharp transients called interictal spikes or discharges (IIS, IID) or high frequency oscillations (HFO), which could be presumable biomarkers of the irritative zone or the epileptogenic zone. As part of the clinical investigation, the patient is subject to various, low and high frequency electrical stimulations through the implanted electrodes, to investigate the function of the underlying brain area. The electrical and behavioural responses can also become potential biomarkers of malfunction too [14-16].

One of our main aim is to find biomarkers which precisely determine the epileptogenic zone in the brain of epilepsy surgery patients. Since temporal lobe epilepsy is recommended to surgery in the highest rate and most of our patients suffer from this kind of epilepsy, we handle it with special attention.

2.1.4 TEMPORAL LOBE EPILEPSY

The most commonly occurring epilepsy is temporal lobe epilepsy (TLE) which covers approximately the 40% of adulthood focal epilepsies [17, 18]. Two subtypes of TLE can be distinguished. In lateral TLE, seizures arise in the neocortical part of the temporal lobe. When seizures emerge from the limbic regions or the hippocampus, it is called mesial TLE [19]. The majority of temporal lobe epilepsy patients suffer from mTLE syndrome [20] which is characterized by a high rate of pharmacoresistance, on the other hand it is well treatable by surgery [18, 21-25]. The surgery depends on the size of the involved areas, which in some cases are only the deep structures (amygdala- hippocampus), while in other cases the whole temporal lobe is removed. [24, 26, 27]. Generally speaking, the bigger the resections is, the

DOI:10.15774/PPKE.ITK.2016.004

better the epileptological outcome will be along with a potentially worse cognitive outcome, while more focused resections result in better neuropsychological, but slightly worse seizure outcome [28].

The hippocampus is the structure of the temporal lobe which is involved in the largest portion (about 60%) of the temporal lobe epilepsies [29].

2.1.5 HIPPOCAMPUS

The hippocampus is an ancient part of the brain that plays an important role in declarative, episodic, spatial and emotional memory. It receives converging information from almost every part of the brain. The main role of the hippocampus is to code and associate pieces of incoming information to form memory traces, then sends them back to the area it came from in the form of thousands of strengthened connections between neurons. Once the temporary associations of cortical neurons become stable, they become independent of the hippocampus. Among all types of memory, spatial memory is an exception, as it appears to be confined to the hippocampus by creating a mental map of space [30].

2.1.5.1 Macroanatomy

The hippocampal formation (HcF) is located at the mesial part of the temporal lobe (Figure 3), named after its resemblance to the seahorse which is 'hippos kampos' in Greek. The human hippocampus is archicortex, the most ancient part of the cortex in the mammal brain, containing only one cell layer. It has three major parts lengthwise: head, body and tail. In animals, various sections of the hippocampal formation are shown to be functionally and anatomically distinct. The dorsal hippocampus corresponds to the posterior hippocampus in primates, performs primarily cognitive functions like spatial memory, verbal memory, and learning of conceptual information. The ventral (anterior in primates) area relates to stress, emotion, and affections. Strikingly, gene expression in the dorsal hippocampus correlates with cortical regions involved in information processing, while genes expressed in the ventral hippocampus correlate with regions involved in emotion and stress (amygdala and hypothalamus) [31, 32].

2.1.5.2 Connections

The hippocampus is part of the Papez's circuit and forms one functional unit with the enthorinal cortex and the medial septal nucleus. It sends axons to the mammillary body and the ventral striatum (nucleus accumbens) through the fornix. The bilateral hippocampi are interconnected via the dorsal hippocampal commissure [33]. As part of the Papez's circuit, the limbic system exerts its influence on the hippocampus and the temporal lobe. The hippocampus facilitates associations among various parts of the cortex.

DOI:10.15774/PPKE.ITK.2016.004

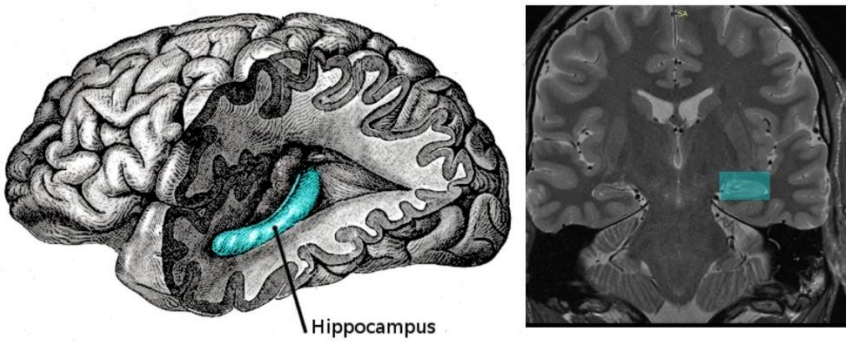

Figure 3. Hippocampus location in the human brain. Hippocampus is the blue coloured anterior-posterior directed structure on the schematic drawing on the left * and on a coronal section of a 2D proton density weighted MRI picture ** – framed with the blue shaded square. (*Source: * 2, **Source: * 3)

2.1.5.3 Microanatomy

We can separate the hippocampal formation into three parts, dentate gyrus (DG), subiculum (Sub) and cornu ammonis (CA) which has three subregions: CA1, CA2, CA3 (Figure 4). The inner connections of the hippocampus are called the trisynaptic loop, which is mainly known from animal studies. Briefly, the main input comes from the entorhinal cortex through the perforant path and terminates on the granule cells of the dentate gyrus. The granule cells give rise to excitatory connections to the pyramidal cells in the CA3 region of the cornu ammonis. The pyramidal cells in the CA3 have multiple recurrent collateral connections with other pyramidal cells in the same region, and project axons into the CA1 region. This pathway is called the Schaffer collaterals. The axons from the pyramidal cells of CA1 end up on the pyramidal cells of the subiculum, from where the axons project back to the entorhinal cortex. Figure 4/B illustrates the trisynaptic loop.

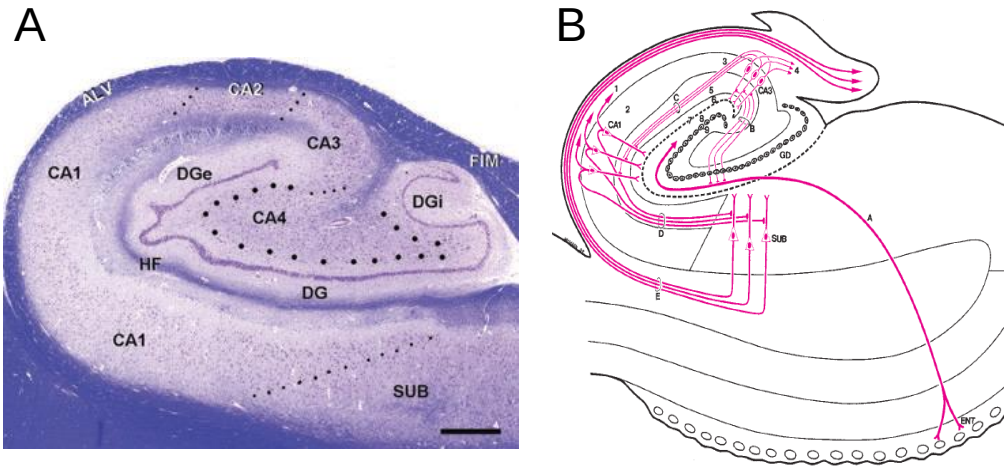

Figure 4. Hippocampus cross-sectional illustration and main connections. A) Human hippocampus sections or subregions as determined by the ILAE [34]. Darker purple line shows the 'blade' of Dentate Gyrus (DG) which contains of the granule cell bodies, bigger dotted layer illustrates CA4 region, and continue with CA3, CA2, and CA1. Subiculum separated from CA1 with smaller dotted lines. B) Schematic representation of the main connections of hippocampus drawn by Duvernoy [35]. The main input comes from the entorhinal cortex through the perforant path and terminates on the granule cells of the dentate gyrus. The granule cells connect to the pyramidal cells in the CA3. The pyramidal cells in the CA3 has multiple recurrent collateral connections with other pyramidal cells within the region, and project axons into the CA1 region. This pathway is called the Schaffer collaterals. The axons from the pyramidal cells of CA1 end up on the pyramidal cells of the subiculum, from where the axons project back to the entorhinal cortex.

DOI:10.15774/PPKE.ITK.2016.004

The excitatory principal cells are the granule cells in the DG and the pyramidal cells in the CA regions which make about ninety percent of all cells within the hippocampus. The remaining ten percent consists of numerous types of inhibitory cells. In contrast to the absolute number, over 80% of the synapses are formed by the inhibitory neurons of the hippocampus, resulting an efficient and well synchronized inhibitory system is the region [36]. Based on the specific termination pattern along the dendritic tree of the pyramidal cells, the inhibitory cells may control selectively the influx or efflux of the information to and from a given subregion. This network plays an important role in learning and memory.

Studies have shown that the subiculum has a possible role in controlling the input and output of the hippocampal formation through its position between CA1 and entorhinal cortex, furthermore it may also integrate the information of the limbic network and redistribute it to other brain structures through its connections [37-44]. The Subiculum therefore has an essential role in both normal and pathological processes. The local connections of subicular pyramidal cells form a characteristic pattern, hypothesized to facilitate the appearance of internal recurrent network activity [45-48]. This might lead to synchronized reverberating circuits and epileptogenic plasticity under pathological conditions [49, 50].

Hippocampal sclerosis (HS) is a typical histological finding of temporal lobe epilepsy patients, characterized by reorganized excitatory and inhibitory circuits, cell loss, axonal sprouting and gliosis[51-56]. However, the Subiculum is relatively well preserved in HS patients [57, 58]. In vitro slice studies on excised human hippocampal tissue showed that spontaneous rhythmic synchronized network activity similar to interictal discharges are present in the subiculum - sometimes even in the absence of hippocampal sclerosis [59-63]. Subicular responses to hippocampal or cortical electrical stimulation also reproduces some basic features of subicular interictal spikes [39, 44, 64, 65]. Cohen et al. measured the activity of surgically removed human epileptic hippocampal slices in vitro, and demonstrated that only the subiculum produced spontaneously recurring interictal discharges, but other sub-regions of hippocampal formation did not [59].

2.1.5.4 Electrophysiology of the hippocampus

Two electrophysiological states are known in the hippocampus. 1) theta oscillation (6-10 Hz) is present during exploration and REM sleep and 2) irregular oscillation with sharp-wave complexes in immobile animal and non-REM sleep [66].

Theta activity

Theta activity in the hippocampus was first described in 1959 [67]. In this state hippocampus is forced into a theta frequency oscillation in order to rhythmically control inhibition. Theta is present in the whole HcF and other structures like the entorhinal cortex,

DOI:10.15774/PPKE.ITK.2016.004

cingulate cortex and amygdala. The main current generators thought to be the medial septum and the diagonal band of Broca which is reciprocally connected to the supramamillary region and so are also involved in the generation of the rhythm. [36, 68]. Network patterns arise from collective action of neurons, and theta is a prominent network pattern studied widely in mammals and human [69-72]. Researchers have shown that oscillation of inhibitory networks during theta could be a control signal for timing of action potentials of excitatory pyramidal neurons, such that the coherent oscillations of cell mass during theta allow an ideal mechanism for temporal coding and decoding. The efficient pyramidal cell and inhibitory interneuron feedback allows active pyramidal cells and their common interneurons to break out of the phase of theta, and segregate assemblies of neurons to coding information [73, 74].

According to the human in vivo studies, hippocampal high-delta (2-4 Hz) increases during NREM sleep after learning [75], during memory performance and REM sleep, therefore this frequency band could be analog to the animal theta [76, 77]. Hippocampal rhythmic slow activity (RSA) oscillations between 1-4 Hz shows similar functional properties to the theta oscillations observed in rodents [78-81]. However a recent study showed increased frequency around 7-8 Hz during working memory task [82], while others reported that this frequency increase was not connected to successful episodic memory encoding [81].

Sharp wave – ripple complexes

The other typical activity of the hippocampus is the sharp wave-ripple complex which emerges in resting, motionless mammals, and was first described by Buzsáki et al. in 1992 [83]. Ripples are transient high frequency oscillations (HFO) around 200 Hz originating from the pyramidal cells in the CA regions during immobility and slow-wave sleep omitting the DG [84]. Concurrent recordings from other regions revealed temporal and spatial coherence of neuronal activity during population oscillations. The action potentials of the pyramidal cells were phase locked to the negative phase of the simultaneously recorded oscillatory field potentials and showed a lower rate than the frequency of the population oscillation while the interneurons discharged at the same frequency. This synchronous output of cooperating CA1 pyramidal cells may induce synaptic improvement in other structures of the hippocampus and therefore these oscillations could be the basis of the neural coding and memory consolidation.

Ripples in the hippocampus are frequently triggered by a massive synaptic activation from the hippocampal CA3 subfield, which is called a sharp wave. The network mechanisms involved in ripple oscillations may be relevant for understanding pathologic synchronization processes in temporal lobe epilepsy.

In humans, ripples can be detected in epilepsy patients in their hippocampal – entorhinal circuit during non REM sleep via microelectrodes [85], clinical depth electrodes [86], or

DOI:10.15774/PPKE.ITK.2016.004

foramen ovale electrodes [87]. Two subgroups can be distinguished according their frequency, slow ripples around 80-150 Hz and the fast ripples between 150-500 Hz [88]. The occurrence of fast ripples well predicted the seizure generation in both animal and humans [85, 89, 90], while slow ripple oscillation were present mostly in the not affected hippocampus [88]. Ripples and fast ripples usually appear in natural slow wave sleep (SWS) [85] and the underlying mechanism of HFO generation has been hypothesized to be mainly excitatory in the adult brain [91]. High-frequency oscillations (HFOs) may have a fundamental role in the generation and spread of focal seizures [92-94], and these events are electrophysiological signatures of the epileptogenic brain.

In epileptic conditions fast ripples were present in the DG both in rodents [95] and humans [96]. Fast ripples seemed to be in close relationship to the area's epileptogenic character [[89]. Based on human studies Staba and his co-workers concluded that these oscillations may be the result of pathological neuronal hyper-synchronization of the underlying area [85]. Fast ripples occur on the initiation of focal seizures in temporal and extratemporal epilepsies [93]. Other authors raised the question, whether fast ripples are a summation phenomenon emerging from slower oscillators only, which is supported by the fact that they have spatially different generators and there is evidence that fast ripples mirror synchronized cooperation of abnormally firing neurons [97, 98].

If we live with the assumption that ripples or fast ripples could be a result of an abnormal local hypersynchronous activity, it could be a useful tool to declare the expansivity of the epileptic area. Since the generators of the fast ripple oscillation are confined to a very small area [92], a special technique is needed to reliably detect them.

2.2 BIOMARKERS OF EPILEPSY SURGERY

2.2.1 SPONTANEOUS MARKERS

2.2.1.1 Interictal discharges

Interictal discharges (IID) are characteristic electrical patterns which can be measured in epileptic patients. Their occurrence is specific rather to the irritative zone in comparison to the seizure onset zone [99]. Interictal discharges have a precise description and are easily recognizable even for an inexperienced observer. Original reports using surface EEG [100, 101] were followed by demonstration of similar waveforms from surface or deep brain electrodes.

DOI:10.15774/PPKE.ITK.2016.004

IID or spikes in the epileptological literature appear around the affected area and consist of a sharp, spike like waves lasting 50-70 ms, usually ending up in a several hundred millisecond long slow wave [102-104].

The underlying mechanism of the genesis of interictal spikes is still a question of recent studies. We know from the literature that neuronal activation is evolving in the hippocampus and parahippocampal structures during medial temporal lobe epilepsy spikes [105, 106] while multiple independent foci can be present in epilepsy syndromes affecting the neocortex [107, 108]. Cohen et al found that the intrahippocampal spikes originated from one of the subregios of the Hippocampus, called Subiculum on ex vivo resected hippocampal transversal slices [59].

Combined deep brain and scalp recordings showed that scalp recorded IIDs reflect the neocortical involvement in this process, while intracranial electrodes demonstrated the deeper structures to be more active compared to the cortex, and the coupling between them varied with stages of vigilance [109-112].

2.2.1.2 Interictal spikes and high frequency oscillation correlation

High frequency oscillations (HFOs) are associated to IIDs and seizures both in animal and human TLE [94] and are also present within the epileptic focus [113]. Clemens et al. provided evidence that the ripples in parahippocamal region are linked to IISs and are modulated by thalamo-cortical oscillations [87]. Therefore IIS and HFO have been suggested as new biomarkers for the epileptogenic zone [114]. These studies report strong high frequency augmentation during spikes and high HFO rates over different brain locations. In identifying the seizure onset zone, the rate of HFOs proved to perform well, but the identification of distinct high-frequency oscillations during spikes delineates the seizure onset zone better than just high-frequency spectral power changes alone[115].

2.2.1.3 High Frequency Oscillations and Epilepsy

High frequency oscillations (HFOs) are uniquely associated with side of seizure onset of mesial temporal epilepsy and cortical epilepsy in animals and humans and there is evidence for an association between degree of hippocampal atrophy and the number of HFOs present [85]. There is further evidence [116] for improved outcome in surgery if regions inducing HFOs are removed. Figure 5 illustrates whether fast ripples or ripples were more specific to the epileptogenic area across different studies. Blanco et al. analysed enormous amount of data and showed that ripples with mean frequency around 137 Hz increased in the seizure-onset zone more frequently than fast ripples [117]. When using macroelectrodes in neocortical extratemporal epilepsies, the seizure onset zone might be better determined by the ripple range [118].

DOI:10.15774/PPKE.ITK.2016.004

TABLE: Studies Comparing Interictal Ripples and FRs to the Potential Epileptogenic Region

Study	Subjects	Site	Electrodes	Epileptogenicity Parameter	Study Conclusion
Bragin and colleagues (1999)[5,9]	Rats (KA) and human	MT	Micro	Epileptic individuals and seizure onset side	FRs
Bragin and colleagues (2002)[35]	Human	MT	Micro	Multiunit neuronal synchronization	FRs
Bragin and colleagues (2004)[29]	Rats (KA)	MT	Micro	Side of KA injection, having seizures	Both
Staba and colleagues (2004/2002/2007)[11,13,78]	Human	MT	Micro	Seizure onset side and region atrophy	FRs
Urrestarazu and colleagues (2006)[49]	Human	MT/F	Macro	Seizure onset zone	FRs
Jacobs and colleagues (2008)[43]	Human	MT/F	Macro	Seizure onset zone	FRs > ripples
Worrell and colleagues (2008)[42]	Human	MT	Micro and macro	Seizure onset zone	Both
Jacobs and colleagues (2010/2009)[50,56]; Zijlmans and colleagues (2011)[48]	Human	MT/F/P/O	Macro	After discharges and seizure onset zone	Both
Ogren and colleagues (2009)[79]	Human	MT	Micro	Hippocampal atrophy	FRs
Jiruska and colleagues (2010)[30]	Rats (TT)	MT	Micro	Side of injection	FRs > ripples
Jacobs and colleagues (2010)[8]	Human	MT/F/O	Macro	Surgical outcome	Ripples > FRs

The conclusion describes whether fast ripples or ripples were more specific for the presumed epileptogenic area or whether no clear difference was found.
F = frontal; FR = fast ripple; KA = kainic acid; MT = mesiotemporal; O = occipital; P = parietal; TT = tetanus toxin.

Figure 5. Relation between ripples, fast ripples and epileptogenic area according to different research groups. Studies collected till 2012 by Zijlmans et al. [115] shows that ripples or fast ripples were more specific to the epileptogenic area.

Fast ripples are reported to be augmented at the time, before seizure onset, or even several hours beforehand [119]. Researchers observed that secondarily generalized focal seizures are characterized by a small area of pathological HFO generation at seizure onset that can move along the cortex and increase in size as the seizure progresses [120]. Bragin et al suggested that the size of the HFO generating region can account for transition to an ictal state [92].

One study showed that while spikes increase after seizures, the number of high-frequency oscillations decreases. The number of HFO events increase after medication reduction so the behaviour of the HFOs are similar to the seizure's. This implies that spikes and HFOs have different pathophysiologic mechanisms and that HFOs are more tightly linked to seizures than spikes. HFOs seem to play an important role in seizure genesis and can be a useful clinical marker for disease activity [121]. More complete resection of the regions with high-rate fast ripples significantly correlated with a better seizure outcome while high-rate ripples only improve seizure outcome. Therefore interictal ripples may not be as specific of a marker for the epileptogenic zone as interictal fast ripples. [122] Another study concluded that ripples were more relevant in the seizure onset zone than in the surrounding area, but the surgery outcome correlated significantly only in the case of temporal lobe epilepsy [123].

The occurrence of fast ripples well predicted the seizure generation both in animal and humans [85, 89, 90]. High-frequency oscillations (HFOs) may have a fundamental role in the generation and spread of focal seizures [93, 94, 124], and thus they may be the

DOI:10.15774/PPKE.ITK.2016.004

electrophysiological signatures of the epileptogenic brain. These oscillations can be found on scalp recordings also with careful selection and artefact elimination (Figure 6) [125].

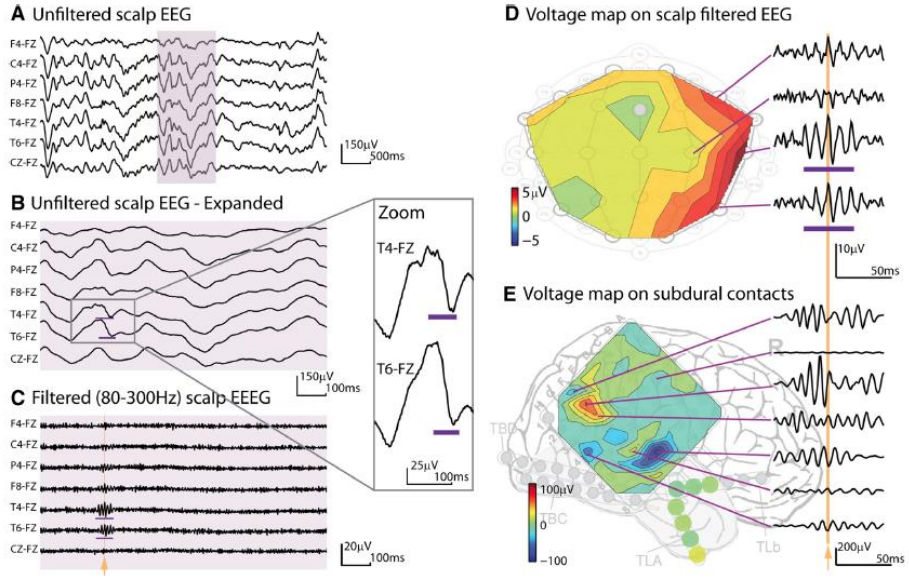

Figure 6. High frequency oscillation on scalp EEG [125]. Zelmann and colleagues had proven with simultaneous intracranial and surface recordings that HFO events even with small generators can be visible with spatially wider extension on good quality scalp EEG verified by experienced reviewer.

Ripple oscillations can be detected in humans by clinical depth [126], or foramen ovale electrodes. Researchers have found fast ripples in the dentate gyrus of the hippocampus in epileptic rats, while in healthy controls there weren't any to detect, not even ripple oscillations [84, 96]. Fast ripples seem to be in a close relationship to the epileptogenic feature area [89]. Staba and his co-workers showed that the fast ripples appearing during NREM sleep and the epileptiform desynchronization events during wakefulness in the epileptogenic zone prove that these oscillations are the result of pathological neuronal hypersynchronization of the underlying area [85]. Fast ripples occur on the initial of the focal seizures in temporal and extratemporal epilepsies [93]. This raises the question whether fast ripples are the harmonics of ripples, but this suggestion is probably wrong, as there is evidence that fast ripples are mirroring synchronized, 'out-of-phase' cooperation of normally firing neurons [97, 98]. If we live with the assumption that ripples or fast ripples could be a result of an abnormal local hypersynchronous activity, it could be a useful tool to declare the expansivity of the epileptic area.

2.2.1.4 Detection algorithms of ripples

From the beginning, many detection algorithms have been made because the gold standard visual inspection of filtered data is time consuming and the reviewer fatigue, vigilance, distractions can cause missed events or artefact confusion. Figure 7 illustrates some examples

DOI:10.15774/PPKE.ITK.2016.004

causing the difficulties of the visual selection like different filter settings or muscle artefact, electrode movement, sharp transients.

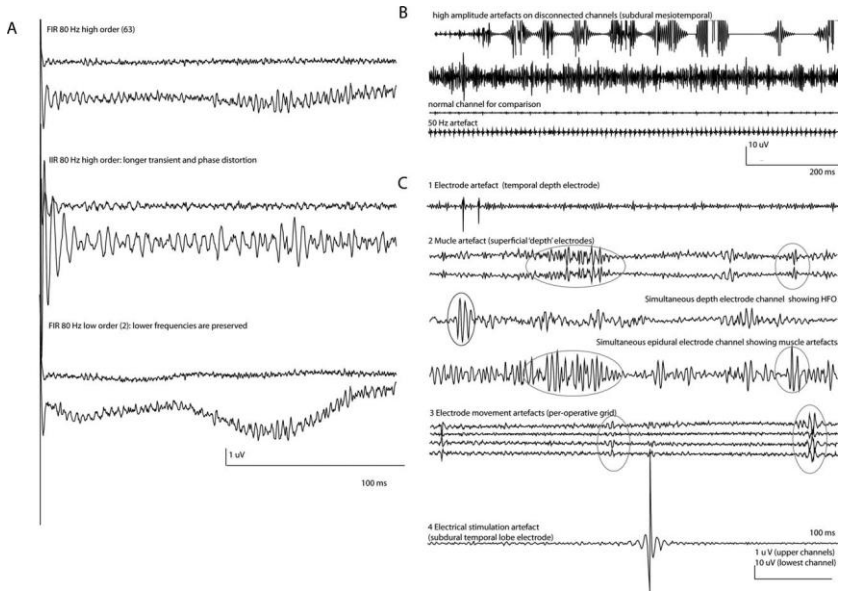

Figure 7. Example of visual ripple detection by Zijlmans 2012 [115]. The detection of ripples run into difficulties which originates from different filter settings, or artefacts. The artefacts could be derived from bad electrode contact, muscle artefact, electrode movement, and stimulation sharp transient.

To overcome visual algorithms, first semi-automated, than automated methods shall be developed. The solution for this problem is not so obvious though, since there is still no agreement in the exact definition of the ripple events up to date. So – while developing the detector – basic research was needed for the missing definition.

The first detection algorithm by Staba and colleagues was invented for microelectrode recordings from the hippocampus. They used two filtering paradigms at the same time, one quadratic (root-mean-square -RMS) mean smoothed and another rectified bandpass filtered data between 80 and 500 Hz. They considered the detection to be successful when the RMS data exceeded a threshold (five times the standard deviation) longer than 6 ms and at the same time at least 6 consecutive peaks were detected on the rectified data above three times its standard deviation. [88]. They visually revised the results and found that 84% of the events were correctly detected.

Since then, a great number of research groups have developed some kind of ripple detection method, in the following I will list these. In 2005 Khalilov et al. worked on hippocampal slice preparation *in vitro* and introduced new thresholds with three times standard deviation on the frequency power amplitude and 5 cycles as calculated on the Morlet wavelet transformed data [113, 127]. Gardner‘s research group published a method [128] based on short – time line length which results in less false positive detections, and they chose a 97.5% threshold on the empirical cumulative distribution function of the line length values. They observed that the distribution of short-time energy (RMS) and short-time line length values are both skewed and

DOI:10.15774/PPKE.ITK.2016.004

kurtotic therefore they are not normally distributed ($p \ll 0.01$), and so the standard deviation derived thresholds may be inappropriate. They verified each of the candidate HFOs identified by either human or computer with human reviewers. This algorithm detected the majority (89.7%) of events, but also produced extra detections. Their results raised the important question if the majority of unlabelled, extra events are due to errors made by the human experts during identification (e.g., false negatives), or due to the errors made by the automated detector (e.g., false positives).

Crepon et al worked with intracranial depth electrodes and subdural strips in human epileptic patients. Their semi- automatic detection procedure is based on wavelet decomposition, and the signal envelope is computed using a Hilbert transform with threshold set to 5 standard deviation of the envelope calculated over the whole recording. The automatically detected events are confirmed by a visual reviewer [129]. They used benchmark events visually identified by a human reviewer (B. Crepon) and measured the performance of their algorithm which was 100% on sensitivity with 90.5% specificity.

Zelmann et al. worked with depth electrodes used for stereo EEG in epileptic patients [130]. They developed an automatic detector called MNI, which first detects baseline segments and then computes the energy threshold using the detected baselines. The baseline detector previously described [131] and based on another work [132] describes that the wavelet entropy (the degree of randomness or orderliness in the time-frequency domain) significantly decreases while “a more rhythmic and ordered behaviour of the EEG signal” appears which could correspond to the “dynamic process of synchronization in the brain activity”. They tested the performance on those events which were jointly marked by two reviewers [126]. Their detector achieved 96.8% in sensitivity with a mean false positive rate of 4.86%.

Blanco et al applied a data-mining technique [117] on an enormous amount of high frequency oscillation events detected by an automatic method in epileptic patients with subdural implanted electrodes and microwires. Their previously described method [133] is based on Staba’s approach [88] when reducing data size and in finding putative events, then an automatic process dismisses events showing statistical similarity to the local background surrounding the candidate event in a 2.5 s window. Afterwards, computational features are extracted from these candidates and applied as inputs to a classifier using the k-medoids algorithm. The groups are then correlated to other epileptic features.

Many other detection methods are available at the moment [134-143]. Based on expert reviewers, visual analysis is considered to be the gold standard with two major problems: poor inter-rater reliability, and limited applicability for large data sets [144]. Supervised detection algorithms usually employ high sensitivity but poor specificity automated detection algorithms

DOI:10.15774/PPKE.ITK.2016.004

that is further specified by the visual review. Unsupervised, fully automated detectors must meet the requirements of high specificity and sensitivity [145].

After numerous studies, researchers examined the question whether the difference between macro and microelectrodes can cause inequality in the HFO detection and found that electrode size has no influence on ripple detection. Châtillon et al suggest that commercially available intracerebral electrodes (0.2 - 5 mm^2) have similar HFO detection abilities [146].

In summary, none of the above mentioned methods are able to fulfil our requirements postulated above. Furthermore, the adjustment of parameters can have significant effects on the data and analysis, thus this is a fairly significant problem in the field currently. Also we still have problems with definitions and characterization of ripple events [141, 147].

2.2.2 EVOKED MARKERS

As previously described, during invasive EEG monitoring, the neurologists are looking for biomarkers which are probably related to the seizure onset zone. The observation in the long-term EEG monitoring unit consists of the examination of the patient's behaviour and concurrent electrical brain activity, during invasive and non-invasive stimulation some kind of evoked responses are expected.

2.2.2.1 Electrical stimulation mapping

During electrical stimulation mapping (ESM), the epilepsy surgical team applies electrical current through the electrodes to map eloquent cortical areas like language, motor or sensory cortex. We have limited understanding of the mechanism, nevertheless stimulation-based cortical language mapping has resulted in minimized postoperative language deficits in countless patients and revealed cortical relationships on a way that has been inaccessible until by any other means [148]. The method was firstly used to identify motor and sensory cortex (by Foester in 1929 and Krause & Schum in1931 [149]) and then applied in clinical utility by many others [150-153].

The electrical stimulation method uses square wave electrical impulses of alternating polarity with a pulse width of 0.2-0.5 ms and a frequency of 20-50 Hz delivered for 1–3 seconds with variable electrical current (1-15 mA) depending on the tissue excitability [148, 154]. Evoked behavioural changes or movements are registered and corresponded to the stimulated area. One study examined the microscopic histology of human cortical tissue from the anterior temporal lobe after direct subdural electrical stimulation was performed in 3 patients. They found no structural damage for the 2-5 s long, 12.5-15.0 mA stimulation and there were no differences in pathologic features which could be correlated with the presence of the electrodes or with the amount of electrical stimulation [154]. The electrocorticogram signals recorded during and after the stimulation were usually not used, but a recent study

DOI:10.15774/PPKE.ITK.2016.004

processed and concluded that the distribution of the largest frequency component of the evoked activity (60–80 Hz) allows one to define different clusters of contacts that retrospectively correlate to the epileptogenic zone identified by the clinicians [155].

2.2.2.2 Cortico-cortical evoked potentials (CCEPs)

Instead of high frequency stimulation used for functional mapping, some centres use single pulse electrical stimulation (SPES) which evokes electrical changes in local and distant cortical areas as recorded on the surrounding electrodes. This phenomenon is named cortico-cortical evoked potential (CCEP) and is illustrated on Figure 8. [14-16, 156-165]

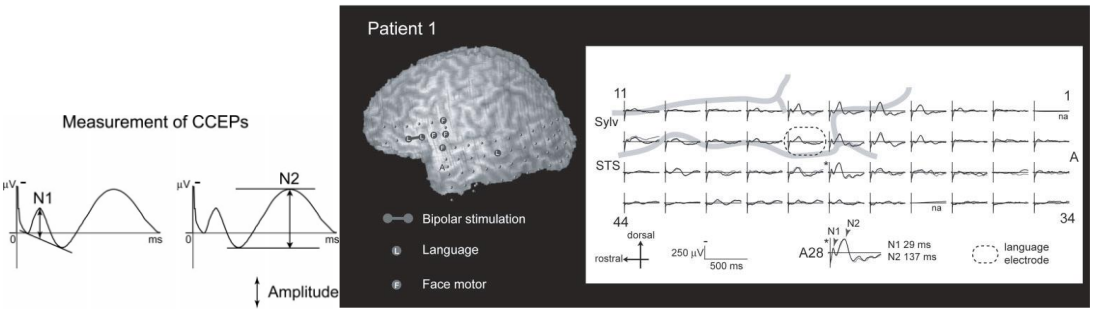

Figure 8. Illustartion of cortico-cortical evoked potentials from Matsumoto's original article [156]. The measurement of the N1 and N2 component are seen on the left and a representation of the stimulation on the right. The first negative peak is N1, the second is N2.

Low frequency (0.5-1 Hz) single pulse stimulation typically does not elicit the behavioural effects that are observed with clinical electrical stimulation mapping [148, 154].]

Cortico-cortical evoked potential (CCEP) consists of an initial early (10–50 ms) biphasic activation and a delayed (50–500 ms) slow wave [164, 166]. The first wave is thought to reflect direct activation of the local cortex [156, 167, 168], while the second wave may represent a later inhibition [166, 169], similar to spontaneously recorded and induced human slow oscillations generated by cortical and subcortical (thalamic) interactions [156, 159, 170-175]. Both responses have been shown to be predicted by resting functional connectivity measures using fMRI [176].

We can assume that evoked potentials are the result of a functional connection between the stimulated area and area where the evoked potential appeared. Defining connections between brain areas is essential to understand the complex functional organization of the human brain system and could also help to elucidate the pathophysiology of ictal semiology and to map the ictal network.

Application of cortico-cortical evoked potentials (CCEPs)

Many studies conclude important information when analysing results of the CCEP analysis. For example, Matsumoto and co-workers used it to map connections of different parts of the brain like the language, the motor and the sensory cortex. They suggest that the perisylvian

DOI:10.15774/PPKE.ITK.2016.004

and extrasylvian language areas have feed-forward and feed-back projections, furthermore they found bidirectional connections between Broca's and Wernicke's area probably through the arcuate fasciculus and/or the cortico-subcortico-cortical pathway. The CCEPs were recorded from a larger area than the identified language area suggesting the existence of a broader neuronal network [156]. They found that stimulation of the positive motor areas in medial motor cortex elicited CCEPs at the regions in the lateral motor cortex and they could evoke evoked potentials from the other direction also [157]. Furthermore, they stimulated the negative motor areas and found connections to the frontal or parietal association cortex, indicating the importance of the fronto-parietal network associated with a higher level of motor control [163, 177]. Based on these results, intraoperative language network monitoring also became feasible using the CCEP technique [165].

Ictal correlation of CCEP

Since the cortico-cortical evoked potential is elicited in the brain of epilepsy patients, it is plausible to examine the correlation with the increased excitability of the neuronal tissue itself. A research group measured the cortico-cortical evoked potentials in ictal-onset regions and found that the amplitude of the first negative wave of the CCEP was significantly higher in the ictal onset region than that of the non-ictal regions in seven out of eight patients. In one patient, the amplitude was higher in normal regions and in the primary eloquent cortex. [178].

With single pulse electrical stimulation, interictal electrical discharge can be induced in the cortex of human epilepsy patients. [14-16, 164, 179]. Valentin et al. described two kinds of late responses, one being the spikes or sharp waves occurring between 100 milliseconds and 1 second after stimulation. They suppose that the late spike generating areas are part of the ictal network. The other response is a repetitive, two or more consecutive sharp-and-slow-wave complexes, which appeared only when the stimulation was performed in the frontal lobes. They assume that areas in which stimulation results in these repetitive response are the abnormal regions. According to their results, the total resection of the sites which produced late responses was also associated with better seizure outcome [14, 15].

A recent study used CCEPs to demonstrate that bidirectional connectivity during the first wave is a prevalent feature that characterizes contacts included in the epileptogenic zone and may contribute to the detection [160].

2.2.2.3 Networks based on cortico-cortical evoked potentials (CCEPs)

We can assume that the cortico-cortical evoked potentials (CCEPs) are hallmarks of the connections between the stimulated and the recording areas therefore we can use them as a measure of connections in neuronal networks.

DOI:10.15774/PPKE.ITK.2016.004

Researchers have also used different methods to create networks where brain regions represent the nodes and the connections between them are the edges [180]. Such studies of brain networks have provided new insight into the interactions that underlie cortical information processing and the pathophysiology of neuropsychiatric diseases [181-183]. The direction of information flow is a facet of this research that has been difficult to ascertain. This is because connectivity measures in humans, like resting fMRI and diffusion tensor imaging cannot resolve the direction of cortico-cortical or subcortical interactions. Anatomical tracer studies can elucidate fine-grained directional connections in experimental animals [184] but are more difficult in humans [185]. A number of non-interventional methods, such as Granger causality and dynamic causal modelling, can demonstrate causal interactions by statistical inference [186, 187], but may be difficult to confidently interpret [188]. Direct cortical stimulation provides an interventional method to test causal relations (or "effective connections") between brain regions. Electrical stimulation at one location on the neocortex can trigger an electrical response at a remote location in proportion to the strength of the effective connection between the two locations.

Physiological network properties based on our work

Our research group have made functional connectivity networks with Brodmann Areas [189] [3].

Cortico-cortical connectivity was assessed creating connectivity measurements from the normalized amplitude of the evoked potential A1 and A2 component between stimulated and recording Brodmann's Areas (BA) for each individual patients.

In this study the network for each patient was averaged together to create an overall connectivity map (Figure 9). We found high A2 amplitude values between the SS (BA1-2-3), BA6, BA9, BA40, BA41, BA42 and motor cortex (BA4). Strong connections start from BA20 aiming the frontal, temporal lateral and medial, parietal and occipital lobes. BA21 and BA22 showed the strongest connections with BA41 & BA42 but moderate connectivity with other cortical areas. The stimulation of the visual cortex V2 & V3 showed strong intralobar connectivity. V2 had strong connections to BA41 & BA42 and posterior cingulate areas while V3 elicited great amplitude response in BA22, BA37 and the posterior cingulate areas. The amplitude value of the A2 component revealed central role of the motor (BA4), premotor (BA6) and somatosensory (BA1-2-3) areas. These connections were consistent across patients [3].

The stimulation of the prefrontal cortex (PFC) results in larger A2 response with an average amplitude of 10.17 z-score in BA21, but in the opposite direction this connection is weaker

DOI:10.15774/PPKE.ITK.2016.004

with an average z-score of 6.25. This asymmetry was found in several areas, but the underlying biological significance needs further evaluation.

The strong A1 connections between BA20 and BA21, BA22, BA37 and BA38 lost their significance in the A2 network and only BA37 showed a very strong connection with BA20. The somatosensory (SS) cortex stimulation evoked very strong connections to BA7, BA39 and BA40 within the A2 network, however the A1 amplitude of these connections were much lower. The amplitude value of the well-known anatomical connection between Broca (BR) and Wernicke (BA22) area was large in both directions with the A2 component, but average or lower with A1. The connectivity based on the A1 and A2 peaks have showed similar properties however there was greater rate of the reciprocal connections in the A2 based network. The differences between the networks based on A1 and A2 still an aim of the future investigations.

The somatosensory, motor, premotor area, BA9 and BA10 had the highest centrality derived from the incoming and outgoing connections across patients.

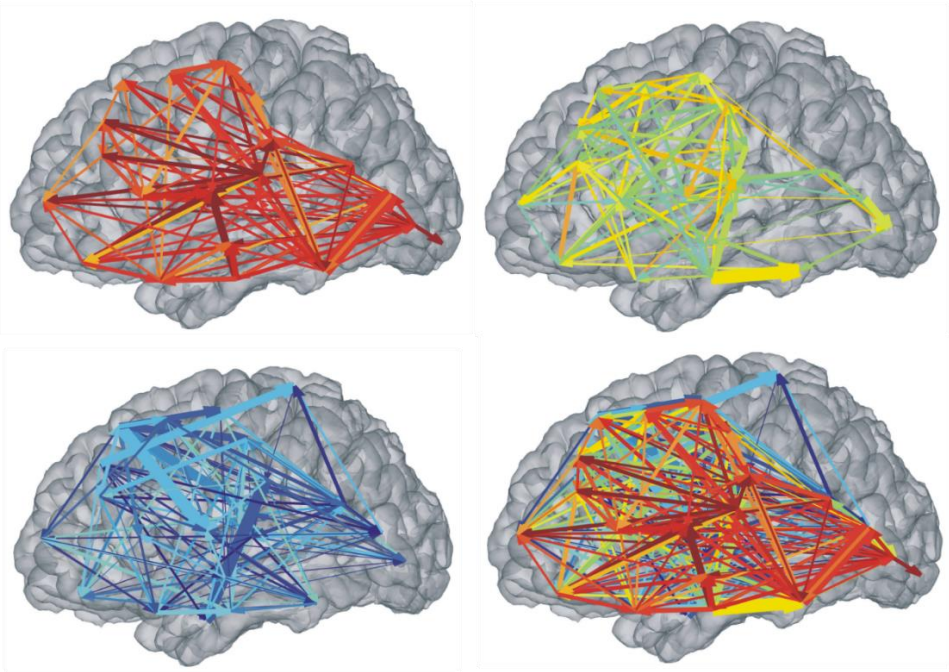

Figure 9. Illustration of the connections between Brodmann Areas, based on A2 component of CCEP. The color of the edges represent the connection stability (warmer colors represent higher percentage of patients exhibiting the connection), the width of the edge highlights the average z-score between the areas. Every connection are visible on the bottom right and separated according to the stability of the evoked slow component (A2) on the others. The more stable connections not always associate with higher amplitude, as it can observe on the top left.

We have created the first connectivity based matrices which allows to describe the connectivity between any two (except those which were not covered with electrodes) Brodmann's area [189]. We defined two measures two specify the connection: 1. The average amplitude between two BAs show if there is at least one significant connection between the selected two area, 2. the ratio of the amplitude of the in and out going connections for every

DOI:10.15774/PPKE.ITK.2016.004

region regarded as a node of the network. These two measures could describe effective connectivity of the brain on a group level revealing formerly not proven connections directly with in vivo electrophysiological measurements.

The usage of cortico-cortical evoked potentials still raises questions and we must be aware of these. We are still not sure whether the CCEP is reflecting the normal brain networks or not, because it is applied on pathological brains. The validity of the network calculations are insecure due to limited coverage of the brain with electrodes. We still just hypothesize that the underlying mechanism of the bidirectional feature of the connections are real back and forth axonal contacts and not the reflexions of antidromic-orthodromic transmission along the axons.

DOI:10.15774/PPKE.ITK.2016.004

3 MATERIALS AND METHODS

This chapter will present the methods and materials (including equipment and data) used during the current work.

3.1 COMMON STATEMENTS

The following statements are equally valid pronouncements for all analyses. In these studies medically refractory epilepsy patients were involved whom after the non-invasive evaluation, underwent subdural strip, grid and/or depth electrode implantation. The choice of patients for intracranial studies, the location of the clinical electrodes, the duration of the implantation and the excision of cortex were determined entirely on clinical grounds by an independent clinical team without regarding any experimental considerations. Every patient consented to the experimental procedure after a thorough explanation of the risks under procedures monitored and approved by the Institutional Review Boards at the respective centres in accordance with the Declaration of Helsinki. Determination of clinical etiology was made by the primary clinical team and, where possible, confirmed through pathological analysis of tissue removed at the time of resection.

3.1.1 PATHOLOGICAL OR PHYSIOLOGICAL PROPERTIES OF THE BRAIN TISSUE

Since we aimed to analyse the physiological and pathological properties of the brain networks, our expert neurologists distinguished between those ECoG electrodes which were over the seizure onset zone or involved in early seizure spread (ictal electrodes) and those which were not involved in early seizure genesis (non-ictal electrodes). The neurologist thoroughly looked through several seizures to determine the ictal electrodes which included those where the seizure started the most often or those which were involved in the first 10s of seizure onset.

3.2 CCEP - MAPPING BRAIN NETWORKS WITH SINGLE PULSE EVOKED CORTICO-CORTICAL POTENTIALS

Mapping directed connections can provide new insight into large-scale brain networks. Here, we used a method of deriving robust effective connectivity networks with high spatiotemporal resolution. These methods may give insight into the large-scale information processing architecture of the human cortex and broaden the knowledge about functional networks.

DOI:10.15774/PPKE.ITK.2016.004

As part of the epilepsy investigation, we could also apply cortical single pulse electrical stimulation, which elicits cortico-cortical evoked potentials from different brain regions. The exact parameters of the stimulation and off-line analysis method details are described in the following part.

My aim was (Aim 1) to develop algorithms for cortico-cortical evoked potential (CCEP) detection and analysis. In a more detailed sense, to analyse the effects of single pulse electrical stimulation (SPES) on the neocortex and in the hippocampus recorded with macro- and microelectrodes and mapping functional and epileptic areas using cortico-cortical evoked potentials (CCEPs).

3.2.1 DATA PREPARATION

3.2.1.1 Patient selection

Twenty-five patients (11 Male, 14 Female) with medically refractory epilepsy were included in the study from the Comprehensive Epilepsy Centre at North Shore LIJ Health System (LIJ, New Hyde Park, NY USA) and the National Institute of Clinical Neurosciences (NICN, Budapest, Hungary). Detailed patient demographics are seen in Chapter 9 - Appendix - Table 2.

3.2.1.2 Electrode placement

After the non-invasive evaluation, patients underwent subdural strip, grid and/or depth electrode implantation (NSLIJ: Integra Lifesciences Corp., Plainsboro, New Jersey, USA and NICN: AD TECH Medical Instrument Corp., Racine, WI, USA). The target area was defined by the Epilepsy Surgical Team. The implantation of subdural electrodes were always done with the aid of neuronavigation and fluoroscopy to maximize accuracy [190].

Grids were implanted through standard craniotomy. In case of implanting only strip electrodes, the burr whole technique was applied. The electrode placement decision and duration of clinical observation was made entirely on clinical grounds, regardless of the purpose of research.

In some cases a 350 μm diameter 24 contact experimental laminar multichannel microelectrode array (ME) was placed in that area, which was presumably removed at the time of the definitive surgery. This ME, called ‘Thumbtack electrode’, was embedded vertically to the cortical surface under the grid silicone layer between the grid contacts [191, 192]. The thumbtack microelectrode has 24, 40 μm diameter Platinum-Iridium contacts evenly spaced at 150 μm providing local field potential gradient (LFPg) recordings reaching through cortical layers from I to VI. To avoid the electrode sliding more than 100 μm below the pial surface, a silicone sheet was attached to the top of the ME shank [191], causing the thumbtack

DOI:10.15774/PPKE.ITK.2016.004

form. After every explantation, ME was visually inspected under a microscope for structural damage. In the lack of diversification, we can hypothesize that the cortex tissue remained intact throughout the recordings.

The intracranial electrodes were referred to contralateral mastoid electrodes. External frontal scalp (sometimes occipital, parietal) electrodes at NIN and to an inversely implanted strip electrode facing the bone at NSLIJ, ECG and zygomatic electrodes were also placed on the patients.

3.2.1.3 Recording parameters

Video-EEG monitoring was made over the course of clinical exploration of spontaneous seizures and ictal activity through 5 - 17 days after electrode implantation surgery. The long-term video-EEG recording of the patients took place at a highly specialized unit, with 24 hour service of EEG assistants and nursing care. The electrocorticogram (ECoG) from the clinical strip and grid electrodes (32-128 channels with mastoid reference) was recorded simultaneously with the video using the standard hospital system band-pass: 0.1-200 Hz, acquisition rate: 2000 - 5000 Hz / 16 bit, Xltek EMU 128 LTM System San Carlos, CA at NSLIJ and acquisition rate: 1024 Hz / 16-22 bit, Brain Quick System 98 Micromed, Mogliano Veneto, Italy at NICN. The ECoG and video data were stored besides the clinical system on hard disks as well for later analysis.

In the case a Thumbtack electrode was placed, spatial LFP gradient (voltage difference between adjacent laminar electrode contacts) was recorded simultaneously with the ECoG. This was provided by a special preamplifier placed inside the head bandage of the patient [191]. The spatial potential gradient is expressed in μV unit rather than the formally correct μV per inter-contact distance (150 μm). This measurement method was proven to be effective in minimizing the motion related head movement and electro-magnetic artefacts [191]. This LFPg recording is defined as the microscopic (~0.1 mm) approximation of the local field potential gradient which mirrors only the locally generated potentials [193]. Since we were curious about the current field which generates the local field potential, we usually used the first and second spatial derivatives as the base of Current Source Density (CSD) analysis to localize synaptic activity [191]. However, we should bear in mind that this recording technique (the potential difference between ~100 μm short distances) could be less applicable to register the far-field effect or precise local synchronous activity.

The LFPg was split to EEG range (0.1-300 Hz) and single (SUA), multiple unit activity (MUA) frequency range (300-5000 Hz) by analogue band-pass filtering at the level of a custom made main amplifier [191], and recorded using custom made LabVIEW (LabVIEW, © National Instruments Corporation, Austin, TX, USA) script. EEG range signal was sampled

DOI:10.15774/PPKE.ITK.2016.004

at 2 kHz/ 16 bit; multiple unit activity (MUA) range was sampled at 20 kHz/ 12 bit and stored on a hard drive. Considering the examination of the ECoG and microelectrode recording correlation, synchronization signal with millisecond precision was given to each recording system simultaneously.

3.2.1.4 Electrical stimulation of the neocortex

Functional Mapping

To identify the functional cortical areas (sensory, motor, language), standard clinical electrical stimulation mapping (ESM) was applied in presence of an epileptologist and neuropsychologist (bipolar stimulation, amplitude: 1-15 mA, frequency: 20-50 Hz, pulse width: 0.2-0.5 ms, train lengths: 2-5 s). If the stimulation resulted in speech arrest, the area was identified as an expressive language site. In case of non-expressive language site, some naming deficit occurred during auditory or visual cues or halt in reading or comprehension. Sensory and motor areas were identified when stimulation caused movement or changes in sensation. Visual and other functional responses were also noted when they occurred. The functional areas were mapped with the lowest current to find the most specific function under the stimulated contact pairs.

Single pulse stimulation

During epilepsy surgery monitoring (approx. 1-2 weeks), single pulse electrical stimulation (SPES) was applied (on average on 5th day after the implantation surgery) across each pair of adjacent electrodes with a Grass S12 cortical stimulator at NSLIJ (Grass Technologies Inc., West Warwick, RI, USA) or an IRES Surgical 600 cortical stimulator at NICN (Micromed S.p.A. Via Giotto, 2-31021, Mogliano Veneto - Italy). Pulse width was 0.2 ms, amplitude 10 mA, frequency 0.5 Hz or 1 Hz and there were various number of trials from 20 to 150 per electrode pair.

The cortico-cortical evoked potentials (CCEPs) were recorded on all other, non-stimulated electrodes. We choose the current amplitude to be 10 mA in order to minimalize the risk to induce epileptic after discharges or other behavioural changes but maximize the number of activated neuronal elements. The 2 s or 1 s inter stimulus interval intended to eliminate the overlapping evoked responses. The different stimulation intervals had no effect on evoked potentials [176]. We performed stimulation while the patient was in an awake but still resting state and in some cases in deep, non-REM sleep.

3.2.1.5 Brain surface reconstruction and electrode localization

As part of NSLIJ and NICN co-operational research program, we developed our method to visualize the electrodes on the individual brain surface. Details have been described previously

DOI:10.15774/PPKE.ITK.2016.004

[3, 176]. Briefly we made native, high density MR images before, CT and MR images after the electrode implantation, followed by the synchronization of these images into the same space using linear transformations (Figure 10). After this step, we used BioImageSuite (BioImageSuite : An integrated medical image analysis suite , 1998, X. Papademetris, M. Jackowski, N. Rajeevan, H. Okuda, R.T. Constable, and L.H Staib., Section of Bioimaging Sciences, Dept. of Diagnostic Radiology, Yale School of Medicine., New Haven, USA, http://www.bioimagesuite.org) electrode localization interface to identify the centre of the electrodes and subsequently snapped to the closest point on the reconstructed pial surface of the pre-implantation MRI in MATLAB using custom scripts [194]. The reconstructed pial surface was computed using Freesurfer [195]. This protocol has been validated with intraoperative photographs.

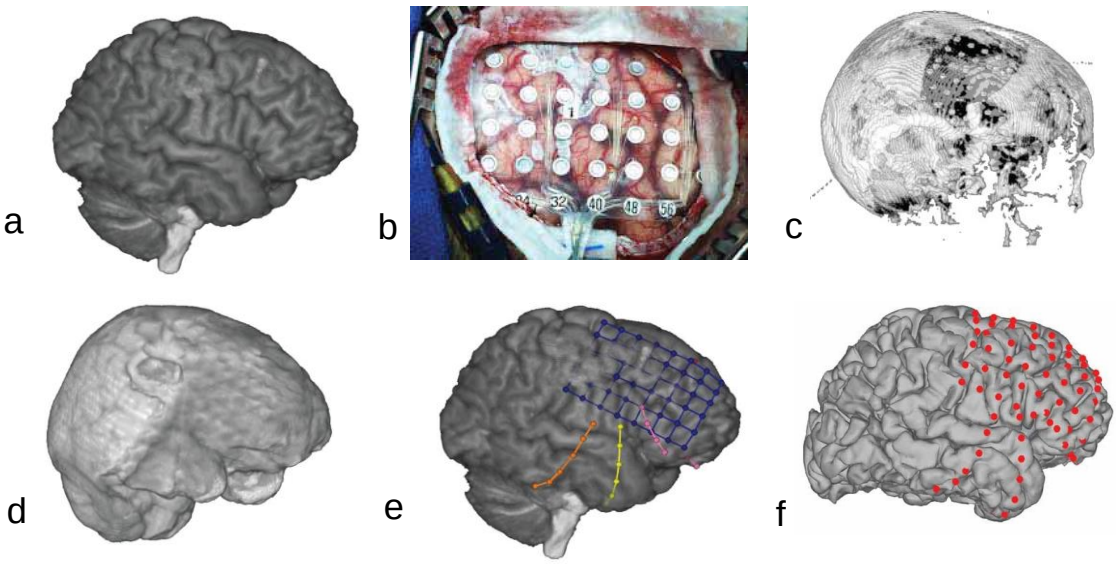

Figure 10. Electrode localization pipeline a) MRI before the implantation, b) Picture during the implantation, c) CT after the implantation, d) MRI after the implantation, e) Localized electrodes after the merged preop. MR, postop. CT, postop. MR, f) Reconstructed brain surface with the electrodes. Every picture is from Pat1 except b) which source is * 4.

3.2.1.6 Electrode distance

Our goal was to examine the appearance of the evoked potentials and the distance from the stimulated area. To measure the distance between two implanted electrodes we used the coordinates derived from the electrode localization procedure. To measure the distance between two implanted electrodes we used the coordinates derived from the electrode localization procedure. The distance between electrode sites were calculated using the Euclidean distance between the midpoint of the two stimulated electrodes and the centre of the recording electrode [156]. With this calculation method, the distance was always the shortest path between the two nodes regardless to the curvature (the gyruses and sulcuses) of the brain.

DOI:10.15774/PPKE.ITK.2016.004

3.2.2 DATA ANALYSIS

Electrophysiological data analyses were performed using Neuroscan Edit 4.3 software (Compumedics, El Paso, TX) and freely available or own made MATLAB scripts (MathWorks, Natick, MA).

In order to determine the connectivity between brain regions, we applied basic graph theory methods. In the following part, I describe how we defined the different nodes (electrodes or electrodes grouped by distance) and the metric values (e.g. z-score, connectivity rate) of the connections.

3.2.2.1 Data preparation

To reduce the amount of the data and to facilitate the handling, I divided the continuous data into smaller parts with NeuroScan Edit. The data was cut into 1 or 2 seconds length epochs, -200 ms to +800 ms or -500 ms to +1500 ms time-locked to the stimulation pulse. We designated the data as baseline between -200 ms to -50 ms for 1 Hz, or -450 ms to -50 ms for 0.5 Hz prior to the stimulation, where we assumed the neuronal activity was at normal, physiological state. The epochs were first averaged, then a high pass (2nd order Butterworth above 0.3 Hz) and a low pass (2nd order Butterworth below 30 Hz) filter was applied. Finally we amplitude rectified the data (we took the absolute values of the amplitude).

3.2.2.2 Peak detection

The cortico-cortical evoked potential waveform in the human cortex consists of an early sharp spike (10–50 ms after the stimulation) followed by a slow-wave (50–250 ms). In previous studies, these were called N1 and N2 referring to the negative voltage deflections within these time periods [156]. Considering the high variability in the polarity and latency of such evoked potentials, we analysed the rectified, filtered data and referred to the peak between 10 and 50 ms as A1 and A2 between 50 and 500 ms after the stimulation [176]. According to this, we measured the magnitude of the cortico-cortical evoked potentials (CCEPs) in between +10 ms to +50 ms for A1 and +50 ms to +500 ms for A2 after the stimulation on the filtered, rectified data.

3.2.2.3 Z score calculation of the CCEP amplitude.

To get an inter-subject comparable value of the evoked potential amplitude, we calculated the statistical z-score of every evoked potential. For the maximal peaks we computed a z-score using the standard deviation and mean of the baseline (of the above described filtered, rectified data) based on the equation (1) below, where z is the calculated z-score value, x is the relative maximum amplitude value, μ_B is the mean and σ_B is the standard deviation of the rectified, filtered data of the baseline between -450 ms to -50 ms (for the 0.5 Hz stimulation) or -200 ms to -50 ms (for the 1 Hz stimulation) before the stimulation artefact.

DOI:10.15774/PPKE.ITK.2016.004

$$z = \frac{x - \mu_B}{\sigma_B} \quad (1)$$

If there weren't any peaks, the mean amplitude of the signal was counted. We used this z-score value as an indicator of the strength of connection between the stimulated and recording areas.

3.2.2.4 Timing of the evoked potentials

We measured the latency of the maximal peak and the distribution of the peak latencies as well.

3.2.2.5 Artificial signal and signal noise handling

The noisy channels (e.g. high amplitude background noise, or contamination of 50 Hz electrical noise) were identified with visual inspection. These channels and those evoked responses which exceeded ± 500uV were left out from the analyses.

3.2.2.6 Significant response criterion

Based on the previously described amplitude measuring technique, we got a value for every channel and every stimulation. From these values, we were able to draw a connectivity map between the stimulated electrode pair and all the others, where the z-score value shows the strength of the connection. In this way we created a directed, weighted graph. To see the significantly relevant connections, we had to specify a threshold.

To find the significant evoked potentials, we calculated two thresholds. To increase sensitivity of the method, we used 3SD (+mean of the baseline) statistical threshold, called "three sigma rule of thumb" statistical theorem which is applicable for non-normally distributed variables too [196]. In order to increase specificity, we described 6SD (+mean of the baseline) threshold determined from the ROC analysis of the connections between Broca's and Wernicke's areas [189, 197]. If we consider the z-score calculation based on equation (1), the 3SD (+mean of the baseline) threshold is corresponding to 3 z-score and 6SD (+mean of the baseline) to 6 z-score. Equation (2) illustrates the calculation of 3 z-scores, after sorting (3), it becomes to the exact definition of the threshold (4) if σ_B =SD (standard deviation) of the baseline and μ_B = mean of the baseline.

$$3 = \frac{x - \mu_B}{\sigma_B} \quad (2)$$

$$x = 3 * \sigma_B + \mu_B \quad (3)$$

$$threshold = 3SD + mean\ of\ the\ baseline \quad (4)$$

DOI:10.15774/PPKE.ITK.2016.004

3.2.3 GRAPH THEORETICAL ANALYSIS OF BRAIN NETWORKS

Our aim was to map the connections between normal and pathological brain areas, therefore we applied basic graph theoretical measures in order to reveal the underlying networks [180, 198, 199]. First, we defined the electrodes as nodes of a graph, and the z-score of the evoked potential amplitude as the strength of the connection between them. Secondly, we redefined the nodes grouping the electrodes according to distance. In order to obtain information with a more reliable significance we've drawn the threshold from the wide distributional z-score values.

3.2.3.1 Connectivity

To analyse the connectivity within the network, connection matrices were built, where electrodes represented the nodes. The values in the connection matrix represent the significant response presence (0 or 1) between the two nodes according to the adjusted threshold (3SD or 6SD) or the z-score value of the evoked potential.

The stimulations were applied on two adjacent electrodes, usually including all possible electrode combinations, with the noisy channels (according to standardized and automatized criteria) always being left out. This resulted in an asymmetric connectivity matrix. The distinction between pathological and non-pathological electrodes also caused asymmetry in the connection matrix.

In-out degree, path length

The in degree of one electrode is calculated based on the ratio of the number of significant responses elicited on that electrode and number of stimulations (possible maximum number of connections) in order to reduce variability due to different electrode configurations and stimulation trials. Out degree of the electrodes were calculated based on the number of activated electrodes with the stimulation which was then divided by the total number of electrodes. This ratio was called normalized outgoing connectivity rate.

We distinguished between the ictal (pathological, P) and non-ictal (normal, N) electrodes. This kind of grouping gave four possible connections according the ictal or non-ictal feature of the stimulated and recorded electrodes. In this way we could map the connectivity when the stimulated area was ictal, and the recorded electrode was ictal (PP), or non-ictal (PN), and the opposite: where the stimulated electrode was non-ictal, and the recording was ictal (NP) or non-ictal (NN).

I calculated the connectivity rate for these four cases in seven distance bins (0-10 mm, 10-20 mm, 20-30 mm, 30-40 mm, 40-60 mm, 60-80 mm, 80-∞ mm), with A1, A2 for 3SD and 6SD threshold.

DOI:10.15774/PPKE.ITK.2016.004

For the electrode level connectivity analyses I created symmetric connectivity matrices filled with the significant events (binary, directed graph) or the z-scores (weighted, directed graph) of the evoked potential. As each stimulation was applied on two electrodes at the same time, I had to duplicate the results of every stimulation to create a symmetrical matrix. With the 3SD or 6SD threshold, I could binarize this connectivity matrix.

From this I could calculate the path length of the electrode level graph. The characteristic path length is the average shortest path length in the network, calculated as the global mean of the distance matrix, including distances on the main diagonal. The path length was calculated with the Brain Connectivity Toolbox by Olaf Sporns & Mika Rubinov [200] on the NN and PP cases since these were symmetrical matrices. For the path length on the cross cases like NP and PN, I had to modify the calculation because these were asymmetrical matrices since there were less ictal electrodes, than non-ictal electrodes. To achieve the cross path length, I calculated the distance matrix from the original electrode connectivity matrix, and then averaged the only submatrix where the stimulated electrodes were ictal, and the recordings were non-ictal, and vica versa.

DOI:10.15774/PPKE.ITK.2016.004

3.3 RIPPLE DETECTION

Our research group developed a Matlab (MATLAB, Natick, MA) script package, called NSWIEW [4] , which facilitates the handling of different kind of ECoG and local field potential (LFP) data and analysis. The advantage of this script package is the graceful rapid memory management approach which can handle large, even GB (gigabyte) size data, because it reads in only 10-100 seconds long data at one time, depending on the user's purpose. On the other hand, this feature demand carefully through-out mathematical calculations, which had to be taken into account in the implementation of any method especially in the ripple detection.

From the literature we can assume, that ripple detection efficacy always depends on some kind of threshold or even a mixture of thresholds. Results from each automatic method are compared to the visual inspection of an expert reviser. My aim was to design a tool (Aim 2/a), that can facilitate ripple detection alloying the hints of an automatic detector and the experience of the trained reviser.

3.3.1 SEMI-AUTOMATED RIPPLE & PUTATIVE RIPPLE DETECTION METHOD

According to the literature, it is still not obvious what a ripple, fast ripple or high frequency oscillation is. However, we can say that these kind of events should be short (80-100 ms in the case of ripple and 30-50 ms, in the case of fast ripples), 80-500 Hz oscillations distinctively standing out from the background activity [201].

For ripple detection, we applied the method described in Staba's article [88] with some modifications. The original method uses the root mean square (RMS) of the band-pass filtered (80-500 Hz) signal to detect high frequency oscillation (HFO) events. Successive RMS values greater than 5 SD above the overall mean RMS value during minimum of 6 ms marked as putative HFO events with an additional criterion of containing at least 6 peaks that were greater than 3 SD above the mean value of the rectified band-pass signal and 10 ms time limit between different putative events were also applied. Figure 11 shows the applied method details, shaded boxes sign where our interpretation differ from the original (blue sign for the modifications which was necessary because of our data handling technique and green sign where I intentionally used other parameter than in the originally method - lower, 3*SD+mean threshold). More details can be found in the following session.

As mentioned earlier, our Matlab software, NSWIEW handles the data by dividing it into smaller (e.g. 10 s long) data therefore we had to apply modifications in the mean and standard deviation calculations.

DOI:10.15774/PPKE.ITK.2016.004

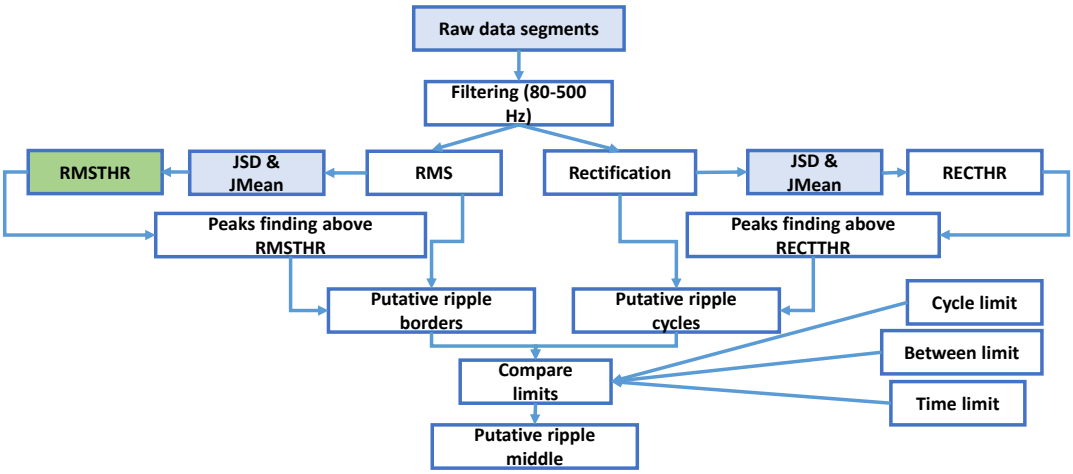

Figure 11. Description of the ripple detection method pipeline. Ripple identifying steps according to the Staba criteria [88]. The root mean square (RMS) of the band-pass filtered (80-500 Hz) signal to detect high frequency oscillation (HFO) events. Successive RMS values greater than 5 SD above the overall mean RMS value during minimum of 6 ms marked as putative HFO events. Additional criterion of containing at least 6 peaks that were greater than 3 SD above the mean value of the rectified band-pass signal and 10 ms time limit between different putative events were also applied. The blue shaded boxes sign where our methods needed some modifications and the green shaded box signs where I used lower threshold than the original.

3.3.1.1 Baseline activity calculation

First, we had to calculate the standard deviation of the 80-500 Hz bandpass filtered (2nd-order Butterworth), rectified data (RECTFdata) and Root Mean Squared (RMS) filtered data (RMSFdata) from smaller data parts for all channels on the whole data. The Root Mean Square calculation described in equation (5):

$$RMS(x_{i,i=n/2}) = \sqrt{\frac{1}{n}(x_1^2 + x_2^2 + x_3^2 + \cdots + x_n^2)} \qquad (5)$$

$$x_1, x_2, \ldots, x_n \; are \; the \; datapoints \; of \; the \; filtered \; data \; in \; the \; window$$

From the smaller (not necessarily equal long) RMSFdata or RECTFdata parts, we calculated the joint standard deviation (JSD) and joint mean (JM) for all channels, described in equations below. In equation (6) D contains N data points (the whole data e. g. 10 minutes long), where we would like to find high frequency oscillatory events, and $d_i - s$ are the smaller parts with m_i length. The Joint Mean (8) is the sum of the length weighted means of the smaller parts divided by the total length. The Joint Standard Deviation (10) is the square root of the sum of the variance of the smaller parts and var^* (9) (which is the length weighted sum of the difference between the means of the smaller parts and the Joint Mean), divided by $N - 1$. The variance of the small parts is calculated as described in equation (11).

$$D = [d_1, d_2, \ldots, d_M]; \qquad (6)$$

$$where \; every \; d_i \; is \; one \; smaller \; data \; part \; and$$

DOI:10.15774/PPKE.ITK.2016.004

$$m_i \; is \; the \; length \; of \; d_i$$

$$N = \sum_{i=1}^{M} m_i \tag{7}$$

$$Joint\ Mean(D) = \sum_{i=1}^{M} \frac{mean(d_i) * m_i}{N} \tag{8}$$

$$var^* = \sum_{i=1}^{M} [mean(d_i) - Joint\ Mean(D)]^2 * m_i \tag{9}$$

$$Joint\ Standard\ Deviation\ (D) = \sqrt{\frac{var(d_1) + var(d_2) + \cdots + var(d_M) + var^*}{N - 1}} \tag{10}$$

$$var(d_i) = \frac{1}{m_i - 1} \sum_{e=1}^{m_i} |d_{i_e} - mean(d_i)|^2 \tag{11}$$

The calculation of Joint Standard Deviation and Joint Mean of RMSFdata and RECTFdata aims to assess the baseline activity. The baseline activity could change in longer data, and the baseline calculation from the whole recording causing low sensitivity rate [131], because the HFO activity involved to the baseline activity calculation. We usually selected 5 minutes or longer data sections from sleep recording, where the baseline activity was quasi stable to avoid baseline fluctuations

3.3.1.2 Putative ripple event selection

My aim was to design a detection method that finds all putative events with high sensitivity even with relatively poor specificity with an option that allows the user to review the events and decide about the their validity based on the hints specified by the program. Therefore I used a lower threshold (3 SD) than did the method (5 SD) described by Staba [88] and made an application which shows several features of the events.

The first step is to specify the threshold for RMSFdata (RMSTHR) and for RECTFdata (RECTTHR), with the calculated JSD and JM. To adjust higher sensitivity, we set RMSTHR= 3 * JSD(RMSFdata) + JM(RMSFdata) and RECTTHR=3 * JSD(RECTFdata) + JM (RECTFdata). The beginning of a putative ripple (PR) event is where the RMSFdata exceeded the threshold value (first green circle on the RMSFdata on Figure 12/A). The time point at which the RMSFdata falls behind the RMSTHR is the end of the PR event (last green circle on the RMSFdata on Figure 12/A), and the middle point is the half-length between the beginning and the end point (middle green circle on the RMSFdata on Figure 12/A). Events

DOI:10.15774/PPKE.ITK.2016.004

with shorter than 6 ms duration or less than 6 RECTFdata peaks above RECTTHR were automatically rejected and events closer than 10 ms were combined.

With the aim to characterize the detected PRs after the automatic detection, we calculated several values, as duration length D (difference between the end point and the begin point in milliseconds illustrated on Figure 12/A, horizontal blue line); rectified peak number (the peaks on the RECTFdata above the RECTTHR, the numbers of the green circles in the pink box of Figure 12/B); and the normalized maximum amplitude (A) on the RMSFdata (illustrated by the vertical blue line on Figure 12/A).

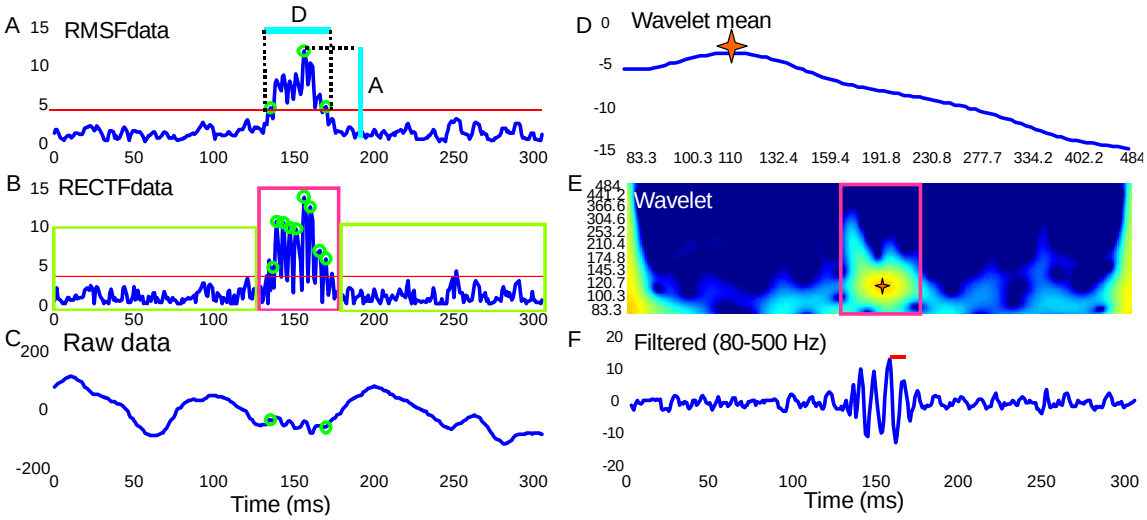

Figure 12. Feature description to characterize the putative ripples. A) The root mean squared, filtered (80-500 Hz) putative ripple – visualization of RMSFdata, with its 3*SD+mean threshold (red line). Green circles illustrate the beginning, the middle and the end of the ripple event, A signs the amplitude and D the duration of the event. B) The rectified, filtered putative ripple data – RECTFdata, with its 3*SD+mean threshold (red line). The Rectified Peak Ratio (RPR) is calculated from the sum of the peak amplitudes in the green boxes in ratio of the sum of the peak amplitudes in the pink box. C) Raw data. D) Wavelet mean calculated from the data in pink box on E. Orange star signs the highest amplitude frequency which characterize the main frequency. E) Wavelet of the putative event. F) Filtered (80-500 Hz) event.

To describe the relationship between the PR and its surrounding area, Rectified Peak Ratio (RPR) was calculated around every PR in a 300 ms window (-150 to +150 ms) as follows. The sum of peak amplitudes on the RECTFdata were calculated around the PR in a 50 ms window (in the pink box on Figure 12/B) and were proportioned to the sum of the peak amplitudes in the -150 to -25 and +25 to +150 ms range (in the green boxes on Figure 12/B). We formed a sorting number without expansion from the multiplication of RPR, the duration (D) and the amplitude (A) of the PR (RPRDA).

The frequency of the event was calculated with wavelet transformation (Figure 12/E). The wavelet coefficient matrix was averaged in a 50 ms window around the PR middle point (pink box on Figure 12/E). For detailed description of wavelet transformation see Materials & Methods - 3.4.2.2 - Cross Frequency Coupling (CFC). On this average curve, the maximal peak indicated the frequency of the PR event (orange star on Figure 12/D). Instant maximum,

DOI:10.15774/PPKE.ITK.2016.004

minimum and average frequency were also calculated from the peak numbers of the rectified, filtered data during the PR event.

3.3.1.3 Visual revision

The putative ripples were then plotted with a specific viewer. A sign was given to those satisfying the Staba criteria and the reviser could see the raw, the filtered, the Root Mean Squared filtered, the rectified filtered and the wavelet transformed data around the middle of the PR event within a 300 ms window.

With this viewer, the reviser could accept and reject the putative ripple events as ripple events. The interface show the filtered waveform, the scales from 80 to 500 Hz of the Morlet wavelet based continuous wavelet transformation of the unfiltered data, the filtered rectified waveform indicating significant peaks over RECTTHR threshold and the RMSFdata signal with the beginning, the middle and the end of the event. After the revision, the accepted events were indicated as ripples.

The time requirement of the visual revision mainly depends on the experience of the reviser, the decision time on average is 1 s per event.

After the ripple analysis and revision, we have information about the distribution in time and space, the frequency domain and occurrence probability of the ripples.

3.3.2 VISUALIZATION ON 3D BRAIN - AIM 3

Our group (with the cooperation with NSLIJ) developed a Brain Visualization Tool (BVT) in order to facilitate the interpretation of the ripples or any kind of events, like interictal spikes, evoked potentials, functional responses or seizures originating from the brain. As part of NSLIJ and NICN co-operational research program, we developed a method to visualize the electrodes and present them on the brain surface. Details were described previously in Methods-CCEP- Brain surface reconstruction and electrode localization [3, 176].

The BVT could import files (txt, xls) with which the user can change the colour and the form of the electrodes according to the features of the desired phenomenon like ratio of the ripples, spikes per minute or the seizure propagation. The program package allows the user to rotate and set the appropriate view of the brain, and then make snapshots from it.

DOI:10.15774/PPKE.ITK.2016.004

3.4 CHEP - EVOKED HIGH FREQUENCY ACTIVITY

With a special kind of experimental setup, we can elicit potentials from the human hippocampus by electrical stimulation of the temporal cortex. We named these events cortico-hippocampal evoked potentials (CHEP). My aims were (Aim 2/b) to develop algorithms for evoked high frequency oscillation (HFO) detection and analysis, characterize the overall variability of evoked potentials and evoked high frequency activity (HFA) of hippocampus in anaesthetized condition. The analysis and the details are described in the following parts.

3.4.1 THE HIPPOCAMPAL RECORDING TECHNIQUE

3.4.1.1 Patients & data

The intrahippocampal recordings were performed before the anterior temporal lobectomy of medically intractable mTLE patients with unilateral seizure starting, after video-EEG monitoring procedure. The seizure onset zone identifying procedure was done in the Epilepsy Centre of the National Psychiatry and Neurological Institution (2004-2007), the electrode implantations and the surgery were done in the National Institution of Clinical Neurosciences (NICN). Eight patients were enrolled in this study (for details see Chapter 9.-Appendix Table 1.), all of them were consented and informed of the risks of this intervention. The permission to the experimental process was given from the Hungarian Medical Research Council, in accordance with the Declaration of Helsinki.

3.4.1.2 Electrode description

The used multielectrode (ME) has been mentioned and described previously [191, 192, 202]. This electrode has originally been developed to record the electrical activity from the layers of the neocortex (Figure 13/B). As it is not applicable for hippocampal recordings, our research group designed a deep multielectrode (dME) to record from the internal brain structures. The 24 contacted dME (linearly arranged contacts, Ø: 25μm, Platinum-Iridium wires, 100 μm or 200 μm centre to centre distance, first contact is 5 mm far from the tip) is a 10 centimetres long, 350 μm diameter, stainless steel needle (Figure 13/A).

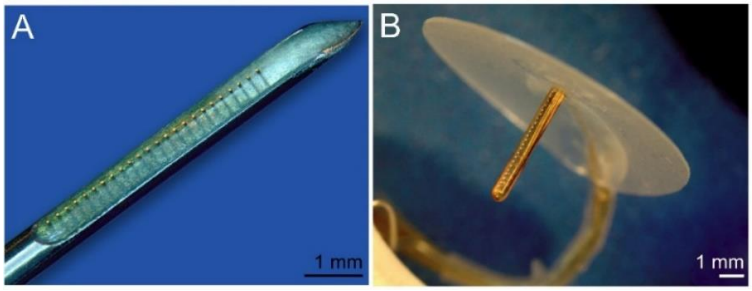

Figure 13. Microelectrodes used in our studies. (A) Laminar microelectrode for hippocampal intraoperative recordings (Source of the picture:* 5) (B) Thumbtack microelectrode for long-term recordings from the layers of the neocortex (Source of the picture: * 6).

DOI:10.15774/PPKE.ITK.2016.004

3.4.1.3 Surgery, electrode insertion, recording details, cortical stimulation and histology description

The technique was previously described in [4, 191, 203]. With the aim of preserving the temporal input pathways of the hippocampus, the lateral medial temporal structures should remain intact. To carry this out, the tip of the multielectrode was positioned to the surface of the hippocampus through a small cut of the lateral ventricle and slowly slipped into the brain tissue with 2-4 mm increments. The dMEs insertion was done by a precision hydraulic micro-manipulator with approximately 200 μm/sec speed, which minimalized the traumatic effect of the dME. The micro-manipulator structure gave the opportunity to hold one or two dME, in some cases, two parallel electrodes were inserted with 6 mm distance.

The field potential gradient recording was continuous during the insertion and the extraction of the electrode. The recordings were taken with custom made equipment, described previously. [191, 203]. The signal was recorded simultaneously, being filtered between 0.1-500 Hz, sampled at 2 kHz/channel with 16 bit precision; and filtered between 150 Hz-5000 Hz, 20 kHz/channel on 12 bit.

An eight contacted clinical strip electrode (Ad-Tech Medical Instrument Corporation, Racine, USA) was placed around the temporal pole regions, to explore the temporal neocortical spiking activity. Through the adjacent electrode contact sites, we applied low frequency (0.5 Hz, 5-10-15 mA, 0.2 ms pulse duration, 25 or 50 stimuli) stimulation to elicit evoked potentials from the hippocampus, and high frequency (50 Hz, 10-15 mA, 0.2 ms pulse duration, 100 stimuli) electrical stimulation to discharges evoked on the neocortex. Figure 14 illustrates the typical strip electrode arrangement. We measured the electrode distance from the pole of the temporal lobe. We agreed to sign the distance in the lateral direction as negative from the pole while positive as the electrode approach the medial, inner part of the temporal lobe.

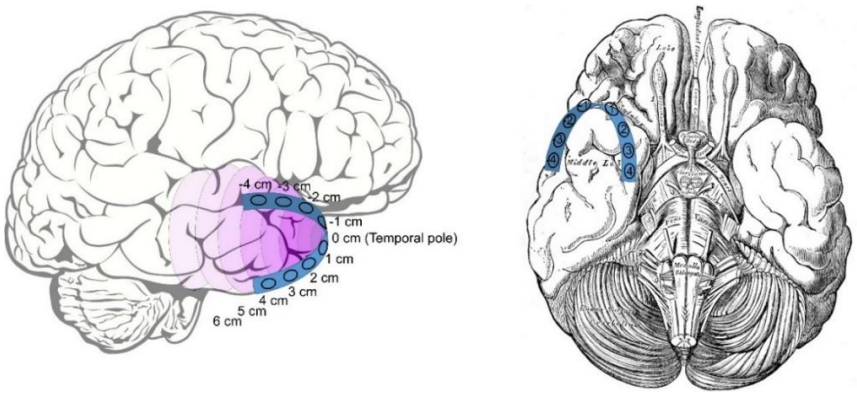

Figure 14. Typical stimulating strip electrode position. The 8 contacted strip electrode reaches the inner part of the temporal lobe, near to the hippocampus. The distance were measured from the temporal pole, negative signs the lateral and positive signs the medial direction. Source of images: * 7, * 8.

DOI:10.15774/PPKE.ITK.2016.004

After the stimulations, the Hippocampal formation and the Entorhinal Cortex was removed “en-bloc” for histological processing.

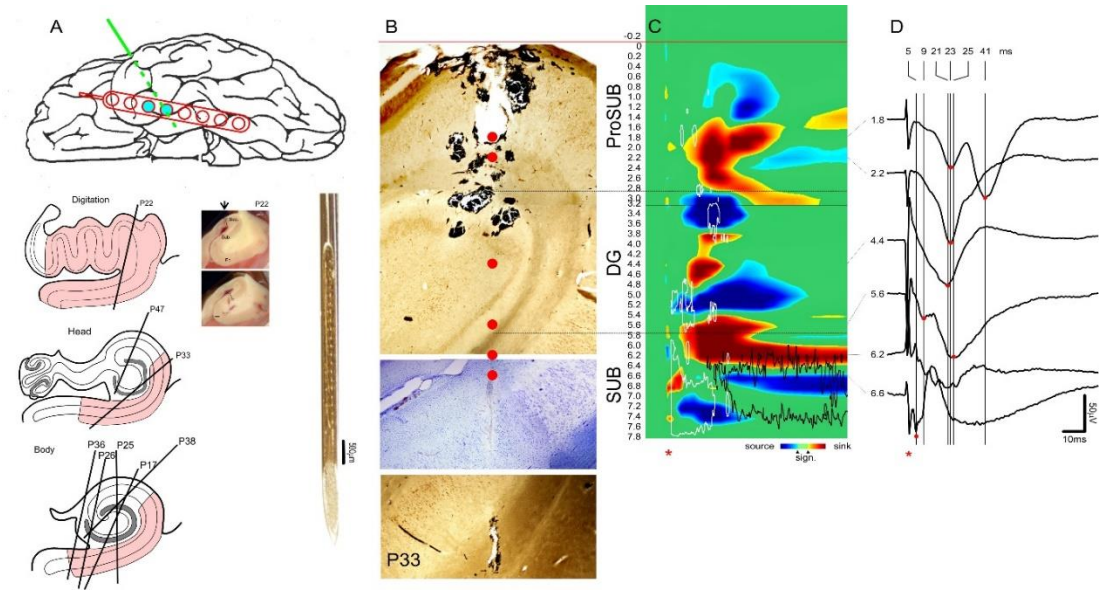

Figure 15. Visualization of the recording situation [4, 203]. A) Schematic drawing of the strip position around the temporal pole, microelectrode positions in the hippocampus and a picture of the microelectrode. The shaded electrodes of the temporo basal strip served for stimulation. Lower panel left: schematic drawing of the hippocampal formation and the subiculum (shaded pink),Black lines: the trajectory of the electrodes and block photo of P22 B) Photo of the hippocampal slice from P33, where the red line sign the surface of the hippocampus, and the red dots show the electrode penetration track and P33 histological reconstruction is shown. The electrode trajectory in the tissue. GluR2-3 immunhistochemistry, and Nissle staining. C) CSD, and MUA map of evoked potential (15mA stim.). Red: sink, blue: source, white contour: MUA increase, black contour: MUA decrease. D) The order of the sinks in different depth indicating the peak latencies. Dashed line: border between regions. Red line: ependymal surface, Asterix: stimulus, CSD: current source density, MUA multiple unit activity, SUB: subiculum, DG: dentate gyrus, ProSub: prosubiculum. Sub I: proximal part of the Subiculum, Sub II: distal part of the subiculum.

The histology verified the electrode penetration, and the affected Hippocampal structures. This work was taken by Zsófia Maglóczky and Lucia Wittner [204].

The penetration of the electrode was identified by light microscopic examination, and later on it was reconstructed from multiple stained sections and analysed in digital picture editing software [4] (Figure 15).

Figure 16 illustrates the regions of hippocampus and the subiculum as we used it in the following analyses. DG is the abbreviation of Gyrus Dentatus, CA3-2-1 are the parts of the Cornu Ammonis. The subiculum could be separated into Pro subiculum (Pro Sub), subiculum (with two part: Proximal subiculum- Prox Sub and Distal subiculum- Dist Sub) and Pre subiculum (Pre Sub).

DOI:10.15774/PPKE.ITK.2016.004

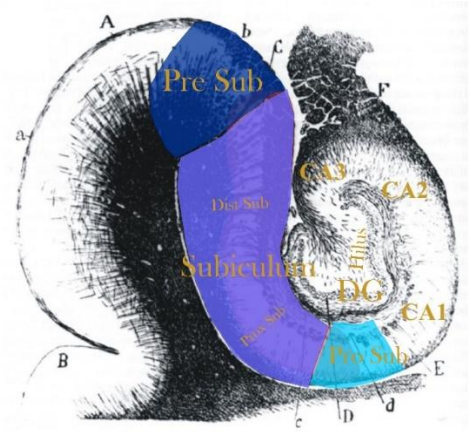

Figure 16. Subregions of the hippocampus and the subiculum. The parts of hippocampus are DG-Gyrus Dentatus, CA3-2-1, the parts of subiculum are Pro Sub-Pro subiculum, Prox Sub-Proximal subiculum, Dist Sub- Distal subiculum, Pre Sub-Pre subiculum. Source of the original picture: * 9.

3.4.2 DATA ANALYSIS

To describe these evoked potential features, we had to apply different kinds of analysis techniques. We wanted to take a closer look at the waveforms, frequency components, spatial presence and the evokability of events.

Thus we analysed the data in the Edit module of Neuroscan (Neuroscan Inc.) and in Matlab (Mathworks Inc.). We used free accessible, open source Matlab packages, like EEGLAB [205] and Fieldtrip (Donders Institute for Brain, Cognition and Behaviour and the Max Planck Institute in Nijmegen), and the previously described [4] script package developed by our laboratory and self-written Matlab scripts.

Our software called NSWIEW [4], can handle different kind of data, like Neuroscan (.cnt, .avg), Brainquick (.trc), Windaqui (.wdq), Brain Vision (.vhdr), and has a lot of useful built in methods and features. One of these is the previously mentioned feature that only smaller parts of the data are imported in the Matlab workspace at one time, so it can handle great amount of data.

3.4.2.1 Data preparation

The surgical technique allowing us to record from the human hippocampus in vivo results in some peculiar tasks to handle. One of these is the electrode slow slipping, which originates from the inertia of the supporting structure. This sliding is not consistent, so the Hippocampal layer recognition, and the analysis became quite complicated. To solve this, we improved a calculation to define the shifting value, which was based on that presumption that the spike like waveform generation is stable in the cell layers. We determined the spike generating layers with CSD, the movement of this source in the time and with linear regression alignment, we could calculate the mm/ms value of the sliding.

DOI:10.15774/PPKE.ITK.2016.004

In the analysis we only used recordings, where the slipping was less than one channel between the beginning and the end of the session. To avoid the probable side effects of the stimulation artefact caused by filtering [206], we replaced it with spline interpolation -4 ms to 4 ms around the artefact transient.

3.4.2.2 Evoked potential analysis

With the aim to thoroughly describe the character of the evoked potentials, we calculated the amplitude, latency, duration, evokability and frequency properties, and arranged them in order of the stimulation features (distance from the temporal pole and stimulation strength) and the hippocampal regions.

Amplitude

For the analysis of the evoked responses, we improved the automated method. Figure 17 explains the steps of the analysis regarding to the channels in the hippocampal layers. Around every stimulation (25-50 occasionally) in a -500 +500 ms window, the hippocampal local field potential data is filtered between 40-500 Hz (2nd-order Butterworth) (Figure 17 /C middle box) for evoked high frequency activity (EHFA) and between 500-5000 Hz (3rd order Butterworth) for multiple unit activity (MUA) from the 20 kHz sampled recordings. After the filtering, Root Mean Square (RMS) calculation was applied in an 11 ms window, 5 times (Figure 17 /C lower box). We assume the RMS of the MUA value corresponds to the action potential summation of the surrounding neurons [207].

From the RMS data, the maximal amplitude between +10 to +100 ms after stimulation (the assumed middle of the evoked potential) is measured and converted to statistical z-score value using the mean and standard deviation of the baseline (-450 ms to -50 ms before the stimulation). The z-score calculation is based on the equation (1), where z is the calculated z-score value, x is the value of the maximum amplitude of the RMS curve between +10 to +100 ms after stimulation, μ is the mean and σ is the standard deviation of the Root Mean Squared, filtered data of the baseline (between -450 ms to -50 ms before the stimulation artefact).

The z-score amplitude values for EHFA after every stimulation on every channels in this special case are colour coded and plotted on Figure 17 /D. The distribution of the z-score values for EHFA (black) and MUA (light blue) are plotted on the boxplots on Figure 17 /E.

DOI:10.15774/PPKE.ITK.2016.004

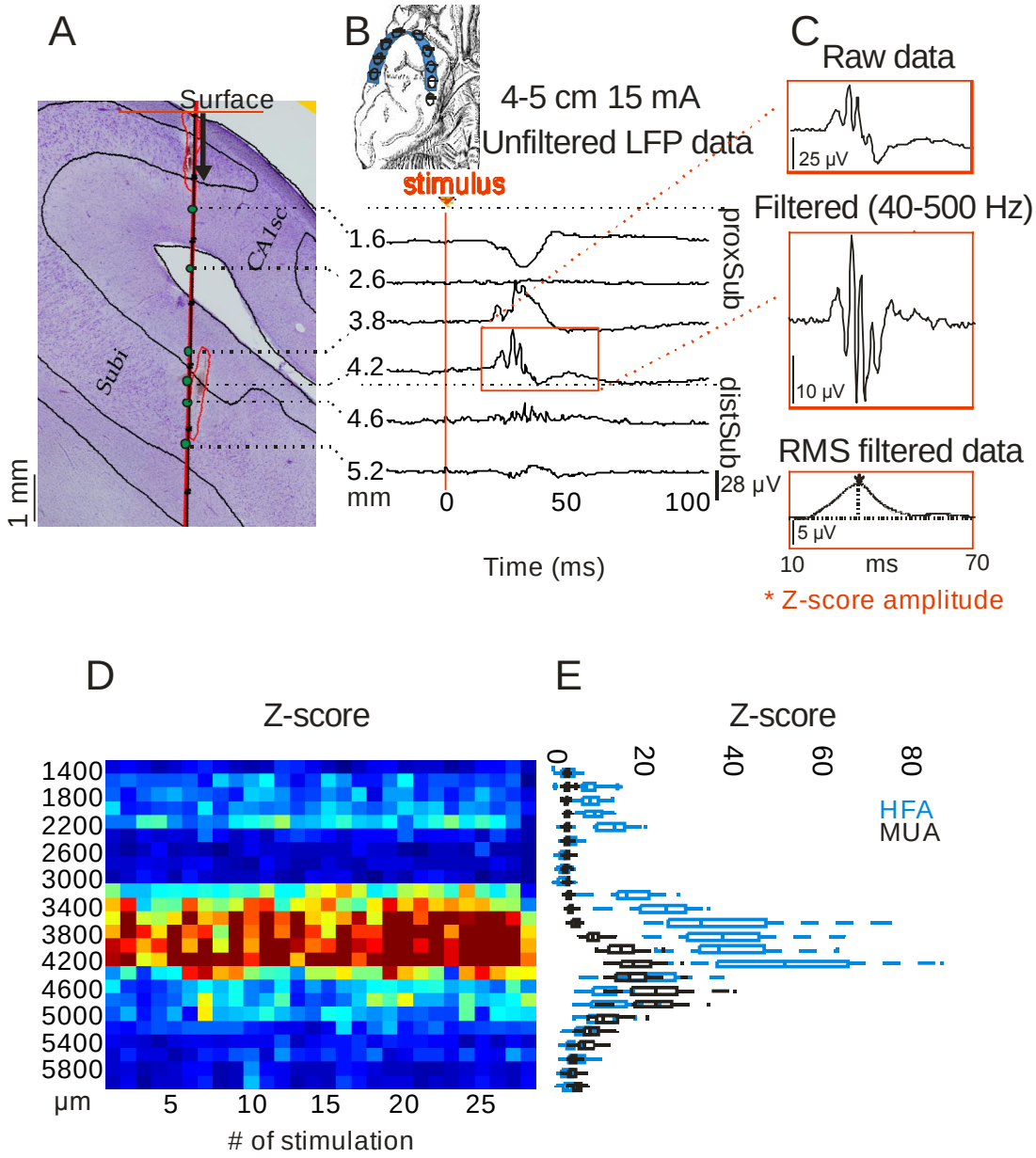

Figure 17. Sample of a Hippocampus slice and recorded evoked potential from Pt22. A) Histology indicates Subiculum (Subi) and CA1sc subregions. B) Local field potential gradients originate from the green electrode contacts. Bottom view of temporal lobe with illustration of current stimulation point. Source of picture: * 8. Data in the red box analysed in the magnified red boxes in C. The red vertical line indicates the time point of the stimulation. C) Illustration of the evoked potential analysis. The raw event is on the top, the bandpass filtered form is in the middle and the RMS of it is on the bottom, where the red dot shows the maximal value, which we take as the middle of the evoked activity. This maximal values are converted into z-scores and plotted on D. D) The z-score of the EHFA after every stimulation is color coded and plotted. E) Laminar profile of the z-score value distribution of EHFA (blue) and MUA (black).

As a comprehensive exemplification, z-score amplitude distribution histograms were made from the amplitude after all stimulations from all channels regardless to the stimulation arrangements or the hippocampal area. In this distribution, density function fitting was calculated with several Matlab built in distributions (Birnbaum-Saunders, Exponential, Extreme value, Gamma, Generalized extreme value, Generalized Pareto, Inverse Gaussian, Logistic, Loglogistic, Lognormal, Nakagami, Normal, Rayleigh, Rician, t location-scale,

DOI:10.15774/PPKE.ITK.2016.004

Weibull, Nonparametric kernel-smoothing). To illustrate the amplitude dispersion of all the evoked events, empirical cumulative distribution function was calculated.

Event differentiation

Based on the findings in the literature [208], we assumed that the evoked potentials would be similar to the well-known ripples. In our first approach, we differentiated the events according to their amplitudes.

Evoked high frequency activity (EHFA)

We hypothesized that the stimulations evoked putative ripple events therefore we applied 5 z-score threshold on the filtered (40-500Hz) and Root Mean Squared data, similar to the method described by Staba [88] to determine the significant evoked high frequency activity (EHFA).

Evoked ripple (HFO, EHFO)

A simple amplitude threshold does not characterize the evoked events well, hence we employed a stricter discrimination. Two expert researchers revised the evoked potentials with the RST (Ripple Selection Tool, See Material & Methods - 3.3.1 Semi-automated ripple & putative ripple detection method) and selected events from every stimulation session, where the 40-500 Hz bandpass filtered evoked high frequency activity were similar to the ripple oscillations with at least 4 cycle described previously in the literature. We described these evoked activities as evoked ripples. Initially, we intended to evaluate the frequency of these selected ripple events. Figure 18/A shows two examples of the evoked ripples, and Figure 18/B specifies several other events excluded from the frequency analyses.

Timing and duration

After the selection, we collected the peak latencies of the evoked ripples, by picking the highest peak on the Root Mean Squared, filtered (40-500 Hz) data after the stimulation 10-100 ms. The duration of an evoked ripple was the period of time while the RMS curve exceeded the half amplitude of the evoked potential.

Frequency

We have several options to measure the frequency distribution of evoked potentials. The most common way to determine the frequency components of a time signal is the Fast Fourier Transformation, but this method does not give us information about the change of the frequency components in time. Time-frequency distributions offer insight into the modification of the frequency components within a time window. We used two kinds of time-frequency transformations. In order to have a precise description of the stimulation dependent frequency component, we applied an Event-Related Spectral Perturbation (ERSP), and to the

DOI:10.15774/PPKE.ITK.2016.004

examination of the interaction of frequencies, we calculated cross-frequency couplings with wavelet transformation.

Event related spectral perturbation (ERSP)

The frequency components of the evoked events were measured with event-related spectral perturbation (ERSP from EEGLAB [205, 209]) in a -150 ms to +150 ms window around the stimulation. Briefly, the ERSP technique uses a bootstrap algorithm to calculate the spectral perturbation before an event. This method indicates the significant changes during and after the event. Our baseline for ERSP was -150 ms to -50 ms before the stimulation and the event related spectral change was calculated between 15.6 Hz- 500 Hz. The highest peak on the time averaged ERSP after the stimulation in 10-100 ms was taken as the middle of the evoked activity. The maximal ERSP coefficients in every frequency bin around the peak of the evoked event in a -25 ms, +25 ms time window characterize the frequency components of the evoked activity. The ERSP of one selected event is plotted on Figure 18/C. The maximum amplitude frequencies across the vertical axis in the depicted time window are plotted with blue curve on where we identified the frequency peaks with the largest power as primary frequency (signed with one white star on Figure 18/C) and lower peaks as secondary frequencies for every events (signed with two and three white stars on Figure 18/C).

Frequency distribution

To get an overview of the typical frequency components, distribution histograms were made from the primary and the secondary frequencies of all the events (evoked) by sorting data into bins from 20 Hz to 650 Hz in steps of 10 Hz. Gauss fitting was calculated on these distributions by using a built in Matlab method to determine the mean and the standard deviation.

DOI:10.15774/PPKE.ITK.2016.004

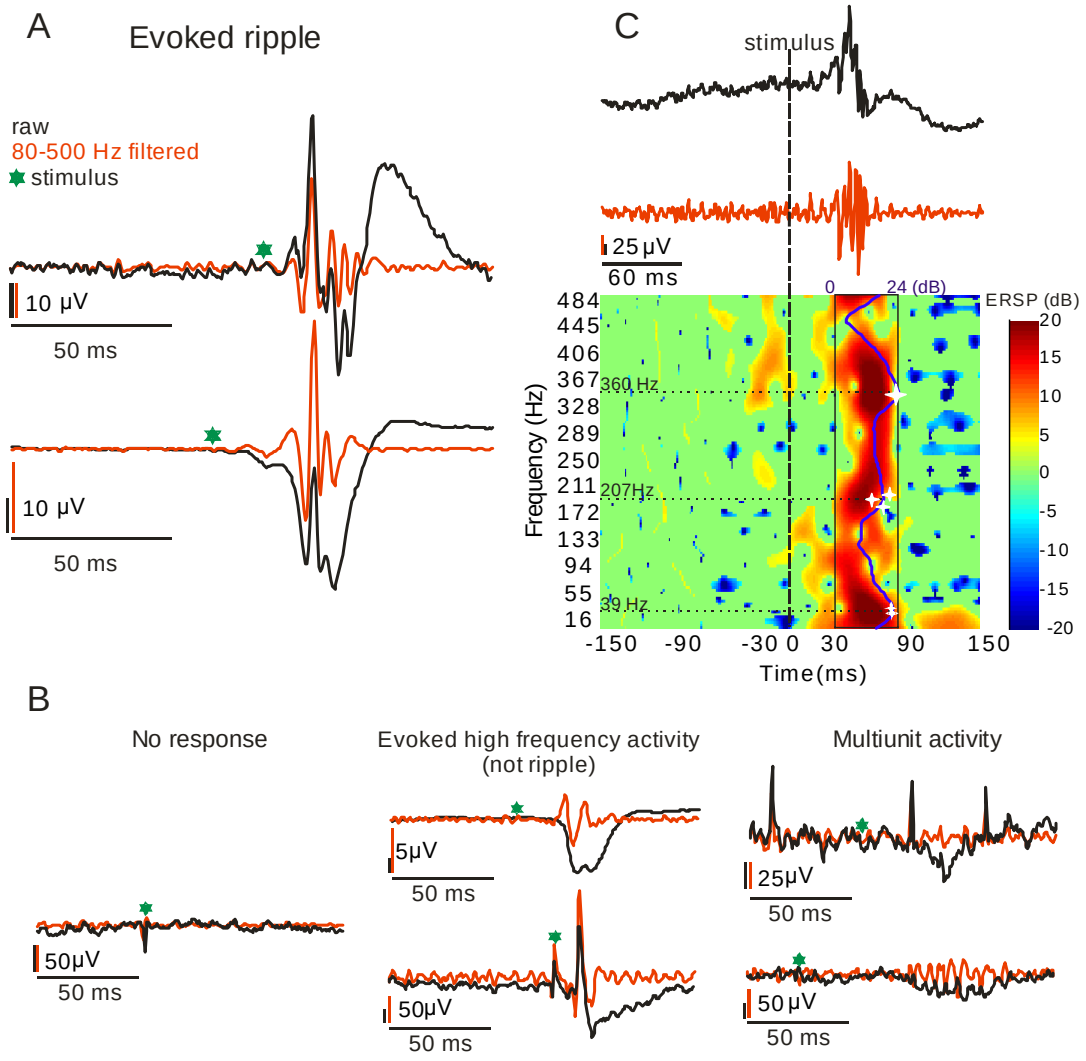

Figure 18. Selection and elimination of evoked high frequency oscillation and illustration of the method for analysis of the frequency components. A) Visually selected evoked potentials identified as ripple, black line signs the raw data, red line signs the 80-500 Hz filtered data and green star signs the time of the stimulation. B) Examples of excluded events, like no response, evoked high frequency activity and multiple unit activity. C) Illustration of the ERSP of the event on the top (black line). The blue line stands for the maximal amplitude frequency component curve, whereas the white stars and the dotted lines sign the maximal values (360 Hz, 39 Hz, 207 Hz).

Cross Frequency Coupling (CFC)

To measure the interaction between frequency components, cross frequency coupling was calculated from all events of one stimulation session. The phase-amplitude coupling (PAC) was determined with calculating the modulation index (MI) (based on the work of Tort and colleagues [210]), which characterizes the strength of the phase-amplitude coupling between two frequencies. The MI value quantifies the phase-amplitude coupling by measuring the distance of the phase-amplitude histogram of two given frequencies from the uniform distribution by means of Kullback-Leibler divergence. Tort's original method applied the Hilbert transformation on filtered signal to get the phase information of one frequency and the amplitude from another filtered signal envelope. Instead of this, PAC values were calculated

DOI:10.15774/PPKE.ITK.2016.004

from the complex Morlet wavelet of the 10-100 ms data after every stimulation from one session.

Wavelet calculation

We have chosen wavelet transformation [211] to measure the changes of frequency components of the evoked potentials. This analysis is especially suitable to represent transient (non-periodic signal with finite-time and relative large finite-energy) waveforms. The Fourier Transformation is not capable to give information of the time component as its basic functions are sine and cosine (12),

$$e^{-j\omega t} = \cos(\omega t) + j\sin(\omega t) \quad (12)$$

being continuous on the range of]-∞, ∞[, and we could not find a part of this interval where this basis function is zero. In contrast, the basis function of the wavelet transformation are localized functions, wavelets that are shifted and compressed (scaled) as variations of a basic wavelet called the mother wavelet. We can choose several mother wavelets that must satisfy the condition listed below (13):

$$\int_{-\infty}^{\infty} \psi(t)dt = 0 \quad (13)$$

where ψ(t) is the mother wavelet function. This condition provides that the wavelet function is becoming zero on the limits of]-∞, ∞[, and we can find a part interval where this is different from zero, which gives the information of the localization in time. In other words, we can choose any mother wavelet function (ψ(t)) if it satisfies the following condition (14):

$$\Psi(\omega) = 0, \qquad if\ \omega = 0 \quad (14)$$

where Ψ(ω) is the Fourier transformation of the mother wavelet function (ψ(t)). Various mother wavelets could gratify this condition, like Haar, Morlet, Mexican hat, etc.

The wavelet transformation uses any of these basis functions to correlate the original signal and obtain the magnitude of the component in the direction of the given basis function. With shifting (time information) and compressing (frequency information) the basis wavelet function, we can get the extent of the frequency component in a given time point of the original signal. Shifting and the compressing are not independent of each other, their calculation is performed depending on powers of a previously specified constant. If we compress the mother wavelet to half, we have to halve the shifting too. Consequently, the low frequency basis function results in poor time and good frequency resolution. In contrast, high frequency basis function leads to good time and weak frequency resolution. This feature will provide us uneven sampled frequency distribution in time.

DOI:10.15774/PPKE.ITK.2016.004

The result of the wavelet transformation largely depends on the proper selection of the basis function. The wavelet function should reflect the type of features present in the time series, therefore we expected that the waveforms of the evoked potentials in the Hippocampal formation will be greatly resembling to the ripple oscillations (described previously in Chapter 2.1.5 Sharp wave – ripple complexes). We have chosen Morlet wavelet because it is very similar to the signal what we are looking for: it is symmetric, complex, contains more oscillations than the Mexican hat, hence the wavelet power combines both positive and negative peaks into a single broad peak [212]. We used Morlet wavelet analysis developed by Christopher Torrence and Gilbert P. Combo. The illustration of the applied Morlet wavelet could be seen on Figure 19, and its exact equation (15) below it.

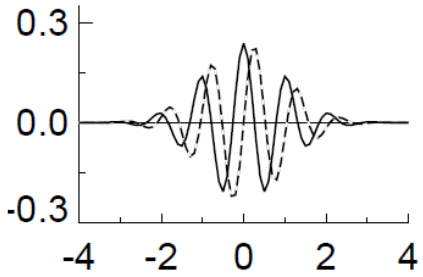

Figure 19. Illustration of the form of the Morlet wavelet (Ψ(η)) with the equation (15) below [212]

$$\Psi(\eta) = \pi^{\frac{-1}{4}} e^{i\omega\eta} e^{\frac{-\eta^2}{2}}, \qquad (15)$$

where ω is the non-dimensional frequency and η is a non-dimensional time parameter[212].

Phase-amplitude coupling

We calculated the phases and the corresponding amplitude values from the complex Morlet wavelet of the 10-100 ms data after each stimulation from one session. The phase-amplitude histograms were calculated on every possible frequency pairs from 11-968 Hz with 131 not evenly divided frequency bins. For the histograms, phases were discretized into 18 bins, followed by the calculation of the mean of the corresponding amplitudes. Finally, the Kullback-Leibler divergence between the resulted mean histogram and the uniform distribution yield the MI value for the given frequency pair. Since only the lower frequency can modulate the higher, phases were taken from the lower frequency and the amplitudes from the higher therefore the resulted MI values were organized into an upper triangle matrix (n= 8515, (131x131)/2). From area (CA, DG, SUB) averaged modulation index (MI) matrices, we determined the maximal MI value which designated one MI curve from the phase and one from the amplitude.

We took these frequency-MI curves as probability density functions, from which the mean and standard deviations were calculated. The frequencies within the mean in one standard deviation were considered as modulating (for phase) or modulated (for amplitude) frequencies.

DOI:10.15774/PPKE.ITK.2016.004

As we collected the MI matrices for all regions, we calculated paired t-tests ($p<0.001$) for significant modulating-modulated frequency pairs. The Bonferroni-correction was not applicable, since the elements of the MI matrices are not independent. However, considering, that each MI matrix consists of 8515 MI values, for $p<0.001$ the expected number of false positive tests is 8.5, which should be randomly scattered through the matrix. Thus, the modulation was considered to be significant, if the number of positive tests exceeded this expected number and they showed patterned distribution in the MI matrix.

Multiple Unit Activity (MUA)

We calculated multiple unit activity from the 20 kHz sampled data with bandpass filtering (3^{rd} order Butterworth) between 500 – 5000 Hz. After the filtering, we rectified and smoothed the data with Root Mean Square within an 11 ms window and we searched for the maximal value after the stimulation artefact 10 ms to 100 ms. Maximal MUA amplitudes were converted to z-score (using the same method as in EHFA case). This value is thought to be corresponding to the action potential summation of the surrounding neurons [207]. The laminar profile of the amplitude of the multiunit activity across channels was correlated to the amplitude of the evoked high frequency activity in all the used recordings.

DOI:10.15774/PPKE.ITK.2016.004

4 RESULTS

In this chapter, the results of applied analyses and methods are described as specified previously in Chapter 3 - Materials and Methods. I will highlight some problems and solutions which appeared during the improvement of the algorithms.

4.1 CCEP

4.1.1 PEAK DETECTION & AMPLITUDE DISTRIBUTION

We recorded consistent and statistically significant CCEPs in each of our patients implanted with subdural electrodes. With a 3SD threshold on average 34.17% (SD 15.51%) of A1 and 59.23% (SD 12.64%) of A2 potentials were significant, with a 6SD threshold 19.91% (SD 11.83%) of A1 and 28.65% (SD 13.28%) of A2 potentials were significant. The time delay from the stimulation artefact for the A1 peak ranged from 10.38 to 49.63 ms (median: 22.52 ms) with two major peaks at 14.72 ms and 34.40 ms. The A2 peaks timed between 50.41 to 499.75 ms (median: 168.00 ms) with two peaks at 60.49 ms and 132.20 ms. Figure 20 shows the time distributions of the A1 and A2 peaks and Figure 21 represents the amplitude (z-score) distribution of the two peaks.

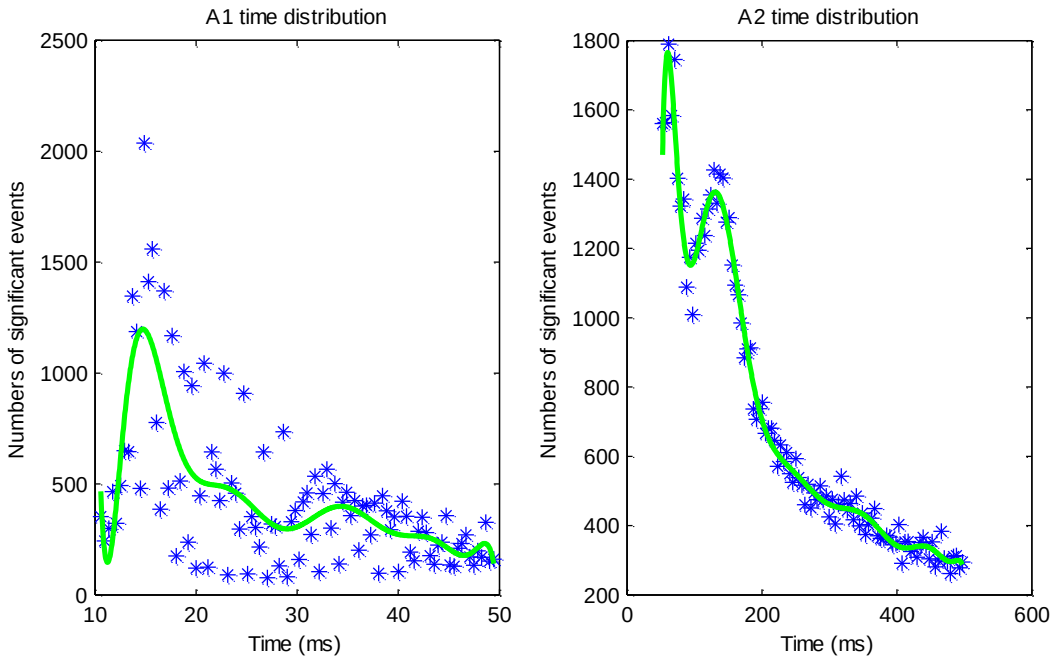

Figure 20. Time distribution of the A1 and A2 peak. On the left, the A1 component has a main peak around 14.72 ms, and on the right, A2 shows bimodal distribution with peak at 60.49 ms and 132.20 ms.

DOI:10.15774/PPKE.ITK.2016.004

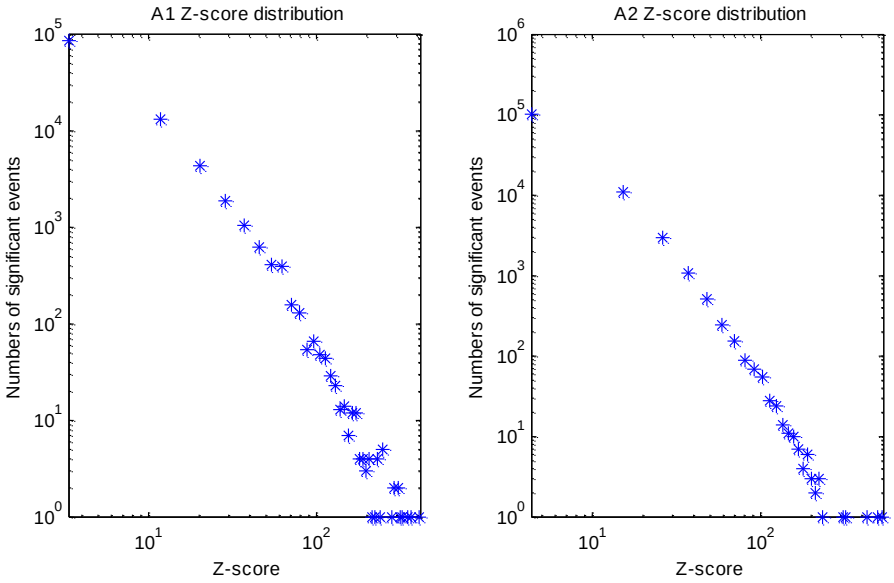

Figure 21. Amplitude (z-score) distribution of A1 and A2 on logarithmic scale. The distribution of A1 is similar to A2.

To investigate the reliability of the evoked potentials, we applied the same stimulation protocol through several days on the same patients. I computed the intra-subject reliability based on the 3SD threshold significant CCEP. CCEP maps recorded on 3 different days within a period of 5 days demonstrating greater than 70% similarity for A1 (70% between day 1 and 4, 71% between day 1 and 5 and 74% between day 4 and 5) and over 75% similarity for A2 (day1-day4: 75%, day1-day5: 76% and day4-day5: 77%).

4.1.2 Asymmetry of connections

The CCEP peak amplitudes were often found to be different on two electrodes depending on which the stimulated and which the recording one is. Namely, the stimulated-recorded electrode z-score was often greater in one direction than in the opposite direction. The asymmetry of A1 connections (if in one direction the amplitude exceeded 3SD) with 81% of connections showing greater than 50% difference and 88% showing greater than 30% difference in z-scores between directions. A similar profile was seen with the A2, with 73% of connections demonstrating greater than 50% difference and 82% demonstrating greater than 30% difference in z-scores between directions.

4.1.3 Connectivity analysis on the level of electrodes

4.1.3.1 Significant response number decrease with distance

The distance between the stimulated and the significant response elicited recording area were calculated using the shortest possible route between the midpoint of the two stimulated electrodes and the centre of the recording electrode regardless to the brain gyrification.

DOI:10.15774/PPKE.ITK.2016.004

In each stimulation series, I grouped the stimulated- recorded electrode pairs according to their distance into seven bins: 0-10 mm, 20-30 mm, 30-40 mm, 40-60 mm, 60-80 mm and 80-∞ mm. To compare the results between the patients, I normalized the average evoked significant potential numbers with the individual electrode numbers in the distance bins.

The normalized number of the CCEPs decreased with increasing the distance between stimulating and recording electrodes. We registered a statistically significant decrease between the 0-2 cm bin and the 8-∞ cm bin ($p<0.01$; ANOVA Kruskal-Wallis test).

4.1.3.2 Normalized connectivity on electrode level in accordance with the ictal (P), non-ictal (N) features

We distinguished the electrodes according to their location as ictal (electrodes in the area affected by seizures) and non-ictal (electrodes outside the areas involved in seizures) electrodes to see if there are any differences between the normal and pathological network properties.

Connectivity

The normalized outgoing connectivity rate between the non-ictal and ictal areas was grouped into seven distance bins (0-10, 10-20, 20-30, 30-40, 40-60, 60-80, 80+ mm) from both A1 and A2. Figure 22 shows the results with a 6SD significance threshold. In the boxplot the central mark is the median, the edges of the box are the 25th and 75th percentiles, the whiskers sign the most extreme data points not considered outliers, and outliers are plotted individually. The left panel shows the connectivity on the A1 peak, non-ictal – non-ictal (NN) coloured with green, ictal-ictal (PP) with red, non-ictal – ictal (NP) with yellow and ictal- non-ictal (PN) with pink. One can notice, that in the near field (0-40 mm) the PP shows higher connectivity rate than the NN, without significant difference. More distantly, this tendency turns out to the opposite and the NN shows higher connectivity than the PP. The red star above the 60-80 mm bin indicates that the non-ictal - non-ictal connectivity is significantly higher (Wilcoxon rank sum test, $p<0.05$) than the ictal-ictal. Interestingly the PN exhibits similar behaviour compared to the PP, except on the most distant, where the PN is higher than PP, and NN.

DOI:10.15774/PPKE.ITK.2016.004

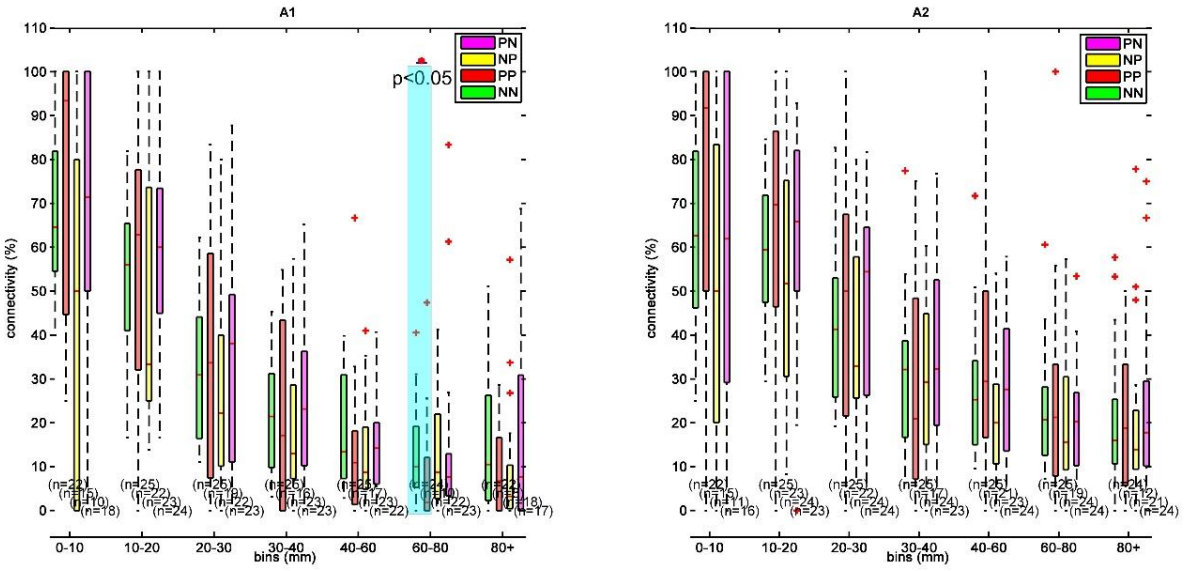

Figure 22. The normalized connectivity rate on the electrode level between the non-ictal (N) and ictal (P) electrodes grouped by distance bins for the A1 (left) and A2 (right) with **6SD** significance threshold. The n below the boxes indicates the patient number from the data originated. Red star and blue box shows the significant difference (Wilcoxon rank sum test, p<0.05) between the NN and the PP in the 60-80 mm range with the A1 component. The n below the boxes indicates the patient number from the data originated.

The right panel of Figure 22 represents the connectivity rate of the network formed with the **6SD** threshold significant **A2** peaks. Firstly we can notice that the A2 connectivity is higher in every distance bin than A1. PP non significantly higher than the NN in each distance bin, and the PN follows the tendency of PP.

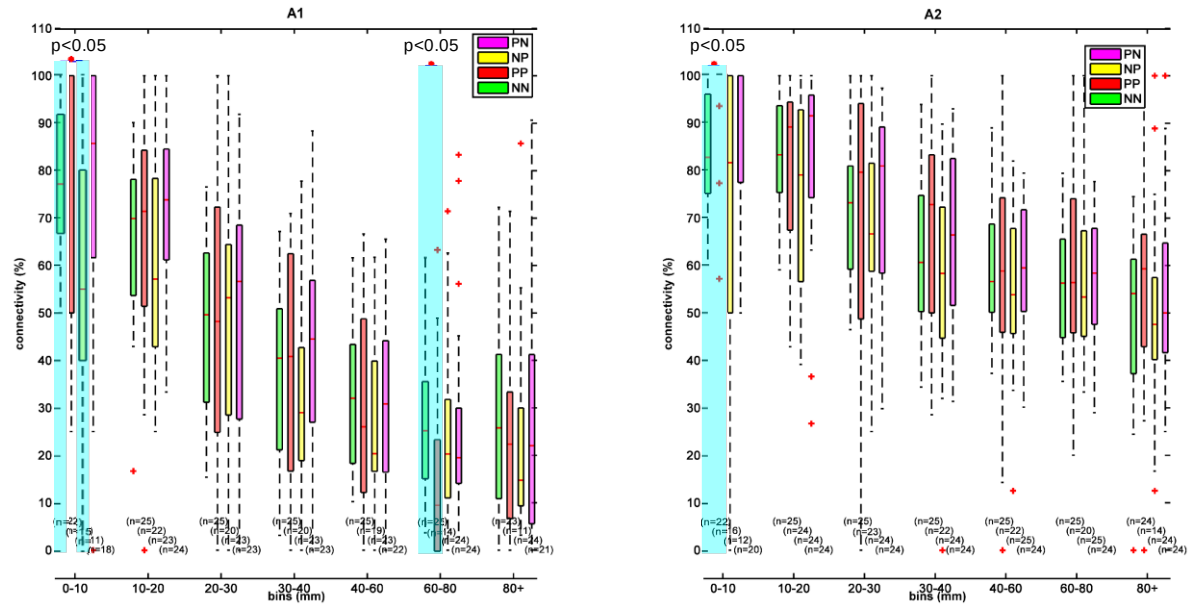

Figure 23. Connectivity measurement boxplot based on **3SD** threshold. The red stars and blue boxes indicates significant difference (Wilcoxon rank sum test, p<0.05) between the NN and NP in the 0-10 mm bins and between NN and PP in the 60-80 mm bin for the A1 component in the left panel; and between NN and PP in the 0-10 mm bin for the A2 component in the right panel. The n below the boxes indicates the patient number from the data originated.

I counted the connectivity rate with a 3SD threshold significant A1 and A2 peaks (results on Figure 23). On the A1 in the left panel we can observe that the PP higher than the NN in 0-

DOI:10.15774/PPKE.ITK.2016.004

60 mm distance moreover this difference is significant (Wilcoxon rank sum test, $p<0.05$) in the first, 0-10 mm bin. This ratio turned out to be the opposite in the 60-80 mm bin, where difference is significant (Wilcoxon rank sum test, $p<0.05$). The behaviour of this network shows similarity to the network formed by a 6SD threshold A1, except the 40-60 mm where the PP remain higher than the NN and the 80+ mm bin where the PP is lower than NN but the PN is not higher than NN like in the 6SD case (Figure 20. left panel, 80+ mm bin).

I examined the connectivity on the A2 peak with a 3SD significance threshold and I illustrated it on the right panel of Figure 23. The connectivity in the PP network was always higher than in the others. This difference is significant (Wilcoxon rank sum test, $p<0.05$) in the 0-10 mm bin.

The amplitude of the CCEPs.

I analysed the amplitude (z-score) of the evoked potential as a metrics of the connection strength between the electrodes and I compared the results between the NN and the PP, NP, PN cases.

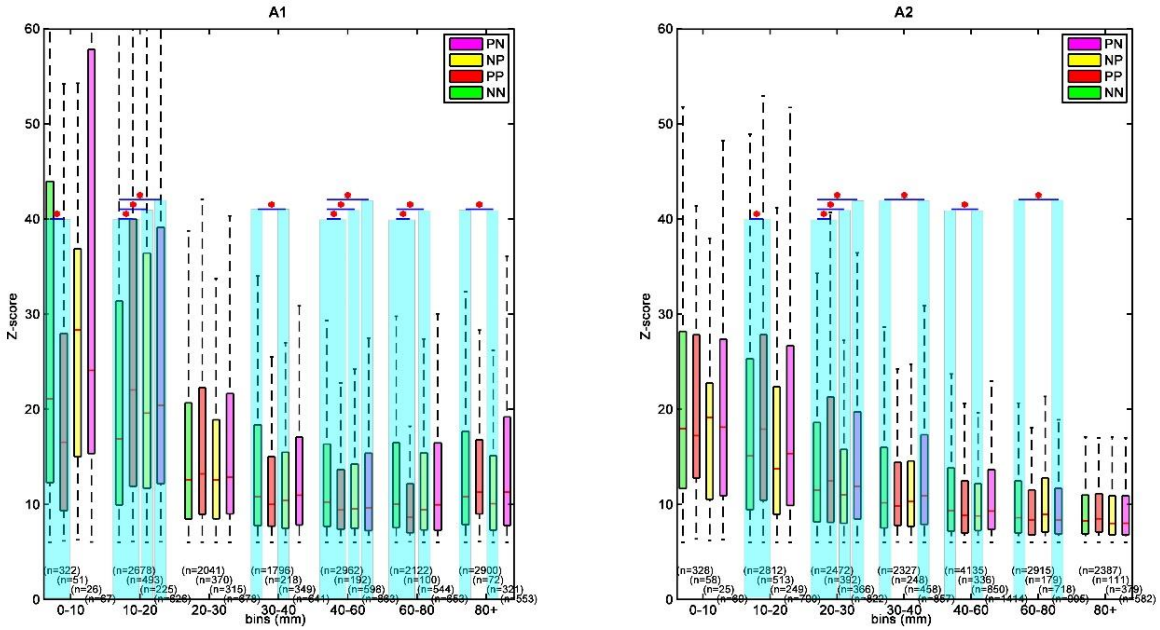

Figure 24. Amplitude for the **6SD** threshold network. The left panel shows the results from the A1 peaks. The red stars and blue boxes indicate significant difference (Wilcoxon rank sum test, $p<0.05$). On the left, in the case of A1 component, interesting to inspect the statistically significant difference between the NN and the other cases in each distance bin, except the 20-30 mm. Generally speaking the PP amplitude is lower than the NN except in the 10-20 and 20-30 mm bin. The higher rate of the PN in the 0-10 mm bin, may reveal some interesting properties of the pathological tissue and the seizure spreading. In the case of A2 based network (on the right) the amplitude in the PP subnetwork is higher than in NN, particularly in the nearby areas (0-30mm), with statistically significant difference between the two subnetworks in the 10-20 and 20-30 mm bins.

Interestingly, there is a statistically significant difference in the amplitude assumed by the A2 peak in the 20-30 mm bin (Figure 24 right panel), while this difference cannot be observed based on the A1 peak in the same bin. In the 30-40 mm bin, the PP connectivity is lower than the NN, while the PN shows greater connectivity with statistically significant difference. From

DOI:10.15774/PPKE.ITK.2016.004

40 mm, z-scores in pathological cases decrease and are lower than in the normal network. It is intriguing to take a closer look at the NP case, which shows lower z-score in each distance.

After the 6SD threshold networks (Figure 24), I analysed the 3SD threshold networks (Figure 25) which shows similar tendency in results. For the A1, the PP is significantly lower than the NN in the first, 0-10 mm bin, but significantly greater in the next two bins (10-20 mm & 20-30 mm) and lower in the 40-60 mm bin. The PN is significantly greater in the 10-30 mm distance, but is significantly lower in the 40-60 mm bin, which pattern follows the PP in these distances. It is interesting to see that the 6SD NP significant differences were lost with 3SD, except in the last bin, further than 8 cm.

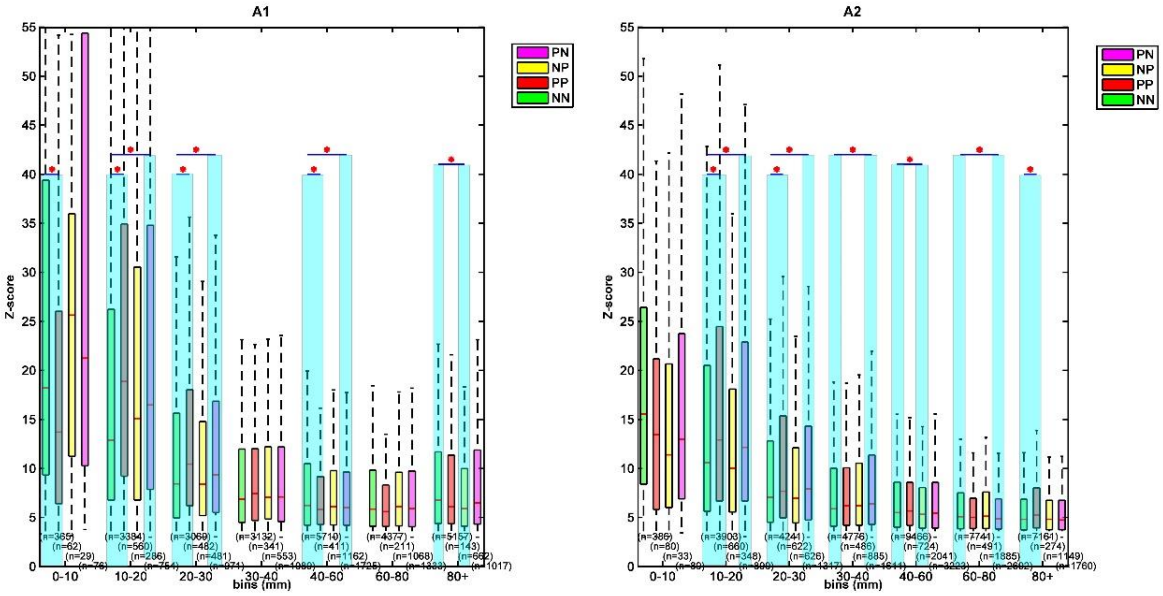

Figure 25. Amplitude of **3SD** threshold significant events decrease with increasing distance between the stimulated and recorded electrodes. The red stars and blue boxes indicate the significant difference (Wilcoxon rank sum test, $p<0.05$) between the NN and PP, NP, PN cases. The n below the bars show the significant event number from the data originated.

On the right panel of Figure 25, **A2** results also show similarities with the 6SD cases. The PP is lower in the first bin than the NN, then greater in the next two bins with statistically significant difference. In 30-80 mm, the PP is lower than NN, but further than 8 cm became greater with a statistically significant difference. The PN shows greater z-score than NN in 0-40 mm with statistically significant difference except the 0-10 mm bin, which is followed by changes and in the 60-80 mm bin it shows statistically significant lower values. The NP is almost everywhere lower than NN with significant difference in the 40-60 mm bin.

Path length

I calculated the path length in NN (non-ictal – non-ictal), PP (ictal-ictal), NP (non-ictal - ictal) and PN (ictal - non-ictal) subnetworks with both 3SD and 6SD on A1 and A2. On the left panel of Figure 26 I illustrate the path length of the network derived from the A1

DOI:10.15774/PPKE.ITK.2016.004

component, and the A2 on the right. The path length in PP (red boxes) is statistically significantly lower than in the NN (green boxes) in every case. It is interesting that for A1 with 6SDs, PN is also lower than NN which ratio ceases in the A2 graph. It is also impressive, that the path length in the A2 network is lower than in the A1.

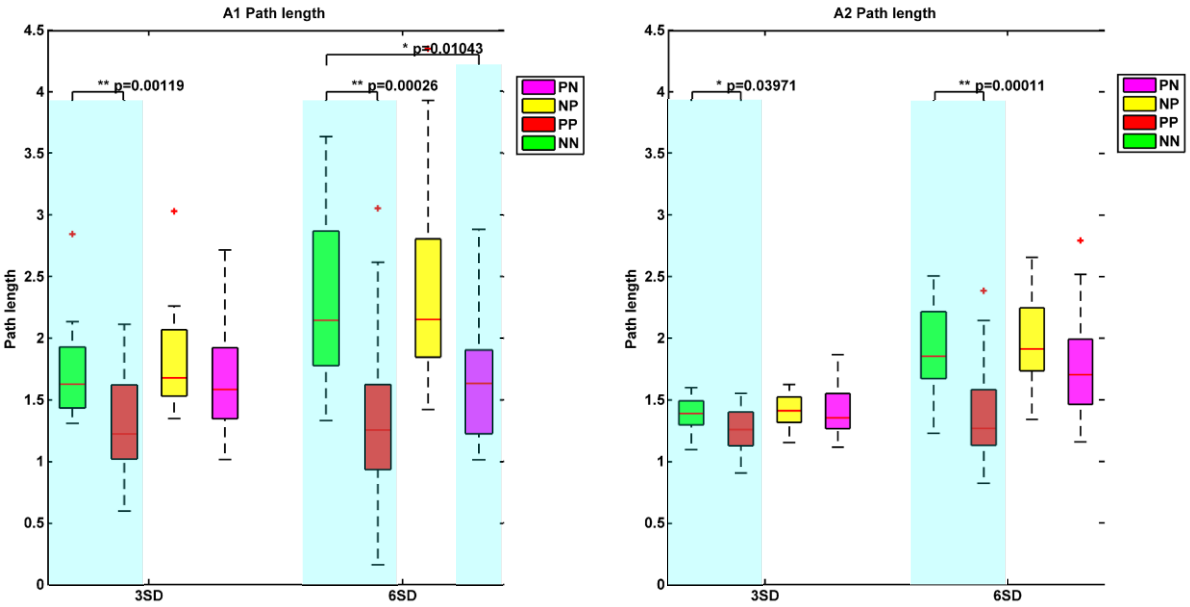

Figure 26. Path length in the NN (green), PP (red), NP (yellow), PN (pink) subnetworks created with 3SD and 6SD significance threshold on A1 (on the left panel) & A2 (on the right panel) peak. The significant differences between the NN and the other groups are calculated with Wilcoxon rank sum test and p values are signed above the corresponding groups, blue boxes sign significant differences. The path length between PP is significantly smaller than NN in every cases.

4.1.4 THESIS I. CORTICO-CORTICAL EVOKED POTENTIAL ANALYSIS AND NETWORK DESCRIPTION.

Thesis I. I have developed an automated CCEP analysis algorithm with which different features (amplitude, timing, placement and distance) can be extracted and graphs with nodes (electrodes or electrode groups) can be generated. I defined effective connectivity by the amplitude (z-score) of the evoked potentials and normalized outgoing and incoming connectivity. The nodes were rated by the ratio of the in and out going connections.

Thesis I.a Based on the applied graph theoretical analysis I experimentally proved that the possibility to evoke significant (>3SD) responses between the elements of the pathological network is significantly ($p<0.05$) higher in the nearer fields (<1 cm) than in normal ones on A2 component (Figure 23).

Thesis I.b From the applied modified graph theoretical analysis I experimentally determined that the path length between the elements of the pathological network is significantly ($p<0.05$) smaller, so the pathological elements are more connected than normal ones (Figure 26).

DOI:10.15774/PPKE.ITK.2016.004

4.2 RIPPLE DETECTION

Our ripple detection method was based on the putative ripple (PR) events provided by the previously described (3.3.1 Semi-automated ripple & putative ripple detection method) semi-automatic ripple detection method. These events were plotted in a Ripple Selection Tool (RST) which showed multiple features of the PR events. We had a window for PR detection parameters: 1) 300 ms raw data 2) Root Mean Squared filtered (80-500 Hz), and 3) a rectified filtered data, and one further window to plot the frequency content of the PR event such as 4) the filtered curve, 5) the results of the wavelet transformation and 6) the time-averaged cross section of the wavelet power and 7) a summary for all the PRs.

4.2.1 RIPPLE REVISION

Our RST was able to let the user review all the PR events in a sequential manner and decide whether to accept or decline them. Figure 27 shows the layout. The summary window distributed the PRs in a two-dimensional coordinate system. The dimensions were the amplitude vs RPRDA (See Materials & Methods - 3.3.1.2 - Putative ripple event selection) measure that allowed the reviser to overview the spectrum of the events in terms of amplitude and duration at glance. As a result of this revision process, a pool of accepted PRs were formed which can be considered as a collection of valid ripple events.

The method was verified on events previously visually marked by two experienced reviewers. The semi-automatic ripple pre-selection application (RST) was proven to be effective with 90.01% sensitivity, although the precision was 22.51%, thus the oppressive majority was composed by false positive matches. It is important to note here that this over representation was my aim. In my opinion it is worth the price if this method manages to find almost every event, because visual revision is always needed as human quality of life depends upon such results.

The visual revision of the recordings is very time consuming [126, 213], thus, in order to give an estimation about the acceleration of this preselection tool, I did an approximate appraisement. According to the literature, the visual revision include at least 4-6 channels within a 0.6 s length window[201], [214] on a 80-500 Hz (or parallel 80-250 Hz and 250-500 Hz) filtered data. The time for the decision and ripple event marking of one 0.6 s length recording is at least 2-3 s long, also depending on the patient's individual ripple density ('rippleness'). If I suppose, that the decision of one 0.6 s length recording may last 3 s, then the approximate time spent on the revision of the recommended 5-10 minutes data [213] with e.g. 80 channels would take 5-10 hours, or more [126]. I made an estimation with 200 s, 773 s and 300 s long, 83 channels data samples, which revision should take 5.76, 22.27, 8.64 hours,

DOI:10.15774/PPKE.ITK.2016.004

and found, that with the ripple selection tool, the revision of the preselected events decreased (with 0.3-0.5 s decision time) up to 1.50-2.60, 5.21-8.69, 1.97-3.28 hours, respectively. This means that the overall acceleration resulted in 74%-55%, 77%-61%, and 78%-63%, average 68% (~2/3) time decrease.

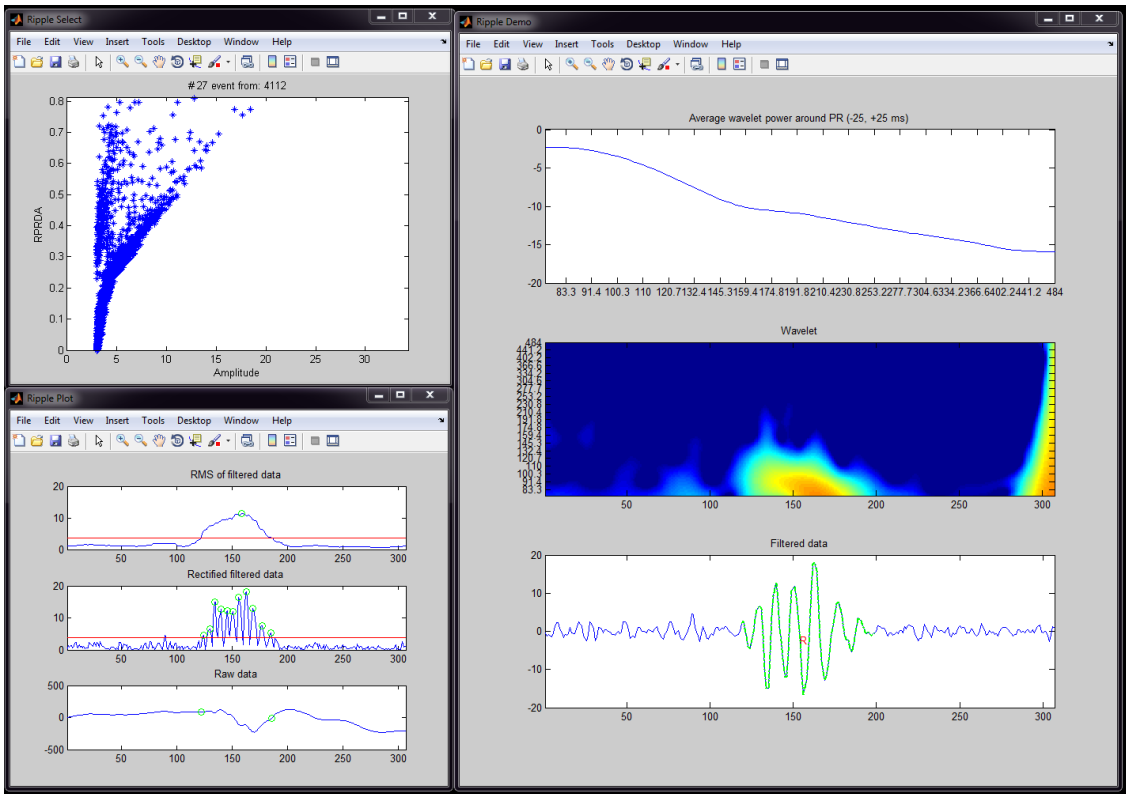

Figure 27. Putative ripple reviser layout. Upper left shows the RPRDA and amplitude values of all the putative events, the actual signed with black star. The upper subplot in the lower left window shows the Root Mean Squared filtered data with the RMS threshold (red line) and the maximal peak (green circle), the middle plots the rectified filtered data with the threshold and the peaks above the threshold and the bottom subplot show the original data in a 300 ms window around the putative event. The top of the right panel represent the mean of the wavelet transformation in a 50 ms window around the putative event, the middle draws the wavelet transformed data, and the bottom illustrates the filtered (80-500 Hz) data in a 300 ms window. Every time window is adjusted to the middle point of the putative ripple event.

4.2.2 RIPPLE VISUALIZATION

After the detection of ripples, the number of ripples per channels (RpC) were calculated. The brain surface was visualized using the BSVT (brain surface visualization tool developed together with Corey J Keller). Briefly, the brain surface vector graphic object (See Materials & Methods - 3.3.2 Visualization on 3D brain) was visualized using a Matlab graphic tool. Electrodes were added as planar circular objects. The position of electrode objects were identified based on the reconstructed 3D position of the grid contacts (See Materials & Methods - 3.2.1.5 Brain surface reconstruction and electrode localization). The colour of the electrode object was determined based on transformed RpC according to the "jet" colourmap distribution (built in function of Matlab), ranging from deep blue (lowest) to dark red (highest).

DOI:10.15774/PPKE.ITK.2016.004

The three-dimensional reconstructed brain surface with ripple rate weighted electrode objects is shown on Figure 28.

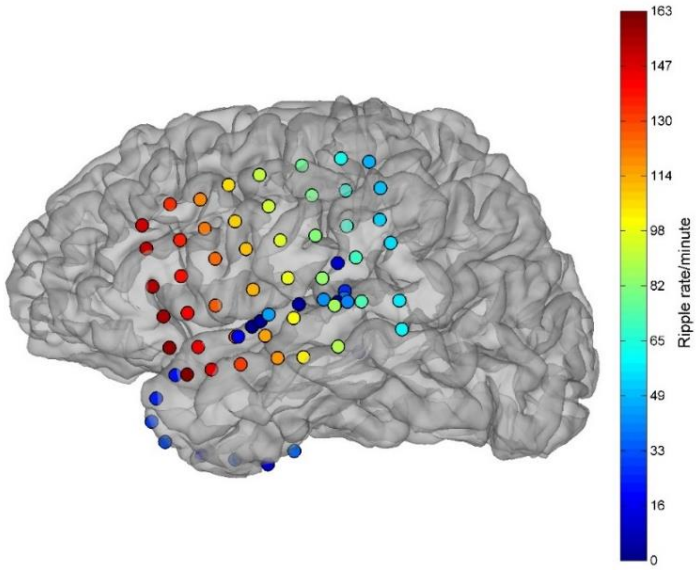

Figure 28. Illustration of the ripple rate on the electrodes. The hotter colours represent higher ripple number. This visualisation is based on not real data.

4.2.3 THE EXTENT OF THE RIPPLE GENERATING AREA

We wanted to describe the spatial extent of individual ripple events. First, we grouped the detected ripple or putative ripple events in a 100ms time window, then channels with coincident ripples were identified. Individual groups were analysed separately, and the area overlapping to the seizure onset zone (SOZ; See Materials & Methods -3.1.1 Pathological or physiological properties of the brain tissue) was mapped.

Ripples usually appeared relatively close to each other in time and space, and it was also common that they emerged on adjacent electrodes within this relatively short time window.

Figure 29 shows two examples from two different patients. The blue electrodes represent one selected representative ripple event, SOZ is shown in red. Overlapping electrodes are indicated with purple colour. The two cases show two essentially different patterns where the ripple was circumscribed in a restricted area that co-localized well with a relatively small SOZ (left side) while on the other case, ripples were encompassed with a wider distributed SOZ (right side).

DOI:10.15774/PPKE.ITK.2016.004

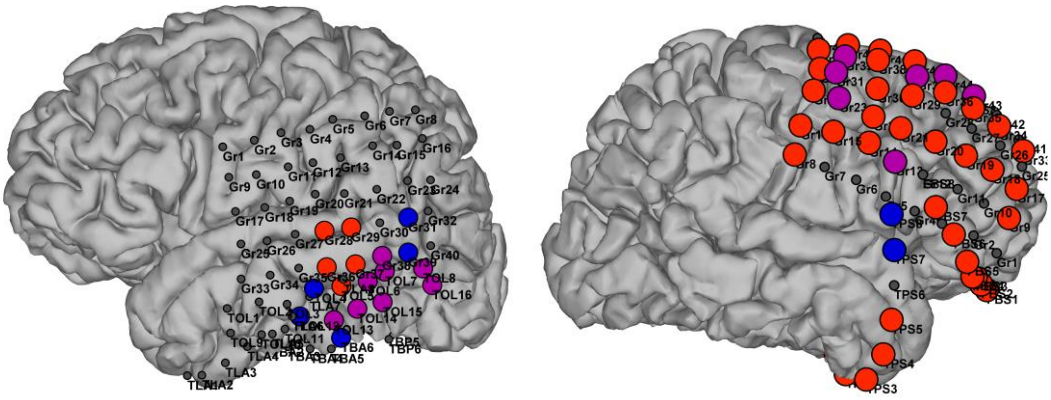

Figure 29. Overlap of ripples with different seizure onset zone areas. Blue electrodes show ripples, red seizure onset zones, and purple electrodes show the overlaping area.

DOI:10.15774/PPKE.ITK.2016.004

4.3 CHEP - EVOKED HIGH FREQUENCY ACTIVITY

The following part consists of the analysis of cortico-hippocampal evoked potentials (CHEP) in the human hippocampus under general anaesthesia during the resective surgery (hippocampus, amygdala, temporal pole, and part of the lateral temporal area resected) of temporal lobe epilepsy patients. Single shock electrical stimulation (amplitude: 5-10-15 mA; pulse duration: positive 0.2 ms; repetition rate: 0.5 Hz; number of pulses: 25-50) was applied to the temporo-basal structures before any kind of resection was performed. Clinical strip electrodes were used for stimulation, evoked responses were recorded with laminar microelectrodes in the hippocampus. Histological reconstruction was performed in order to determine the exact location of the electrode tract, the recorded activity relative to the cell layers and the subfields of the hippocampus after the "en-block" resection of the hippocampus.

Fourteen patients were included in this study. Three cases were rejected due to missing or low quality histological reconstruction, two cases were rejected because the stimulation protocol was compromised (applied after partial resection of the temporal lobe), and one case was rejected due to noisy recording. We analysed the evoked responses in the remaining eight patients (See Table 4 in Appendix). All together 131 CHEP sessions containing 3221 stimuli (25-50 stimuli each) were included. Data was further sorted according to stimulation site, the recorded hippocampal area and the stimulation amplitude. Table 1 summarizes the available combinations of these parameters. Despite not all of the possible permutations were present, we still managed to gain a good representation of the stimulus – response relationship in the temporo-basal – hippocampus system especially from 0 to 5 cm stimulation sites relative to the temporal pole.

	CA			**DG**			**SUB**		
Stim.point	**5 mA**	**10 mA**	**15 mA**	**5 mA**	**10 mA**	**15 mA**	**5 mA**	**10 mA**	**15 mA**
-3 - -4 cm		Pt38			Pt38				
-2 - -3 cm		Pt38 Pt36			Pt38			Pt36	
-1 - -2 cm		Pt38 Pt36	Pt26		Pt38	Pt26		Pt36	Pt26
0 - -1 cm		Pt38 Pt36	Pt26 Pt25		Pt38	Pt26 Pt25		Pt36	Pt26
0 – 1 cm		Pt38 Pt36	**Pt25**		Pt38 **Pt47**	Pt25		Pt36	
1 – 2 cm		Pt38 Pt36	Pt26 Pt25	Pt33	**Pt38** Pt47 Pt33 Pt17	Pt25 Pt33 Pt26	**Pt25** Pt33	**Pt25** Pt17 Pt33 Pt36	**Pt25 Pt22 Pt33** Pt26
2 – 3 cm		Pt36	Pt26 **Pt25**	Pt33	Pt33 **Pt47**	Pt25 Pt33 Pt26	Pt33	Pt33 Pt36	**Pt22 Pt25** Pt33 Pt26
3 – 4 cm		Pt36	Pt26 Pt25	Pt33	**Pt47** Pt17 Pt33	Pt25 Pt33 Pt26		Pt17 Pt26 Pt33 Pt36	**Pt22 Pt25** Pt26 Pt33
4 – 5 cm			Pt26 Pt25	Pt33	**Pt47** Pt33	Pt25 **Pt33** Pt26	Pt26 Pt33	Pt26 Pt33	**Pt22 Pt26** Pt33
5 – 6 cm									**Pt22**
6 – 7 cm	Pt17	Pt17		Pt17	Pt17			Pt17	Pt22

Table 1. Summary of the parameters of the stimulations in all the included cases. Red entries indicate stimulation sessions which evoked ripple events.

DOI:10.15774/PPKE.ITK.2016.004

4.3.1 HISTOLOGY AND CO-REGISTRATION WITH ELECTROPHYSIOLOGY

Based on the histological results, electrodes reached the CA region in six (Pt17, Pt25, Pt26, Pt33, Pt38, P36), the DG in other six (Pt17, Pt25, Pt26, Pt33, Pt38, Pt47) and the subiculum in again six (Pt17, Pt22, Pt25, Pt26, Pt33, Pt36) cases. All available tissue was analysed with immunohistochemical methods [55] with respect to cell loss and reorganization in the CA1 and subiculum. We observed severe cell loss in the CA1 region in five patients (severe hippocampal sclerosis, sHS); and in three patients relatively mild cell loss was detected (mild hippocampal sclerosis, mHS).

Figure 30 shows the co-registration of the electrophysiology with the histological results. The left panel shows the reconstructed electrode trajectory and the histology of the electrode penetrations of Pt22. Single stimulus response waveforms from identified registration points are indicated on the right.

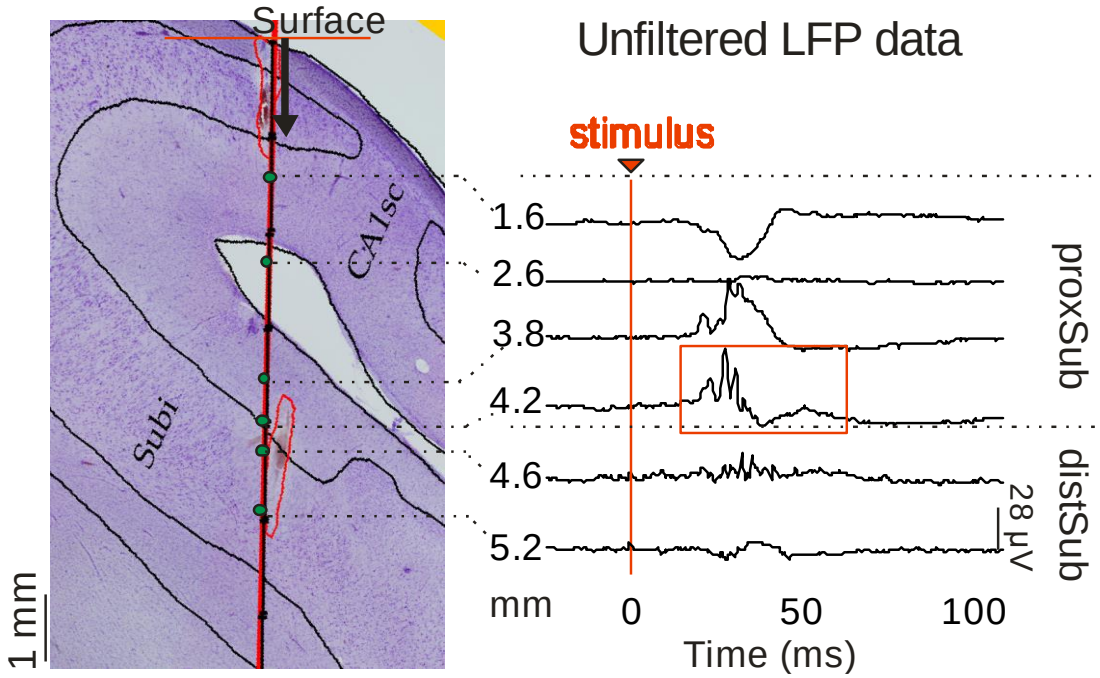

Figure 30. Sample of a hippocampus slice and recorded evoked potential from Pt22. Histology indicates subiculum (Subi) and sclerotic CA1 subregions. Local field potential gradient are shown on the right originated from recording points highlighted with green on left panel. The red vertical line indicates the stimulation time point. The red box sign a typical evoked high frequency oscillation.

4.3.2 HIGH FREQUENCY CONTENT OF EVOKED POTENTIALS

In this study to describe the electrophysiological properties of the cortico-hippocampal network, we focused mainly on the high frequency (40-500 Hz) content of the short latency components (10-100 ms) of the CHEP. Our first approach to detect high frequency activity (HFA) in the hippocampus was a simple threshold cutting method of the filtered FPG. In order to detect the shortest latency responses, we cut out the stimulation artefact from the recording, replacing it with low frequency curve using the spline fitting method. HFA was detected after

DOI:10.15774/PPKE.ITK.2016.004

this preparation based on band pass filtering and threshold cutting method similar to putative ripple identification mentioned earlier (3.3.1.2 - Putative ripple event selection). Recording electrodes were grouped based on the reconstructed location across the major subfields of the hippocampus dividing it into three areas, cornu ammonis (CA) region (including CA1-3a,b,c), dentate gyrus (DG) (including the hilus beside DG itself) and subiculum (Sub) (including pre-, pro-, proximal-, distal-Subiculum).

Based on this division 2335 out of the 3221 stimulation fell in different Hc regions that evoked HFA. Evoked ripples were detected using our Ripple Selection Tool (RST – See Materials & Methods - 3.3 Ripple detection), which was followed by identifying the best channel from each region. The cases and stimulation arrangements showing ripple activity are highlighted in Table 1 with red. The analysis resulted in 504 ripple events out of the above mentioned 2335 HFAs, from which 32 were registered in CA, 86 in DG and 386 in Sub region. Latency, duration, amplitude, evokability and frequency were calculated for all these evoked ripples and HFAs.

4.3.3 Latency and duration of the evoked ripples

Latency and duration of the evoked ripples were measured event by event, average values were determined after Gaussian curve fitting on the histograms. Figure 31 part A-C shows the peak latency histograms for the three regions (CA, DG, subiculum) and Part D shows the duration histogram for all these regions. We determined that the peak latency of the evoked ripples were bimodal in the CA and Sub regions. The more frequent latencies appeared earlier in the CA region (11.84 ms with SD: 0.86 ms), and later in the Sub region (39.52 ms with SD: 1.36 ms). The less frequent ones appeared 88.27 ms with 1.17 ms SD, and 15.40 ms with 1.72 ms SD for the CA and the Sub respectively. The DG showed a unimodal distribution with 26.55 ms with 1.73 ms SD latency. The duration of the ripples were 21.82 ms with 1.89 ms SD, which remained fairly stable regardless to the stimulation parameters or the subregions of the hippocampal formation.

DOI:10.15774/PPKE.ITK.2016.004

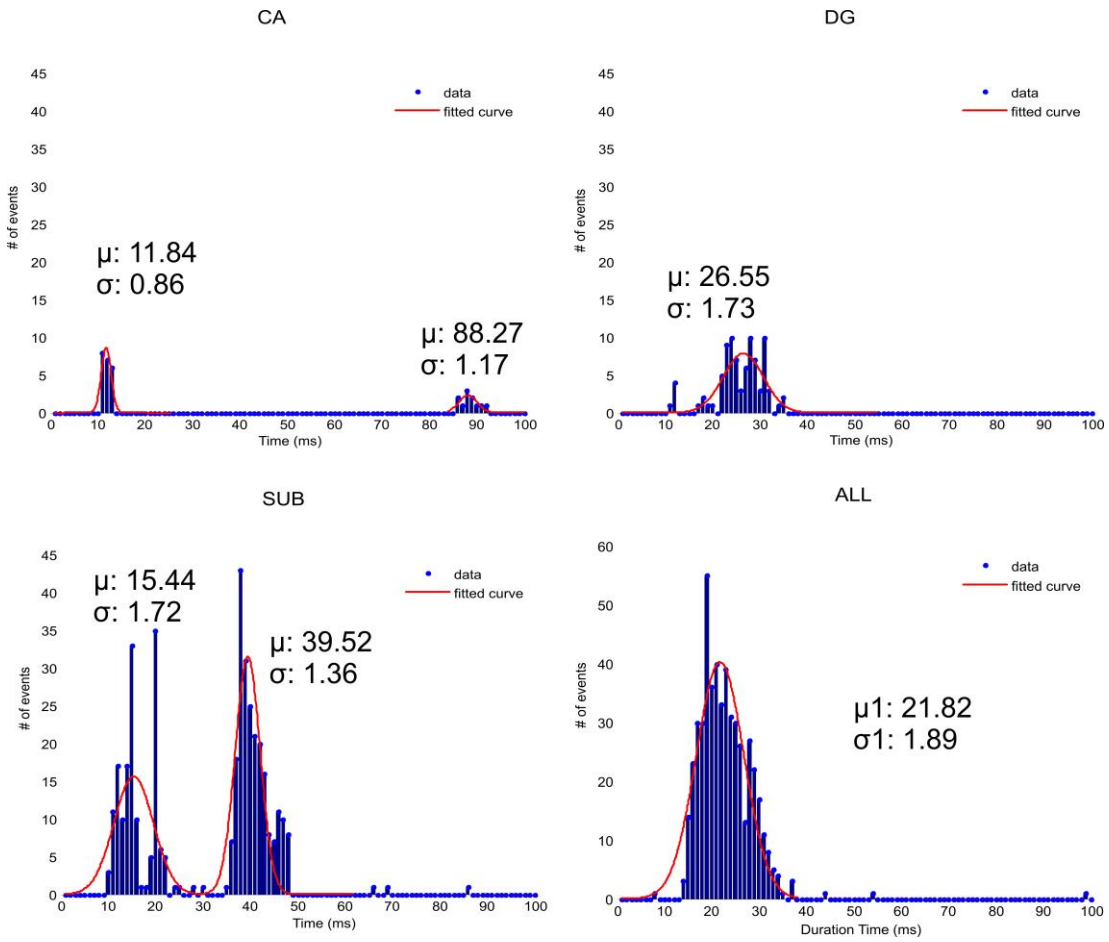

Figure 31. Distribution of timing and duration of selected evoked ripple events. A) Timing of events from CA. B) From DG. C) From subiculum. D) Duration of all events from all regions.

4.3.4 Analysis of the overall amplitude

Figure 32 illustrates the distribution of z-scores of all events. The outliers are hypothesized to be artefacts therefore they were not involved. Based on the Matlab curve fitting procedure, the distribution seemed to be a nonparametric kernel-smoothing distribution. The left and middle part of the figure shows the fitted Kernel distribution (red line). The empirical cumulative distribution function can be seen on the right. We can observe that about 70% of the events have an amplitude value lower than 5.

DOI:10.15774/PPKE.ITK.2016.004

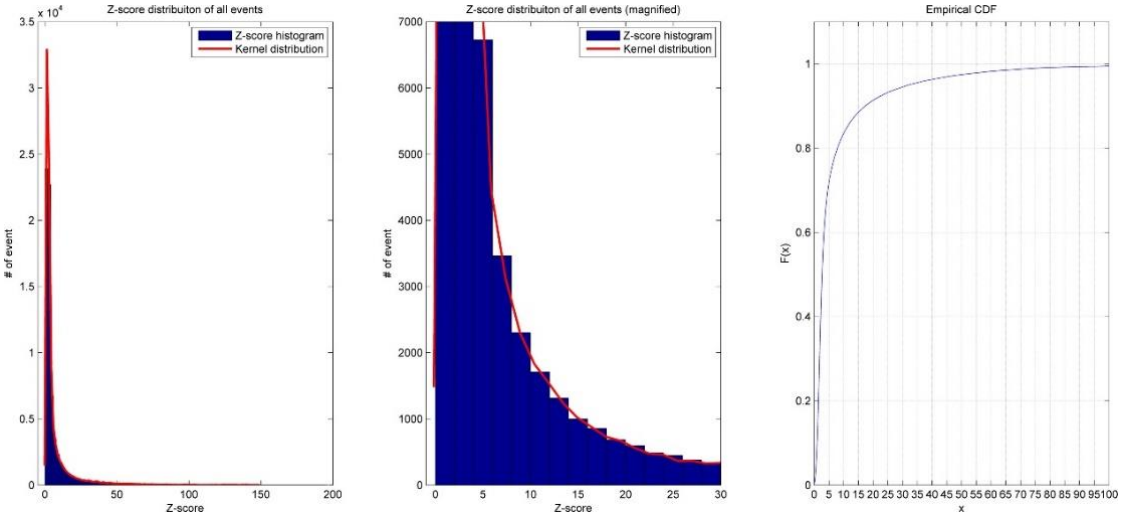

Figure 32. Amplitude (z-score) distribution of the hippocampal evoked potentials. The left and middle part of the figure shows the fitted Kernel distribution (red line). The empirical cumulative distribution function can be seen on the right. We can observe, that about 70% of the events have lower amplitude value than 5.

The amplitude changes of the evoked potentials during a stimulation session from one patient are illustrated on the results in Figure 33. The electrode followed the trajectory of CA2 – DG – CA3 – DG – Sub regions, the heatmaps illustrate the amplitude of every evoked potential, red colour indicates higher z-score values. In this case, 16-20 stimulations were applied from 5 types of distances (0-1, 1-2, 2-3, 3-4, 4-5 cm). The overlaid boxplot shows the overall z-score distribution on the channels. The highest amplitudes were consistently present on channels in the DG and the most efficient stimulation point (from where the highest z-score were evoked) was 3-4 cm.

It is important to note that the simplest amplitude illustration manages to describe the hippocampal layers accurately.

DOI:10.15774/PPKE.ITK.2016.004

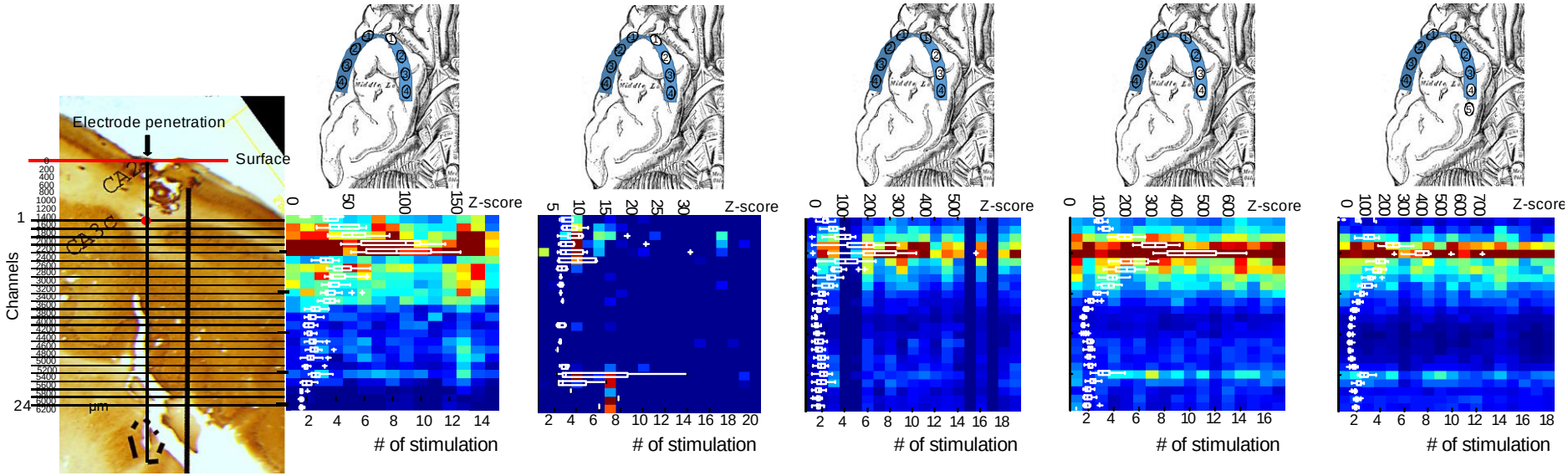

Figure 33. Illustration of the amplitude distribution of evoked potentials across different stimulation points with the same stimulation current from Pt47. The maximal amplitude z-score values of the evoked potentials after the stimulation between 10-100 ms are plotted on the heatmaps. The overlaid boxplots sign the distribution of the amplitude z-scores derived from all events. . On top, the basal brain drawing and the white contacts of the overlaid strip electrode sign the approximate stimulation positions. Source of the original brain drawing: * 8

DOI:10.15774/PPKE.ITK.2016.004

We collected the amplitude of the selected evoked ripples. To give a visual representation, I illustrated the overall results on Figure 34. The height of the coloured columns represent the third percentile value of all z-score amplitudes of the evoked potentials elicited in that subregion of the hippocampus, the ‘hat’ indicates the most extreme data points which are still not considered as outliers (outliers are not plotted). The colours code the current strength of the stimulation, blue for 5 mA, green for 10 mA and red for 15 mA. Not all current strengths were applied on all stimulation distances in each patients. Detailed description about the stimulation points, the stimulation current strength and the recorded areas of the hippocampal formation are plotted in Table 1 (The illustrated amplitudes originate from patients indicated with red letter).

We can observe that as stimulation gets closer to the inner surface of the temporal lobe, amplitude increases especially in the DG and the Sub regions. 5 mA stimulations almost never evoked ripples, except stimulations involving the subiculum from 1-2 cm. At this distance, we could see a reversed ratio between the stimulation strength and the amplitude of the evoked potential in the Sub region. We should notice that the most sensitive and active area is DG, where the highest amplitudes were evoked from all distances.

To get a more precise comparison, I plotted the amplitude of the evoked ripples depending on the stimulation distance and the strength on Figure 35. We can observe that DG responses are especially sensitive to the stimulation from 1-5 cm distance, while CA and Sub regions show less pronounced changes regarding to the stimulation strength or the stimulation distance.

DOI:10.15774/PPKE.ITK.2016.004

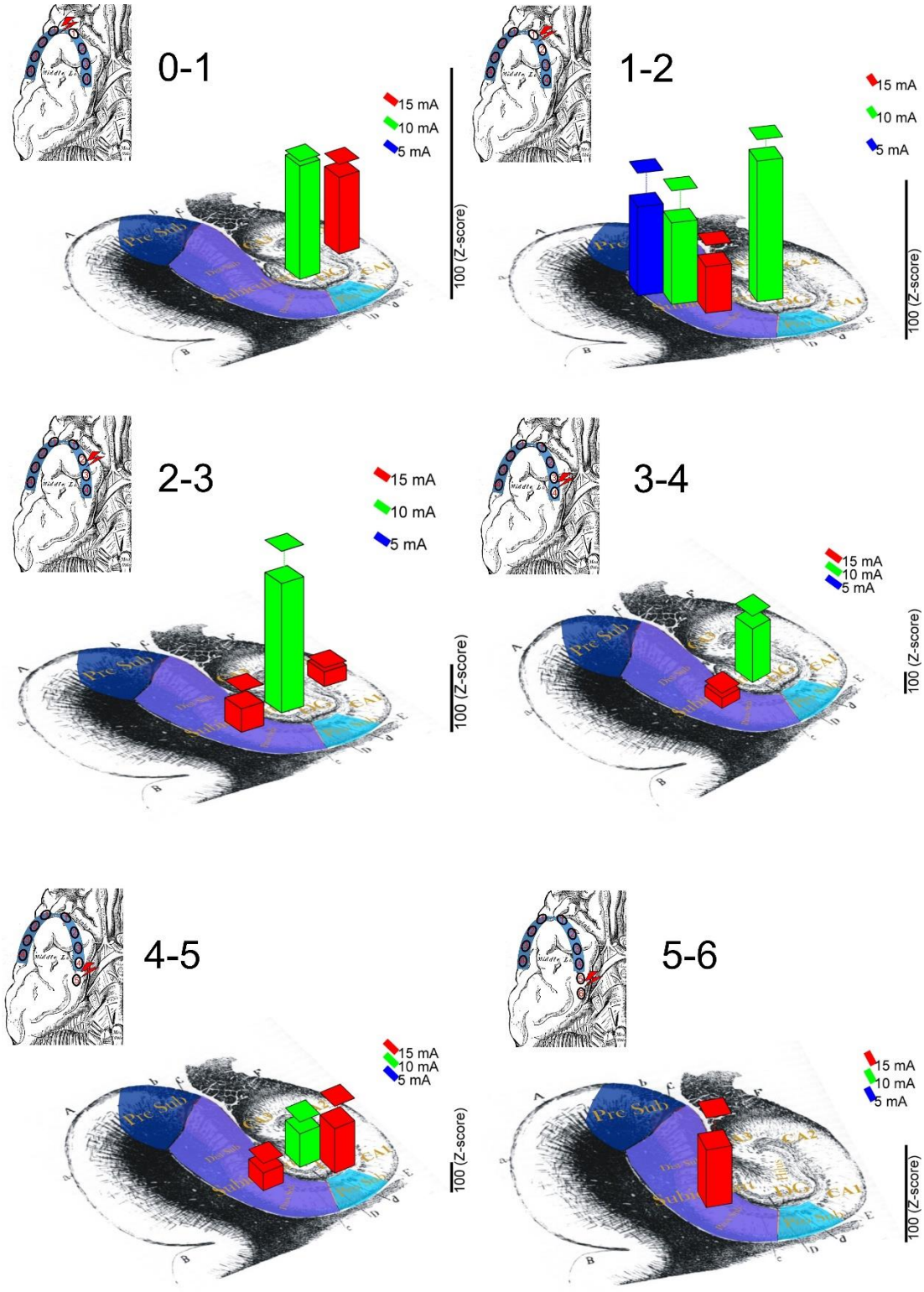

Figure 34. Amplitude of the evoked potentials elicited from the regions of the hippocampus, according to different stimulations moving away from the pole of the temporal lobe to the inner part of the temporal lobe, closer to hippocampus. On top left, the basal brain drawing and the white contacts of the overlaid strip electrode sign the approximate stimulation positions. Source of the original brain drawing: * 8,* 9.

DOI:10.15774/PPKE.ITK.2016.004

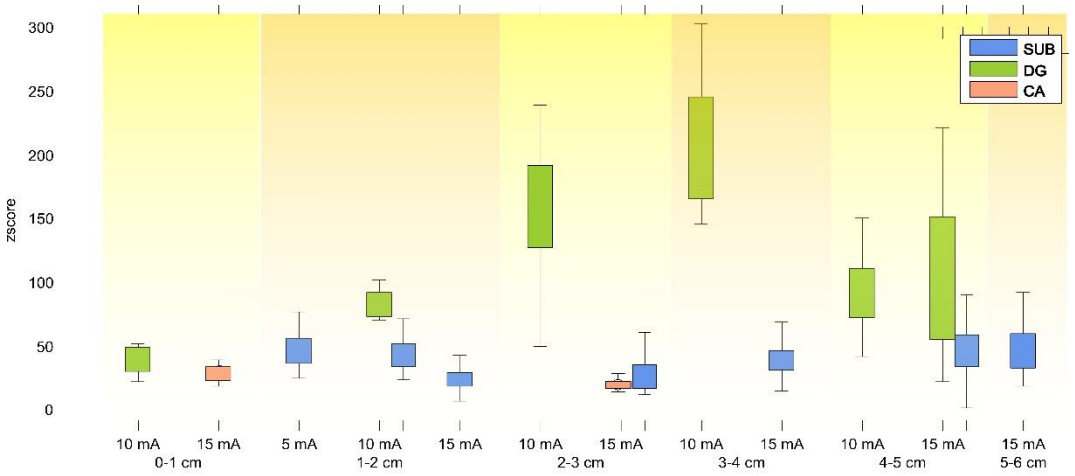

Figure 35. Summary of stimulation placement and stimulation strength dependence. The x axes show the different distance from temporal pole (0-6 cm), y axes show the z-score amplitude values. Different colours denote the subregions of hippocampus (CA-salmon, DG-green, SUB-blue). The edges of the box are the 25th and 75th percentiles, the whiskers extend to the most extreme data points not considered outliers, and outliers are not plotted. The most effective stimulations were from 1-5 cm.

Overall, stimulations could elicit significant potentials in all regions of the hippocampus. We can observe, that the DG region showed the highest amplitude among all the hippocampal regions, especially in the cases where stimulation was applied from a distance of 3-4 cm and the 2-3 cm. Stimulations from 6-7 cm were not highly effective (Figure 35).

4.3.4.1 Response evoking capability – 'Evokability'

Overall results

To characterize the tenacity of the evoked ripples and HFAs, we calculated the rate between the number of the evoked ripples (HFAs) and the number of stimulations which could have possibly elicited ripples (HFAs). Figure 36/A summarizes the specificity of grouping by rate with the stimulation distance, strength and hippocampal regions (CA, DG, SUB-Subiculum). The right figure visualizes the rate of the selected ripples, while the left figure contains the ratio of HFAs (events with an amplitude higher than 5 z-score values). The left figure illustrates all stimulations and all recording area arrangements (64 cases). Warmer colours represent higher ratios in percentage for the possibility of triggering an event (HFA or ripple). We can see that all stimulated hippocampal regions were able to perform HFA, with slightly more frequent incidence in the Sub region, followed by DG and CA regions. The possibility to evoke a HFA is relatively low, around 30-40 % in the CA region (except 3-4 cm, 10 mA, 70%), higher in the DG region (40-100%), and also fairly high (50-100%) in the subiculum. Interestingly, evokability does not necessarily depend on the stimulation strength. In the DG, 10 mA stimulation was the most effective was, while we can only observe a slight simulation strength (5-10-15 mA) dependence in the subiculum.

DOI:10.15774/PPKE.ITK.2016.004

After the strict evoked ripple selection, 16 stimulation-recording area arrangements remained in the analysis (Figure 36/A right). The possibility to evoke a ripple is rather low in the CA region (15 %), highest in the DG (10-50%), and highly varying (5-35%) in the Subiculum.

As we compare the ratio of the evoked ripples and the EHFA (Figure 31/A right and left), we can notice, that the ratio of the EHFA is higher in all positions. From this, we may conclude that the amplitude of the evoked ripple is almost always higher than 5 z-scores, but this is not a sufficient requirement for evoked ripples. Lower evokability rate for ripples may indicate that multiple types of significant HFAs could be present at the same time.

If we consider the results of EHFA evokability (Figure 36/A left), it stands out that the possibility to evoke high frequency activity is less probable from the lateral stimulation sites between -4 cm and the temporal pole (0 cm). The rates of the evoked events are averaged across the hippocampal regions in accordance with the stimulation distance from the temporal pole. Detailed description of the stimulation distance dependence is illustrated on Figure 36/B. The subiculum showed (blue box) the most consequent response to stimulations between 0-7 cm of distance, with a higher than 50% evoking ratio with a maximal peak at 1-2 cm. The evokability of HFAs is high between 0-4 cm in DG (green box) with a wider dispersion around 2-3 cm, and variable but quite low between 0-7 cm in CA region (salmon coloured box). The most effective stimulation point to evoke a HFA is 1-2 cm for subiculum, 3-4 cm for DG and CA. In comparison to these results, the rates of the selected ripples (shown on the right panel of Figure 36/B) shows clearly that ripples could only be evoked - only with moderately low evokability - exclusively from 0-5 cm. The most influential distance to evoke a ripple is 1-2 cm for subiculum, 4-5 cm for DG and 0-1 cm for CA. In general, the most active region according to this comparison is DG.

If we examine the ratio of the evoked activity regarding the stimulation strength (5, 10, 15 mA) and averaged with the regions, we can see a directly proportional increase in the case of CA on Figure 36/C left (salmon coloured box) but not in the case of DG or the subiculum. When considering these comparisons, we should take into account the differences in the sampling, e.g. the data for 5 mA CA originate from only one sample stimulated from 6-7 cm, from where the EHFA evoking ratio is usually low (about 10-30% (Figure 36/A left)). For DG, evokability is almost invariable but there is a small increment with 10 mA in comparison to the 5 mA, however evokability returns to almost the level of the 5 mA stimulation at the level of a 15 mA stimulation. The sensibility of the subiculum is high for the stimulation strength, the mean evokability is around 70% chance at 5 mA, 20% chance for 10 mA and 70% chance for 15 mA - which is the highest within these regions. The ratio of evokability for HFOs (Figure 36/C right) is hardly comparable to the previous results, as the 5 mA stimulation

DOI:10.15774/PPKE.ITK.2016.004

did not elicit ripples , with an exception being the Subiculum from 1-2 cm with 15% chance, DG (5 cases) with average 5% and Subiculum with 5% (in one case) with 10 mA stimulations. 15 mA stimulation evoked ripples in the CA region with 15% chance (2 cases), in DG with 17% chance (one case) and 10% chance in the Subiculum (5 cases). The comparison of ratios of the EHFAs and HFOs could suggest that the amplitude of ripples in the Subiculum and CA regions is not always than 5 z-scores, while amplitude of ripples in the DG always have higher amplitudes.

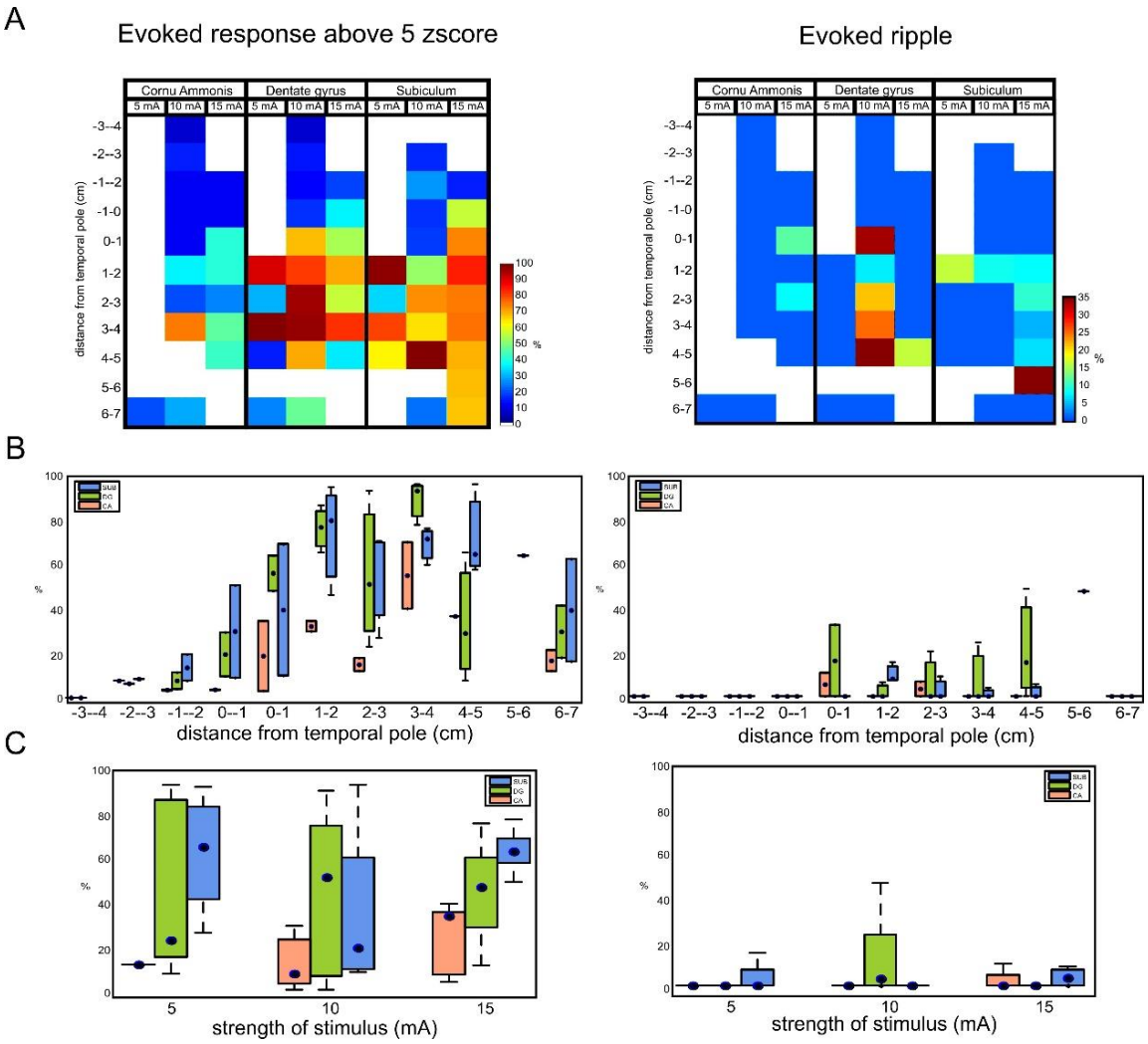

Figure 36. Summary of stimulation placement dependence on the event evoking capability. A) Left: The possibility to evoke a HFA in all stimulation arrangements grouped by the regions Cornu Ammonis-CA, Dentate gyrus- DG and Subiculum. Right: Possibility of evoking HFO. B) The means of evoking rates in the regions grouped by the stimulation distance. Left for HFA, right for HFO. C) The means of evoking rates in the regions grouped by the stimulation strength. Left for HFA, right for HFO.

Possibility to evoke HFOs regarding to hippocampal sclerosis

The possibility to evoke these kinds of oscillations in the CA regions is higher than in DG in mild and severe HS, but the Subiculum exceeded both regions in severe HS cases, and fell behind both regions in mild HS cases. This well-marked difference in the possibility to evoke

DOI:10.15774/PPKE.ITK.2016.004

an event in the Subiculum is significantly (Wilcoxon rank sum test, $p<0.05$) higher in the severe HS cases than in the mild HS cases (Figure 37).

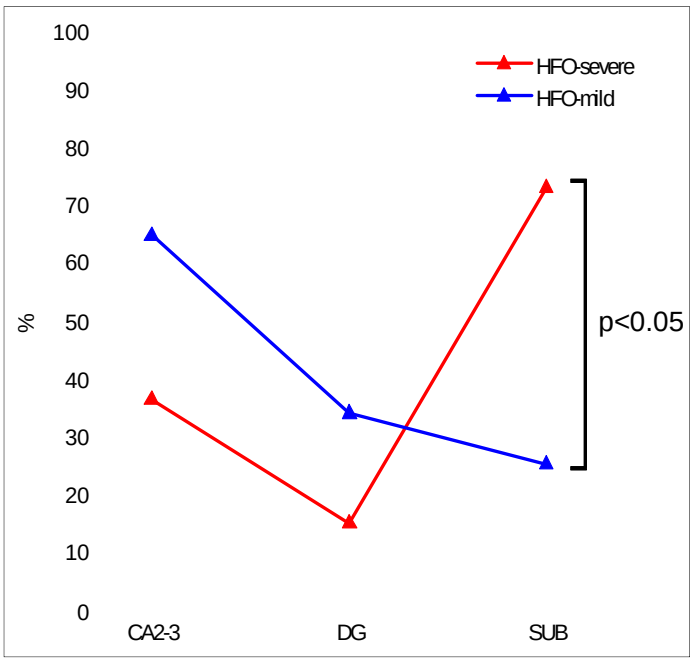

Figure 37. Illustration of the possibility to evoke HFO according to hippocampal sclerosis categories. The possibility to evoke these kind of oscillation in the CA is higher than in DG in mild (blue triangles) and severe HS (red triangles), but SUB exceed both regions in severe HS cases while fell behind both regions in mild HS cases. The possibility to evoked event in the SUB is significantly (Wilcoxon rank sum test, $p<0.05$) higher in the severe HS cases than in the mild HS cases.

4.3.5 Analysis of the frequency distribution

To analyse the frequency distribution of evoked potentials, we calculated the event-related spectral perturbation of the evoked potential and then averaged it in a 50 ms window. See exact description in Materials & Methods - Event related spectral perturbation (ERSP). We classified the maximal power amplitude frequency values (primary frequencies) and the lower power amplitude frequency values (secondary frequencies) of every event into frequency bins from 20 to 650 Hz. Results from Pt47 are illustrated on Figure 38 and on Figure 33.

The analysed recording was registered to the histological preparation of the hippocampal slice. Figure 38 illustrates the frequency distribution (between 80-500 Hz) from all evoked potentials at a given channel according to the different stimulation distances. The overlaid boxplot shows the overall z-score distribution on the channels which is same as on Figure 33. The highest amplitudes were present in DG (upper channels) but this did not always correspond to how high frequencies were. Our observation showed that the most prominent frequencies are around 80-90 Hz on the top five channels. When the stimulation was closer to the hippocampus (2-3, 3-4, 4-5 cm), the most prominent frequency reached 240-260 Hz on the sixth channel and showed a decay on the lower layers.

DOI:10.15774/PPKE.ITK.2016.004

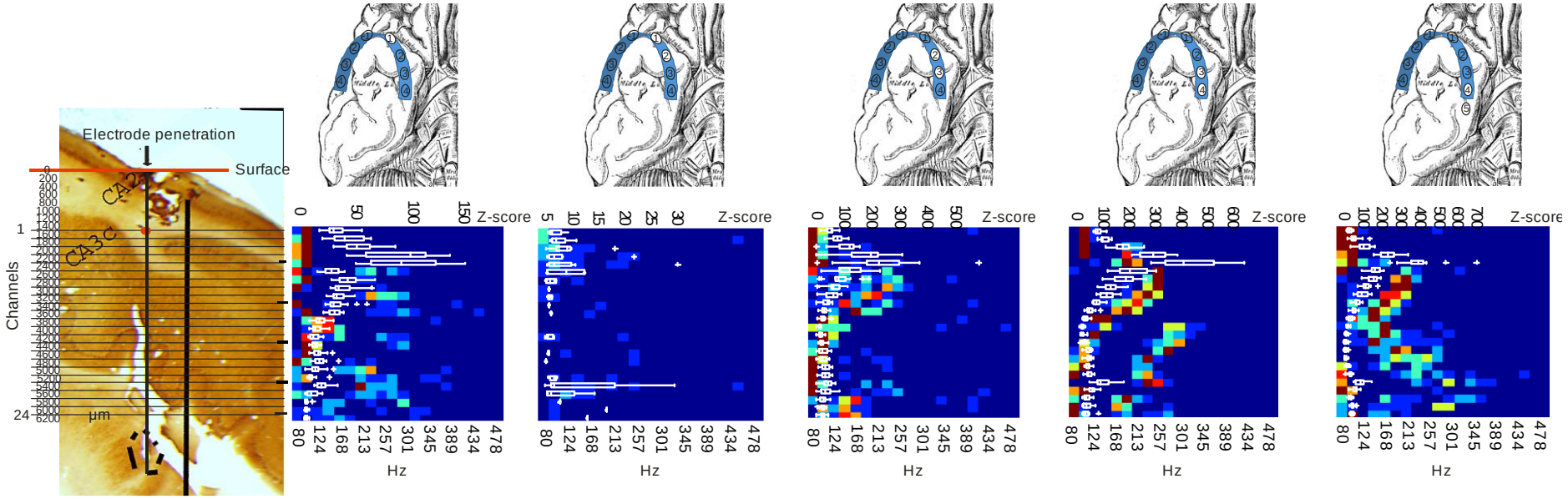

Figure 38. Frequency distribution of evoked potentials from patient P47 in the layers of Gyrus Dentatus. The overlaid boxplots sign the distribution of the amplitude z-scores. The frequency of the evoked potentials changes according to the stimulation placement. On top, the basal brain drawing and the white contacts of the overlaid strip electrode sign the approximate stimulation positions. Source of the original brain drawing:* 8.

DOI:10.15774/PPKE.ITK.2016.004

We grouped the frequency values of evoked ripples and plotted similarly as in the previously described amplitude cases (Figure 34). The height of the coloured columns represent the third percentile value of the primary frequency values of all evoked potentials elicited in the subregions of the hippocampus. The ‘hat’ signs the most extreme data points which are still not considered as outliers, outliers are not plotted. The colours code the current strength of the stimulation, blue for 5 mA, green for 10 mA and red for 15 mA. Not all current strengths were applied on all stimulation distances in every patients. The stimulations could evoke greater than 100 Hz oscillations in every region independently of the position of the stimulation. Interestingly, the higher stimulation currents evoked higher frequencies - as we can observe in the 1-2 cm stimulation of the subiculum.

DOI:10.15774/PPKE.ITK.2016.004

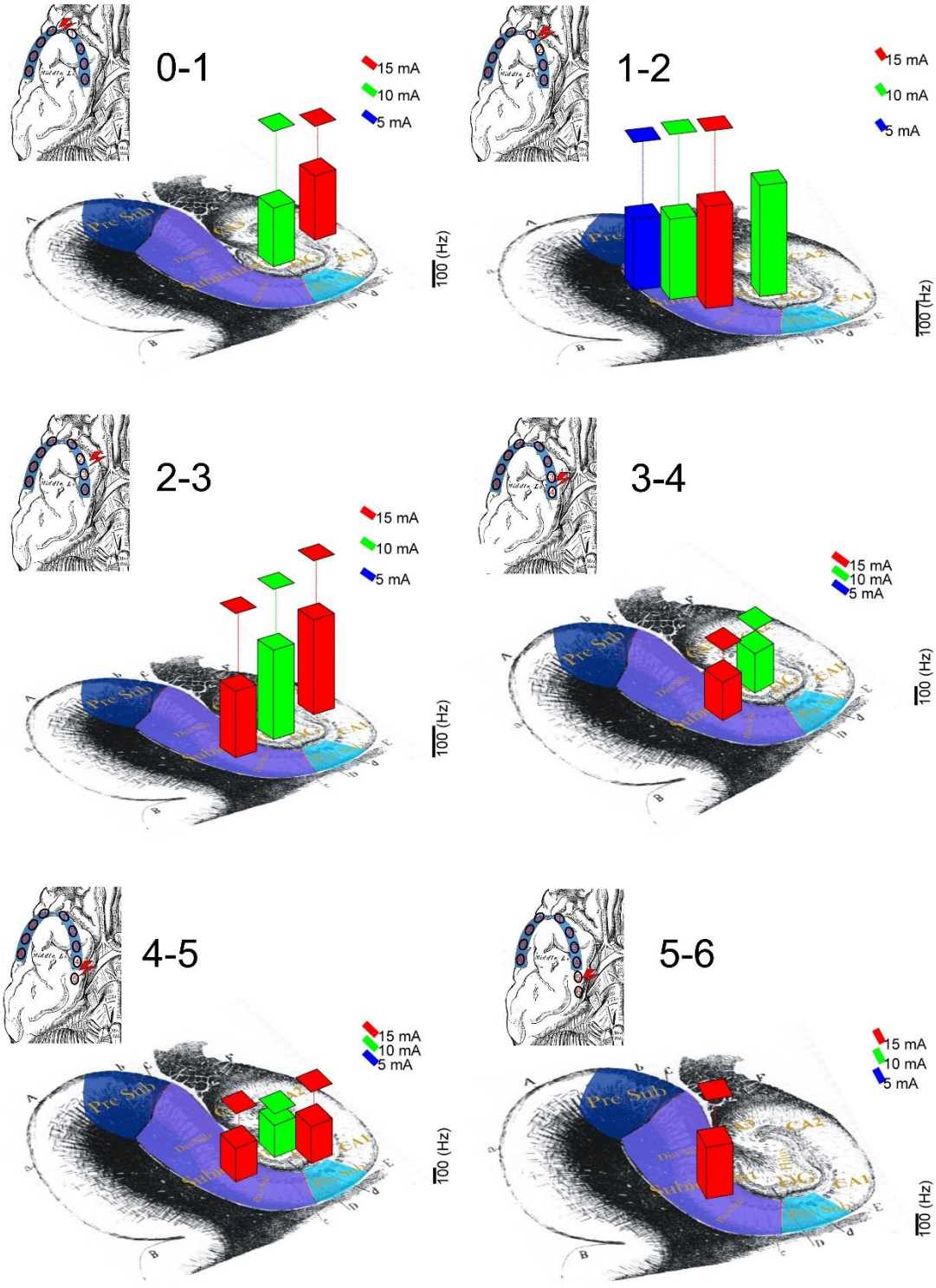

Figure 39. Frequency of the evoked potentials elicited from the regions of the hippocampus according to different stimulations moving away from the pole of the temporal lobe to the inner part of the temporal lobe, closer to hippocampus. On top left, the basal brain drawing and the white contacts of the overlaid strip electrode sign the approximate stimulation positions. Source of the hippocampus illustration:* 9 and the brain drawing:* 8 .

To analyse the frequency components of the CHEPs, we used event related spectral perturbation (ERSP from EEGLAB). Highest power frequency peaks were measured on time-averaged (50 ms window around the maximal peak of the event) ERSP values. (See exact description in Materials & Methods).

DOI:10.15774/PPKE.ITK.2016.004

We classified the maximal power amplitude frequency values as primary frequency values, the lower ones as secondary frequency peaks for all events, and sorted them into frequency bins from 20 to 650 Hz. Figure 40 show the result, where the four panels demonstrate the data for CA, DG, Sub, and all together (A, C, B, D respectively). In all of the four panels the upper and middle subplots stand for the primary and secondary ERSP frequency peaks (blue and red respectively). In the CA region (Figure 40/A), the primary frequencies were in the slow ripple range (mean: 95.75 Hz with SD: 10.46 Hz; range: 66-130 Hz). A relatively separated subset of this peak was in the gamma range (mean: 27.53 Hz with SD: 12.75 Hz; range: 20-46 Hz). The secondary frequencies were in the fast ripple range (mean: 200.00 Hz with SD: 4.98 Hz; range: 170-493 Hz). The highest frequencies appeared around 130.00 Hz from the range of 66-220 Hz.

The frequency of DG showed (Figure 40/C) a somewhat different pattern, pointing out a three peaked distribution. The most prominent primary frequencies were around 15.00 Hz with 50.00 Hz SD, 108.30 Hz with 10.80 Hz SD and 194.40 Hz with 10.30 Hz SD. The secondary frequencies were similar, but the highest incidence was around 206.70 Hz with 4.10 Hz SD and 303.70 Hz with 6.10 Hz.

Most of the events occurred in the Subiculum (386). The primary frequencies of these showed a bimodal distribution (Figure 40/B) with a peak around 45.00 Hz with SD: 11.50 Hz and 166.90 HZ with SD: 48.00 Hz. The secondary frequencies had similar distribution, the highest peak being around 41.80 Hz with SD: 8.90 Hz and 169.80 Hz with SD: 21.80 Hz which draw a long tailed distribution with almost 500 Hz maximal value. In summary (Figure 40/D), we found a bimodal distribution in the primary and secondary frequencies. The primary frequencies were most prominent around 41.50 Hz with SD: 14.10 Hz and 172.80 Hz with SD: 48.80 Hz while the secondary had 40.30 Hz with SD:10.80 Hz and 186.40 HZ with SD: 30.50 Hz showing a long tailed distribution which reached even 500 Hz in rare cases.

We found events with combined frequency components with dominant frequencies between 110 - 208 Hz and less prominent higher frequencies between 100-500 Hz in the Subiculum and also in the CA and DG regions in rare cases.

DOI:10.15774/PPKE.ITK.2016.004

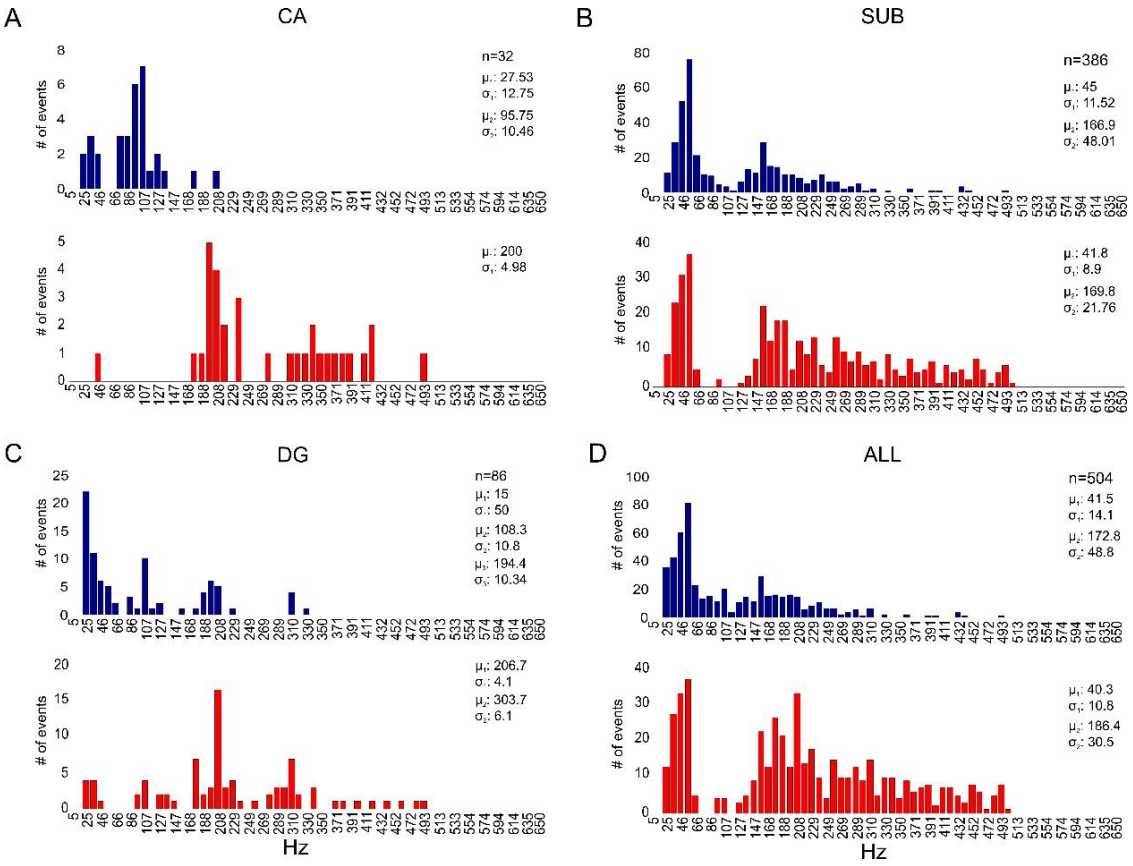

Figure 40. Frequency distribution of evoked HFOs grouped by regions (CA, DG, SUB). In every region the blue bars illustrate the first greatest frequency components, and red bars the secondary peaks. In every region the gamma band is prominent and the higher frequencies (>80 Hz) appear mainly in the subiculum.

We presuppose that the frequency of an event can consist of different frequencies. To validate this presumption, we visualized frequency changes with a wavelet transformation. A typical case is plotted on Figure 41 (from DG). The original LFP data are plotted on the left, the typical ripple filtered data is demonstrated on the middle with an illustration of the two mixed signals, the wavelet transformed data could is placed on the right. The dominant frequencies (around 95 Hz and 230 Hz) of the two mixed signals are clearly visible on the overlaid wavelet mean curve (light pink curve).

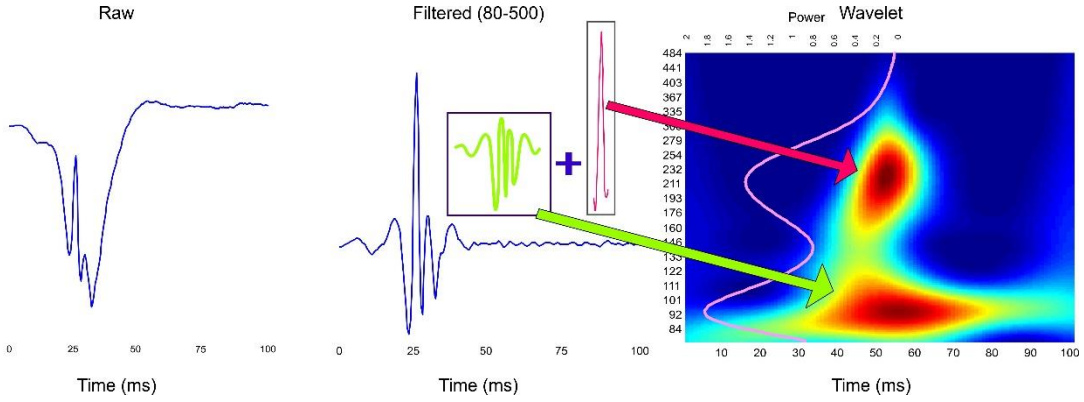

Figure 41. Mixed frequency sample from DG in Pt47. Combination of two frequency is clearly visible on the wavelet transformed data.

DOI:10.15774/PPKE.ITK.2016.004

4.3.5.1 Cross Frequency Coupling (CFC)

We analysed the interaction of frequencies calculating phase-amplitude coupling. Figure 42 illustrates the mean modulation index (MI) between the frequencies from 11 to 968 Hz grouped by CA, DG, Subiculum regions. The left column contains the results of the evoked ripples, the right column shows the frequency coupling of the background activity. The three regions show a slightly different coupling pattern. In the CA region, the most influential frequencies are between 11-33.4 Hz (peak 20 Hz), also affecting frequencies in the range of 14.60-322.70 Hz (n=2). In the DG the interaction is between 11.00-57.30 Hz and 47.00-478.90 Hz (peak 400 Hz). The Subiculum is very similar to DG, with 11.00-35.90 Hz influencing the 46.30-507.70 Hz range (peak 230 Hz). The volume of this effect is the highest in the DG (max MI values: 0.40), followed by the Sub (max MI: 0.25), and lowest is in the CA region (max MI: 0.14). The background activity reveals poor MI values in all areas with an interesting, but very small coupling between gamma band (15-80 Hz) and the multiple unit activity range (684-968 Hz).

Statistical analysis resulted in a significant difference between active and background activity in terms of the interaction of the 11-60 Hz range modulating the 30-814 Hz range during the active phase. Interestingly, a significant increase in modulation was also measured as 85-160 Hz and 575-968 Hz ranges modulated the 814-968 Hz ranges during resting condition (Figure 42 bottom right grey stripped areas).

DOI:10.15774/PPKE.ITK.2016.004

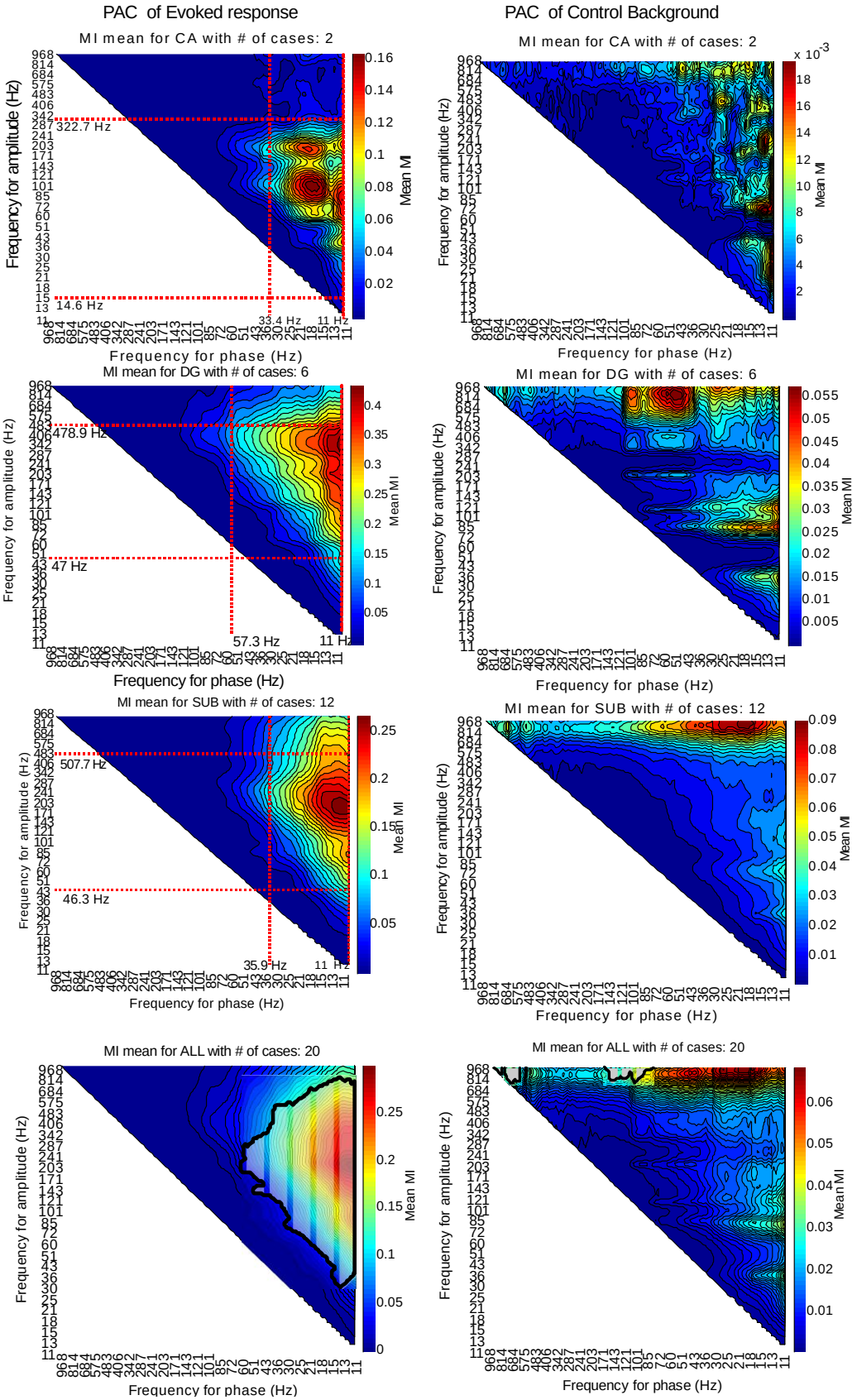

Figure 42. Cross frequency coupling during evoked ripples and their background activity averaged by hippocampal regions CA, DG, SUB and all. The modulation index (MI) values sign the strength of the phase-amplitude coupling, the hotter colour represents stronger relation between the phase of the frequency on the horizontal axis, and the amplitude of the frequency on the vertical axis. The red dotted lines and the black line framed, striped area represents the limits of the most significantly influential and affected frequencies.

DOI:10.15774/PPKE.ITK.2016.004

4.3.6 THE OVERLAP BETWEEN EVOKED HIGH FREQUENCY ACTIVITY AND MULTIUNIT ACTIVITY

An example is shown on Figure 43 where the electrode reached the CA2, DG, hilus, CA3 and also distal subiculum regions. The blue boxplots represent the amplitude of the HFA events and the green shows the amplitude of the MUA.

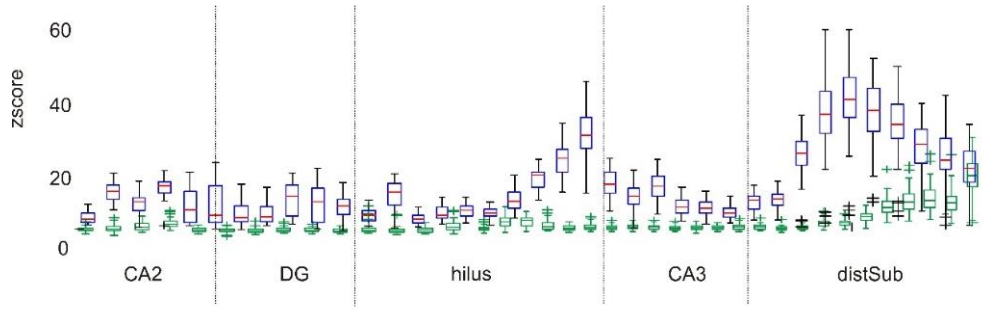

Figure 43. An overall comparison of MUA and EHFO amplitude (z-score) from Pt25. The x axes show the regions, y axes show z-score values. The EHFOs (blue boxes) can be detected in hilus and distal subiculum, by contrast MUAs activity (green boxes), which can be observed just another layers of distal subiculum. The two detected activities are not overlapped. (Stimulation point: 2-3 cm, current: 15 mA)

We correlated the laminar profile of MUA and the EHFO activity, and found that out of all the cases only 31.30% correlated significantly, which brought us to the assumption that the detected high frequency activities did not originate from the summed action potentials of the cell layers.

4.3.7 THESIS II. CORTICAL STIMULATION INDUCED HIGH FREQUENCY OSCILLATION ANALYSIS

Thesis II. I have implemented a semi-automated HFO pre-selection application (RST Figure 27), which was proven to be effective with 90.01% sensitivity with 22.51% precision and the estimated revision time was reduced to 32%. Cortical stimulation of the temporal lobe cortical stimulation evoked high frequency oscillations in the human hippocampus, which shows clear evidence for the connections between the temporal lobe and the hippocampal layers.

Thesis II.a Based on the analysis of data from eight hippocampi recorded intraoperatively I demonstrated that evoked high frequency oscillation appear in every sampled area of the hippocampal formation (DG, CA2-3, subiculum), and contain high frequency activity around 172.8 Hz (124-221.6 Hz). This frequency may vary in the subregions of the hippocampus.

Thesis II.b With the implemented high frequency oscillation pre-selection and evoked high frequency potentials analysis method package, I demonstrated experimentally that the possibility to evoke high frequency oscillations in Cornu Ammonis is 1.88 times higher than in Dentate Gyrus and 2.53 times higher than in the subiculum in mild hippocampal sclerosis

DOI:10.15774/PPKE.ITK.2016.004

cases. In severe hippocampal sclerosis, the evokability in the subiculum exceeds the other regions (CA, DG) and itself 2.85 times compared to the mild cases (Figure 37).

DOI:10.15774/PPKE.ITK.2016.004

5 DISCUSSION

5.1 CCEP

Cortical electrical stimulation has a history dating from 1947 [150, 152]. Single pulse electrical stimulation was first described in the early 2000's [16] with the aim of exploring pathological areas. Since then, significant amount of research has been conducted about the correlation of the motor and language networks and evoked potentials [156, 157, 163]. Our aim was to reliably detect evoked potentials, determine the basic properties and use all this information to map the functional and pathological networks. We have created the first connectivity based matrices which allowed us to describe connectivity between brain areas. We've defined two measures to specify the connection: the average z-scorse between two Brodmann Areas (BAs) and the ratio of the in and out going significant connections. These measures were used to describe the existence of any probable connections between the selected areas, and to indicate their role (governance or integration) in the network. I believe that these two measures can describe the effective connectivity of the brain on a group level.

We found that motor and language systems had high overall connection rates with even higher out-degree measure implying a central position in the network, furthermore a wide-range influence on other systems. Superior parietal, superior temporal, and anterolateral frontal regions received more incoming connections indicating their integrating function. Grand mean average maps were created for all patients including an analysis to create a BA based effective connectivity map of the brain for future reference. From the comparison of normal and pathological networks we could distinguish between pathological and non-pathological brain areas and demonstrate that connectivity within the pathological area is higher, and pathological areas are more affected then the non-pathological ones. Based on our retrospective results, we would like to develop a method that has the potential to describe pathological properties of the network in a prospective way.

We have faced several obstacles during the improvement of the methodology, for example the fluctuation of the brain's baseline activity and some other differences in the sampled brain areas (due to individual electrode positions). We also had to solve a problem arising from the not point-like nature of the bipolar stimulation, and provide a tool for the localization and visualization of the electrodes. We have successfully found solutions of the above mentioned difficulties. We applied z-score calculation for the baseline fluctuation, normalized or modified graph theoretical calculation for the differently sampled areas and bipolar stimulation (for in, -outdegree, and path length computation).

DOI:10.15774/PPKE.ITK.2016.004

5.2 RIPPLE DETECTION

Ripple oscillations are a relatively new electrophysiological phenomenon thought to be a valid marker for epileptic activity [116]. Its accurate description and correct detection have been a long-standing problem. In order to solve this question, we developed an algorithm combining a highly sensitive automatic detector for the putative ripple events, containing a tool that helps subsequent human revision. The tool includes windows for special hints, further helping the judgment. Using this device, we could reach high specificity which is the most important feature in the neurological practice. We can reliably detect ripple events that presumably correspond to the type of the epilepsy and may also give a forecast about the suitability of the planned resection in surgery. The size of the ripple generating area, and the volume of the overlap with the seizure generating area could both be markers of the epileptogenic zone.

Our future aim is to compare epilepsy surgery outcomes with different properties of the HFAs.

5.3 VISUALIZATION

We developed a tool (Brain Visualization Tool, BVT) to have better visualization properties of the functional connections between different brain regions explored by CCEP mapping, which can also integrate the reconstructed brain surface and the extracted features of the electrical brain activity for example evoked potentials, interictal spikes and ripple oscillations. The visualization tool provides outstanding possibilities for clinicians to observe this long-studied question from a new angle.

5.4 CHEP

Spontaneous and evoked high frequency activities (HFA) can be elicited in rodent hippocampus [215], which is a marker of epileptogenic nature [92]. Similarly, we managed to evoke cortico-hippocampal evoked potentials (CHEP) in the hippocampus in humans during anaesthesia, which were different according to the stimulated area within the temporal lobe, the stimulation strength and the recorded hippocampal region. Significant HFO activity was evoked in 6 cases (75%). Stimulation closer to the temporal pole evoked HFOs with higher probability and higher amplitude. CHEPs also contained abundant amount of HFOs. The most active region was the Subiculum and DG, indicating that all these responses - slow or fast

DOI:10.15774/PPKE.ITK.2016.004

ripples - were pathologic. Further investigation is needed to determine the diagnostic role of EHFO in TLE.

Differentiation of the evoked activity is still an unresolved issue. Our results indicate that high frequency activities are not uniform, they can contain ripples, sharp transients, and multiple unit activity as well [147, 216], [141]. These results raise several questions about the basic features of high frequency oscillations.

Is the artificial differentiation valid, does it have any meaning? Or are these events only different forms of the same phenomenon? If not, how should we differentiate properly? In the future, we plan to test new analysis techniques e.g. other kinds of wavelet transformations (db44 from Daubechies family [211, 217] instead of Morlet) and adapt the basic functions of the wavelet to any specific signal to achieve optimal representations of the searched waveforms [218].

The latency of evoked ripples in the hippocampus CA – 11.8ms, DG 26.5ms, Sub 39.5ms mirrors the trisynaptic loop approximately, and indicates that the direct entorhinal, CA1 projection has an essential significance in humans. However, the low number of sampled CA areas somewhat limits this conclusion. The long, 80ms, latency response in the Subiculum can be the results of individual variability of the stimulation site in the – uncontrolled – medial-lateral aspect.

Regarding the CHEP amplitudes, only 70% of all the events following any stimulation had lower amplitude than 5 times the variance of the baseline activity (z-score), which is the threshold that has been regarded as a gold standard [88]. This raises concerns about the validity of the 5 Z-score threshold, and implies that higher thresholds or, maybe, a threshold based on the amplitude of the final ripple events should have been selected. Amplitudes showed great differences between histological layers, thus this feature may be a useful intraoperative to instantly indicate hippocampal layers.

Based on the amplitude and evoking capability measures, the region most prone to be activated was the DG. Previous animal data showed that ripple activity in the DG was a pure consequence of epileptogenic process within the hippocampus [92]. The limitation of this result is our one outstanding case (P47) regarding the DG showing no data from any other hippocampal regions particularly from the Subiculum. Including this limitation, we can still conclude that DG performs ripple activity similarly to the Subiculum that may be the consequence of the epileptogenic nature of the recorded hippocampi. As we analysed the frequency of the CHEPs from this peculiar patient (Figure 41), we noticed at least two dominant frequencies (around 95 Hz and 230 Hz) and we registered two mixed signals on the waveform. We may assume that DG rarely shows evoked ripples, but easily shows high

DOI:10.15774/PPKE.ITK.2016.004

amplitude high frequency activity. We observed that DG responded especially to the stimulation from 1-5 cm, while CA and Sub showed less pronounced changes regarding to the stimulation strength or distance.

Regarding the frequency values, we observed that the most dominant higher frequencies appeared in the DG (mean: 108.3 Hz with SD: 10.8 Hz, mean: 194.4 Hz with SD: 10.34 Hz, and mean 206.7 Hz with SD: 4.1 Hz), in the CA (mean: 303.7 Hz with SD: 6.1 Hz; mean: 95.7 Hz with SD: 10.5 Hz and mean: 200 with SD: 4.9 Hz) and in the Subiculum (mean: 166.9 Hz with SD: 48.1 Hz and mean: 169.8 Hz with SD: 27.8 Hz). These ranges were complemented by an equally distributed gamma (in the range of 15-50 Hz) activity. Importantly, our results of the power spectral analysis of the evoked ripples in the CA are in line with the findings of Schomburg et al [219]. They found three gamma frequency ranges in the CA1, 1) stratum radiatum 30-80 Hz; 2) str lacunosum moleculare 60-150 Hz with mean 85.7±1.8 Hz, 3) str pyramidale 120-250 Hz, 149.4 ± 4.3 Hz mean. The peak values in our CA samples were 27.53 Hz with SD: 12.75 Hz; 95.74 Hz with SD: 10.46 Hz, and 200 Hz with SD: 4.98 Hz, which also reflects the previously mentioned results well [220]. Unfortunately we haven't been able to distinguish between the subregional selectivity of these layers yet, therefore this is a plan for further evaluation, based on our new recordings. The frequency distribution of CHEPs showed a combination of gamma (20-70 Hz) with co-occurring slower (80-140 Hz) and higher (150-500 Hz) HFO frequency components [147]. The HFO bands in our results were slower compared to the ones previously recorded in rats, however another study recording primates resulted similar slower (100–120 Hz) HFO frequencies [221].

We analysed the interaction of frequency ranges and came to the conclusion that similarly to previous findings [210], slow gamma (11-50 Hz) had significant effect on the high gamma-ripple [30-400 Hz] activity. In baseline condition, this effect was absent and was replaced by gamma frequency (11-90 Hz) affecting MUA (680-986 Hz) ranges. This effect during baseline was 4 times smaller than the one during an active condition. This implicates that the hippocampal gamma network entrains neurons responsible for ripple oscillation during the CHEP condition.

As a general conclusion we can say that in the last decade we faced a beginning of a paradigm shift in clinical neurophysiology that requires new data analysis and visualization techniques, and the integration of multidisciplinary knowledge from neurobiology across electrical engineering to information technology. Rapidly developing technical tools could allow medical doctors and clinicians to regularly measure with unusual devices like microelectrodes, in regards of high frequency brain oscillations, electrical stimulations and unitary activities. Our aim was to find solutions for the technical challenges, detect, quantify

DOI:10.15774/PPKE.ITK.2016.004

and visualize useful information on the normal or pathological nature of the human brain for clinical and research purposes.

5.5 APPLICATION

The epileptogenic zone is the target area of the epilepsy surgery investigation. Its resection is necessary and sufficient to eliminate seizures. It can be estimated by different biomarkers for example seizures, sharp transients-spikes, etc. The uncertainty in the definition of the epileptogenic zone underlies the extensive need and research after more specific biomarkers of epilepsy surgery.

Determining the pathological area is not an obvious task, and at the same time, it is equally difficult to describe what is normal in the brain. The characterization of what is normal or physiological and what is pathological is evenly necessary.

The results of CCEP analysis demonstrated that connectivity within the pathological area is higher, and pathological areas are more affected the non-pathological ones. This feature can contribute to the identification of the epileptogenic zone and give hints about the connections within and around it.

Ripple oscillations are a relatively new electrophysiological phenomenon thought to be a marker of epileptic activity. Using my device, we could reach high specificity which is the most important feature in a neurological practice. We can reliably detect ripple events which presumably correspond to the type of the epilepsy and can possibly give a forecast about the suitability of the planned resection. The size of the ripple generating area and the volume of the overlap with seizure generating area could be markers of the epileptogenic zone.

The intraoperative characterization of cortico-hippocampal evoked potentials (CHEPs) and evoked high frequency activity (HFA) of the hippocampus could determine the hippocampal layers, subregions and the categorization of hippocampal sclerosis if present. This technique can help in a better understanding of the fundamentals of the hippocampus in vivo and the epileptic transformation occurring in the hippocampus.

5.5.1 FUTURE OVERVIEW

All of the previously implemented techniques could be the base of future analyses. The long lasting observation of slow changes of the CCEPs can provide information of infraslow oscillations within the network of the brain. Correlating our results with MRI tractography analysis shows that anatomical connections may shed more light on the genesis and spread of the evoked potentials. Intraoperative HFO detection can be extended to cortical areas as well, also, with its help we can obtain more detailed laminar information.

DOI:10.15774/PPKE.ITK.2016.004

After all, we think that low frequency electrical stimulation provides unprecedented information on brain networks and their epileptogenic nature. We think that this method could be used excessively in diagnostic procedures embedded at various phases of epilepsy surgery both before and during the surgical intervention. This sets new horizons for exploring epiletogenicity based on simple and reproducible stimulation methods that can be planned and scheduled before or even under the surgery, unlike the observation of spontaneous seizures of the patient.

DOI:10.15774/PPKE.ITK.2016.004

6 SUMMARY

There are substantial changes in clinical neurophysiology under way. It results in a need for new data analysis and visualization techniques, and the integration of multidisciplinary knowledge from neurobiology across electrical engineering to information technology. The rapidly developing technical tools may allow the clinicians to measure high frequency brain oscillations, neuronal activities and analyse brain changes after electrical stimulations, recorded with macro and micro-sensors. Our aim was to find solutions for the technical challenges, detection, quantification and visualization of useful information on the normal or pathological nature of the human brain for clinical and research purposes.

My main aims were to develop data analysis tools to examine evoked and spontaneous neuronal unit and field activity recorded with different electrodes in epileptic patients. With the ambition to help to better understand the results of the different analyses, my aim was to develop a spectacular visualization tool for biomarkers of epilepsy on 3D brain reconstructions which can be used both in the research and the clinical work.

We selected therapy resistant epilepsy patients undergoing presurgical evaluation, for resective surgery. The analysed data was recorded during the clinical examination period. This way we could test our methods directly in and nearby a clinical environment. We focused on the above mentioned new electrophysiological markers such as 1) high frequency oscillations (HFO), 2) neuronal unit activities and 3) neocortical single pulse electrical stimulation (SPES) elicited cortico-cortical and cortico-hippocampal evoked potential (CCEP, and CHEP) recorded with intracranial macro- and microelectrodes.

6.1 THESIS GROUP I. CORTICO-CORTICAL EVOKED POTENTIAL CHARACTERISATION AND NETWORK DESCRIPTION.

Thesis I. I have developed an automated CCEP analysis algorithm with which different features (amplitude, timing, placement and distance) can be extracted and graphs with nodes (electrodes or electrode groups) can be generated. I defined effective connectivity by the amplitude (z-score) of the evoked potentials and normalized outgoing and incoming connectivity. The nodes were rated by the ratio of the in and out going connections.

Thesis I.a Based on the applied graph theoretical analysis I proved experimentally that the possibility to evoke significant (>3SD) responses between the elements of the pathological network is significantly ($p<0.05$) higher in near field (<1 cm) than normal ones on A2 component (Figure 23).

DOI:10.15774/PPKE.ITK.2016.004

Thesis I.b From the applied modified graph theoretical analysis I determined experimentally that the path length between the elements of the pathological network is significantly ($p<0.05$) smaller, so the pathological elements are more connected than normal ones (Figure 26).

6.2 THESIS GROUP II. CORTICAL STIMULATION INDUCING HIGH FREQUENCY OSCILLATION IN THE HIPPOCAMPUS

Thesis II. I have implemented a semi-automated HFO pre-selection application (RST), which was proven to be effective with 90.01% sensitivity with 22.51% precision and the estimated revision time was reduced to 32%. Cortical stimulation of the temporal lobe cortical stimulation evoked high frequency oscillations in the human hippocampus, which shows clear evidence for the connections between the temporal lobe and the hippocampal layers.

Thesis II.a Based on the analysis of data from eight hippocampi recorded intraoperatively I demonstrated that evoked high frequency oscillation potentials appear in every sampled area of the hippocampal formation (DG, CA2-3, subiculum), and contain high frequency activity around 172.8 Hz (124-221.6 Hz). This frequency may vary in the subregions of the hippocampus.

Thesis II.b With the implemented high frequency oscillation pre-selection and evoked high frequency potentials analysis method package, I demonstrated experimentally that the possibility to evoke high frequency oscillations in Cornu Ammonis is 1.88 times higher than in Dentate Gyrus and 2.53 times higher than in the subiculum in mild hippocampal sclerosis cases. In severe hippocampal sclerosis, the evokability in the subiculum exceeds the other regions (CA, DG) and itself 2.85 times compared to the mild cases (Figure 37).

DOI:10.15774/PPKE.ITK.2016.004

7 LIST OF AUTHOR'S PUBLICATIONS

7.1 PUBLICATIONS RELATED TO THE PRESENT THESIS:

Papers

L. Entz*, **E. Toth***, C. J. Keller, S. Bickel, D. M. Groppe, D. Fabo, et al., "Evoked effective connectivity of the human neocortex," Hum Brain Mapp, vol. 35, pp. 5736-53, Dec 2014. *Authors contributed equally to the manuscript, [185]

C. J. Keller, C. J. Honey, L. Entz, S. Bickel, D. M. Groppe, **E. Toth**, et al., "Corticocortical evoked potentials reveal projectors and integrators in human brain networks," J Neurosci, vol. 34, pp. 9152-63, Jul 2 2014. [197]

E. Toth*, D. Fabo*, L. Entz, I. Ulbert, and L. Eross, "Intracranial neuronal ensemble recordings and analysis in epilepsy," J Neurosci Methods, Oct 8 2015. *Authors contributed equally to the manuscript [206]

Emília Tóth, Virág Bokodi, Zoltán Somogyvári, Loránd Erőss, László Entz, István Ulbert, Dániel Fabó, Evoked High Frequency Activity In Human Hippocampus in vivo, Under submission

Posters

2015

Virág Bokodi; **Emília Tóth**; Zsófia Maglóczky; László Entz; Loránd Erőss; István Ulbert; Dániel Fabó, Evoked high frequency oscillations in the human hippocampal formation, MITT, 2015. 01. 22-23, Budapest, Hungary

Boglárka Hajnal, Dániel Fabó, István Ulbert, **Emília Tóth**, László Entz, Loránd Erőss, Evaluation of the components of the cortico-cortical evoked potentials with single and paired pulse subdural electrical stimulation in epilepsy patients, MITT, 2015. 01. 22-23, Budapest, Hungary

Emília Tóth, István Ulbert, Sydney Cash, Daniel Fabó, Laminar organisation of high frequency oscillation in the human brain, MITT, 2015. 01. 22-23, Budapest, Hungary

B. Hajnal, L. Entz, **E. Toth**, I. Ulbert, D. Fabo, L. Eross, Evaluation of the components of the cortico-cortical evoked potentials with single and paired pulse subdural electrical stimulation in epilepsy patients, SFN, 2015. 10. 17-21, Chicago, USA

2014

DOI:10.15774/PPKE.ITK.2016.004

Emília Tóth, László Entz, István Ulbert, Loránd Eross, Dániel Fabó, Spatial variability of cortical ripples in humans, IBRO, 2014. 01. 16-17, Budapest, Hungary

Emília Tóth, László Entz, István Ulbert, Loránd Eross, Dániel Fabó, Spatial variability of cortical ripples in humans, IBRO-IRUN,2014. 04. 25-27, Krakkow, Poland

Emília Tóth, László Entz, István Ulbert, Loránd Eross, Dániel Fabó, Spatial variability of cortical ripples in humans , From medicine to bionics, 2014. 05. 9-10

Laszlo Entz , Pierre Mégevand , David M. Groppe , **Emilia Toth**, Daniel Fabo, Zianka Fallil, Sean T. Hwang, Cynthia L. Harden, Stephan Bickel, Corey J. Keller, Ashesh D. Mehta, Exploring seizure networks using cortico-cortical evoked potentials: internally hyperconnected, externally hypoconnected?, AES, 2014. 12. 5-9, Los Angeles, USA

Laszlo Entz, **Emilia Toth**, Corey J. Keller, David Groppe, Pierre Megevand, Daniel Fabo, Istvan Ulbert, Lorand Eross, Ashesh D. Mehta, The Human Neocortex Demonstrates Projectors and Receivers of Influence: A Consideration in Neuromodulation Therapy, CNS, 2014. 10. 18-22, Boston, USA

Virág Bokodi, **Emília Tóth**, Zsófia Maglóczky, László Entz, Loránd Erőss, István, Ulbert, Dániel Fabó, Evoked high frequency oscillations in the human hippocampal formation, IBRO, 2014. 01. 16-17, Budapest, Hungary

Balázs Kondákor, Ferenc Kovács, **Emília Tóth**, István Ulbert, Loránd Erőss, Ashesh D. Mehta, Daniel Fabó, László Entz, Cortico-cortical evoked potentials in the seizure onset zone, IBRO, 2014. 01. 16-17, Budapest, Hungary

László Entz , **Emília Tóth**, Corey J. Keller, Dániel Fabó, Stephan Bickel , Loránd Erőss, István Ulbert, Ashesh D. Mehta, Cortico-cortical evoked potentials may reveal pathological and functional networks in the brain, OHBM, 2014. 06. 8-12, Hamburg, Germany

Entz László, **Tóth Emília,** Keller Corey J.,Ulbert István, Mehta Ashesh D.,Erőss Loránd, Direkt kortikális elektromos ingerlés segítségével azonosíthatók a nagy befolyással bíró agyi központok, MIT2014, 2014. 11. 20-22, Budapest, Hungary

Virág Bokodi; **Emília Tóth**; Zsófia Maglóczky; László Entz; István Ulbert; Loránd Erőss5; Dániel Fabó, Kiváltott magas frekvenciás oszcillációk a humán hippocampusban, MIT2014, 2014. 11. 20-22, Budapest, Hungary

Tóth Emília, Entz László, Ulbert István, Erőss Loránd, Fabó Dániel, Humán agykérgi ripple hullámok térbeli kiterjedtsége, , MIT2014, 2014. 11. 20-22, Budapest, Hungary

Fabó Dániel, **Tóth Emília**, Ulbert István, Sydney Cash, Erőss Loránd, Magasfrekvenciás oszcillációk agykérgi szerveződése, MIT2014, 2014. 11. 20-22, Budapest, Hungary

2013

László Entz ,**Emília Tóth**, Corey J. Keller, Dániel Fabó, Stephan Bickel, Lajos R. Kozák, Loránd Erőss, István Ulbert, Ashesh D. Mehta , Anatomico-functional parcellation of the brain based on human electrical stimulation data, MITT, 2013. 01. 17-19., Budapest, Hungary

DOI:10.15774/PPKE.ITK.2016.004

Emília Tóth, László Entz, Corey J. Keller, Dániel Fabó, Stephan Bickel, Lajos R. Kozák, Loránd Erőss, István Ulbert, Ashesh D. Mehta, Cortical electrical stimulation may reveal pathological and functional networks in the human brain, MITT, 2013. 01. 17-19., Budapest, Hungary

Virág Bokodi, **Emília Tóth**, Zsófia Maglóczky, Loránd Erőss, István Ulbert, Dániel Fabó,High frequency oscillations in the human hippocampal formation using single pulse cortical electrical stimulation, MITT, 2013. 01. 17-19., Budapest, Hungary

E. Tóth, L. Entz, I. Ulbert, L. Erőss, D. Fabó; Spatial variability of cortical ripples in humans, SFN, 2013. 11. 9-13, San Diego, USA

E. Tóth , L. Entz , D. Fabó , C. J. Keller , S. Bickel , L.R. Kozák , L. Erőss , I. Ulbert , A.D. Mehta, Pathological and Functional Network connectivity analysis in the Human Brain Using Single Pulse Electrical Stimulation, Congress of International Brain Research Organization 2012, Szeged, Hungary

Emília Tóth, László Entz, Stephan Bickel, Loránd Erőss, István Ulbert, Ashesh D. Mehta, Identifying functional networks in the human brain using single pulse electrical stimulation, Annual Conference of the Hungarian Neuroscience Society, 2011, Budapest, Hungary

L. Entz, S. Bickel, **E. Toth**, C Keller, S Vakili, J Corines, S Stream, L Eross, S Jain, I Ulbert, A.D. Mehta, Identifying brain networks using single pulse electrical stimulation (SPES) and resting state functional MRI connectivity analysis, Congress of Neurological Surgeons, 2011,Washington DC, USA, Poster Award

L. Entz, S. Bickel, C.J. Keller, **E. Toth**, I. Ulbert, L. Eross, A.D. Mehta, Resting state functional MRI and Single Pulse Electrical Stimulation (SPES) are possible new methods to map functional brain networks, Annual meeting of the European Association of Neurosurgical Societies, 2011, Rome, Italy

Presentation

Emília Tóth, László Entz, Corey J. Keller, Dániel Fabó, Stephan Bickel, Lajos R. Kozák, Loránd Erőss, István Ulbert, Ashesh D. Mehta, Analysis of pathological and physiological network connections using cortico-cortical evoked potential ,Kálmán Erika Doctoral Conference, 2012

Emília Tóth, László Entz, Stephan Bickel, Loránd Erőss, István Ulbert, Ashesh D. Mehta, Determination of functional networks in human brain, using low-frequency stimulation, Semmelweis University, Doctoral Conference, 2011,Budapest, Hungary

DOI:10.15774/PPKE.ITK.2016.004

7.2 PUBLICATIONS NOT RELATED TO THE PRESENT THESIS:

B. Dombovari, R. Fiath, B. P. Kerekes, **E. Toth**, L. Wittner, D. Horvath, *et al.*, "In vivo validation of the electronic depth control probes," *Biomed Tech (Berl)*, vol. 59, pp. 283-9, Aug 2014. [222]

DOI:10.15774/PPKE.ITK.2016.004

8 ACKNOWLEDGEMENT

I am indescribably grateful to István Ulbert, László Entz and Dániel Fabó for mentorship on this thesis and the leadership of my way which led me to reach this point. They have given me the opportunity to achieve my proposed aims. I am especially thankful for the possibility to learn from their professional knowledge and human values.

I wish to sincerely thank to the contributors of this work

- for developing information technology solutions to:
    - Virág Bokodi, Zoltán Somogyvári in Hungary and Stephan Bickel, Corey J. Keller, David Groppe, Pierre Mégevand in USA,
- for surgery to:
    - Loránd Erőss in Hungary and Ashesh Mehta in USA,
- for histology to:
    - Zsófia Maglóczky and Lucia Wittner .

I'd like to express gratitude to my family especially to my Mother for her endless support.

I am grateful to the Ph.D. fellows and to the members of our laboratory for their intellectual and scientific inspiration and help.

Supported by Péter Pázmány Catholic University, Faculty of Information Technology and Bionics, OTKA PD101754, KTIA_NAP_13-1-2013-0001

DOI:10.15774/PPKE.ITK.2016.004

9 APPENDIX

	Hospital	Gender	MRI abnormality	Age at surgery	Implanted
Pt1	**NICN**	1	normal	31	R
Pt2	**NICN**	1	L parietal and insular flair	29	L
Pt3	**NSLIJ**	2	L occipitotemporal dysplasia	22	L
Pt4	**NSLIJ**	2	normal	36	Bilateral
Pt5	**NSLIJ**	2	normal	48	R
Pt6	**NSLIJ**	2	R Cortical Dysplasia	17	R
Pt7	**NSLIJ**	1	normal	22	R
Pt8	**NSLIJ**	1	R Temporal lobe	47	R
Pt9	**NICN**	2	R temporo-polar dysgenesis	35	L
Pt10	**NSLIJ**	2	L temporal encephalomalacia	55	Bilateral
Pt11	**NSLIJ**	2	L frontal tumor	39	L
Pt12	**NICN**	2	R cingular and frontal CD	20	R
Pt13	**NSLIJ**	1	L frontal encephalomalacia	18	Bilateral
Pt14	**NSLIJ**	1	L temporal arachnoid cyst	60	L
Pt15	**NSLIJ**	2	R Multiple gangliogliomas	25	R
Pt16	**NSLIJ**	1	normal	15	Bilateral
Pt17	**NSLIJ**	1	R occipitotemporal	30	R
Pt18	**NSLIJ**	2	normal	30	R
Pt19	**NSLIJ**	2	normal	26	Bilateral
Pt20	**NSLIJ**	1	R occipitotemporal	32	R
Pt21	**NSLIJ**	2	normal	23	L
Pt22	**NICN**	1	L occipito-temporal dysgenesis	17	L
Pt23	**NSLIJ**	2	L mesial temporal sclerosis	40	L
Pt24	**NSLIJ**	2	L mesial temporal sclerosis	36	L
Pt25	**NIN**	1	R temporo polar cyst	37	R

Table 2. Summary of all patients included in the CCEP studies. R=right, L=left. NSLIJ: North Shore – LIJ Health System, NICN: National Institute of Clinical Neurosciences. Gender 1=male, 2=female [189]

DOI:10.15774/PPKE.ITK.2016.004

	CA			DG			SUB		
	5 mA	10 mA	15 mA	5 mA	10 mA	15 mA	5 mA	10 mA	15 mA
-3--4 cm		Pt38			Pt38				
-2--3 cm		Pt38, Pt36			Pt38			Pt36	
-1--2 cm		Pt38, Pt36	Pt26		Pt38	Pt26		Pt36	Pt26
0--1 cm		Pt38, Pt36	Pt26, Pt25		Pt38	Pt26, Pt25		Pt36	Pt26
0-1 cm		Pt38, Pt36	Pt25		Pt38, Pt47	Pt25		Pt36	
1-2cm		Pt38, Pt36	Pt25, Pt26	Pt33	Pt38, Pt17, Pt33, Pt47	Pt25, Pt33, Pt26	Pt25, Pt33	Pt25, Pt17, Pt33, Pt36	Pt25, Pt22, Pt33, Pt26
2-3 cm		Pt36	Pt25, Pt26	Pt33	Pt33, Pt47	Pt25, Pt33, Pt26	Pt33	Pt33, Pt36	Pt22, Pt25, Pt33, Pt26
3-4 cm		Pt36	Pt25, Pt26	Pt33	Pt47, Pt17, Pt33	Pt25, Pt26, Pt33		Pt17, Pt26, Pt33, Pt36	Pt22, Pt25, Pt26, Pt33
4-5 cm			Pt25, Pt26	Pt33	Pt47, Pt33	Pt25, Pt26, Pt33	Pt26, Pt33	Pt26, Pt33	Pt22, Pt26, Pt33
5-6 cm									Pt22
6-7 cm	Pt17	Pt17		Pt17	Pt17			Pt17	Pt22

Table 3. List of patients whom data were involved in the analysis of the depicted area from the Hippocampal formation at the given stimulation point and stimulation strength.

DOI:10.15774/PPKE.ITK.2016.004

Patient	Age at operation (years)	Impl. side	Gender	Duration of epilepsy at operation (years)	MRI finding	Hc damage	Analysed electrode localization	Anesthesia	Outcome	Follow up time (years)
P17	31	Right	1	22	Right HS	sHS	body	Isoflurane	1B	3
P22	46	Left	2	10	Bilateral HS	sHS	digitations	Propofol	3A	9
P25	36	Left	2	6	Left HS	sHS	head	Propofol	1A	3
P26	40	Right	2	26	Bilateral HS	sHS	body	Isoflurane	2B	3
P33	51	Left	2	32	TU (left amygdala)	mHS	head	Propofol	3A	2
P36	39	Left	2	37.5	Left HS	sHS	body	Propofol	1A	9
P38	57	Left	1	23	Left HS	mHS	body	Isoflurane	1A	5
P47	38	Left	2	3	Left FCD + HS	mHS	head	Propofol	1A	6

Table 4. Summary of patient characteristics. Abbreviations: Impl. side: implantation and resection side, Gender 2: female, 1: male, MRI: Magnetic Resonance Imaging, HS: hippocampal sclerosis, TU: tumor, FCD: focal cortical dysplasia Hc.: hippocampal, sHS: severe cell loss and reorganization of hippocampus (severe hippocampal sclerosis), mHS: mild cell loss and reorganization of hippocampus (mild hippocampal sclerosis). Outcome: (Engel classification) [223] 1A: Aura and seizure free; 2B: Rare seizures; 3A: Often seizure with worthwhile reduction

* 1 Epilepsy Action Australia Education Resources © The Epilepsy Association 2011 https://www.epilepsy.org.au/about-epilepsy/understanding-epilepsy/seizure-types-classification

* 2 Posterior and inferior cornua of left lateral ventricle exposed from the side. Before 1858. Henry Vandyke Carter - Henry Gray (1918) Anatomy of the Human Body, Bartleby.com: Gray's Anatomy, Plate 739, https://commons.wikimedia.org/wiki/File%3AGray739-emphasizing-hippocampus.png

* 3 A 2D proton density-weighted image acquired perpendicular to the temporal lobes. Copyright © 2016 New Zealand Brain Research Institute, MR images from our studies http://nzbri.org/Labs/mri/Images/, http://nzbri.org/resources/image/pd_weighted_temporal_small.png

* 4 3D Visualization of subdural electrodes. AnalyzeDirect, Inc. http://analyzedirect.com/blog/3d-visualization-of-subdural-electrodes/, http://cdn2.hubspot.net/hub/281820/file-442225838-png/brainthinline.png

* 5 Stainless steel standard electrode (U-probe). Neuronelektród Kft. http://www.neuronelektrod.hu/elektrod-tipusok/acelcso-alapu-elektrodok/standard-acelcsoves.html

* 6 Thumbtack Probe. Plexon Inc. http://www.plexon.com/products/thumbtack-probe

* 7 http://www.clipartbest.com/cliparts/nTX/oqx/nTXoqx5yc.jpeg

* 8 Project Gutenberg's Buchanan's Journal of Man, April 1887,eBook, http://www.gutenberg.org/files/25819/25819-h/25819-h.htm

* 9 Hevner Laboratory Miscellany. Cortical Neurons: Drawings by Cajal, hippocampus, adult human, 1901. Santiago Ramón y Cajal http://faculty.washington.edu/rhevner/Miscellany.html, http://faculty.washington.edu/rhevner/HumanHippo.jpg

DOI:10.15774/PPKE.ITK.2016.004

10 REFERENCES

[1] K. Karbowski, "Hans Berger (1873-1941)," *J Neurol*, vol. 249, pp. 1130-1, Aug 2002.

[2] I. Ulbert, "Investigation of the evoked spontaneous intracortical electrical activity with multielectrodes in humans," Ph.D. Ph.D., Doctoral School, Neurosciences, Semmelweis University, 2001.

[3] L. Entz, "Mapping the human brain with cortical electrical stimulation," Ph. D. Ph. D. Thesis, Doctoral School, Semmelweis University, Budapest, 2015.

[4] D. Fabo, "Properties of spontaneous and evoked discharges in the human subiculum," Ph.D. Ph. D. Thesis, Doctoral School, Semmelweis University, Budapest, Hungary, 2007.

[5] P. Kwan and M. J. Brodie, "Early identification of refractory epilepsy," *N Engl J Med*, vol. 342, pp. 314-9, Feb 3 2000.

[6] J. Engel, Jr., "A proposed diagnostic scheme for people with epileptic seizures and with epilepsy: report of the ILAE Task Force on Classification and Terminology," *Epilepsia*, vol. 42, pp. 796-803, Jun 2001.

[7] J. Roger, F. Dreifuss, M. Martinez-Lage, C. Munari, R. Porter, and M. Seino, "Proposal for Revised Classification of Epilepsies and Epileptic Syndromes," *Epilepsia*, vol. 30, pp. 389-399, 1989.

[8] A. T. Berg and I. E. Scheffer, "New concepts in classification of the epilepsies: entering the 21st century," *Epilepsia*, vol. 52, pp. 1058-62, Jun 2011.

[9] C. A. Schevon, A. J. Trevelyan, C. E. Schroeder, R. R. Goodman, G. McKhann, Jr., and R. G. Emerson, "Spatial characterization of interictal high frequency oscillations in epileptic neocortex," *Brain*, vol. 132, pp. 3047-59, Nov 2009.

[10] J. F. Tellez-Zenteno, R. Dhar, and S. Wiebe, "Long-term seizure outcomes following epilepsy surgery: a systematic review and meta-analysis," *Brain*, vol. 128, pp. 1188-98, May 2005.

[11] M. G. Campos, H. B. Pomata, M. A. Vanegas, and A. C. Sakamoto, "Essentials for the establishments of an epilepsy surgery program " in *Tesxtbook of Epilepsy Surgery*, H. O. Lüders, Ed., ed London, UK: informa healthcare, 2008, p. 1582.

[12] S. Noachtar and I. Borggraefe, "Epilepsy surgery: a critical review," *Epilepsy Behav*, vol. 15, pp. 66-72, May 2009.

[13] F. Rosenow and H. Luders, "Presurgical evaluation of epilepsy," *Brain*, vol. 124, pp. 1683-700, Sep 2001.

[14] A. Valentin, G. Alarcon, J. J. Garcia-Seoane, M. E. Lacruz, S. D. Nayak, M. Honavar, *et al.*, "Single-pulse electrical stimulation identifies epileptogenic frontal cortex in the human brain," *Neurology*, vol. 65, pp. 426-35, Aug 9 2005.

[15] A. Valentín, G. Alarcón, M. Honavar, J. J. García Seoane, R. P. Selway, C. E. Polkey, *et al.*, "Single pulse electrical stimulation for identification of structural abnormalities and prediction of seizure outcome after epilepsy surgery: a prospective study," *The Lancet Neurology*, vol. 4, pp. 718-726, 2005.

[16] A. Valentin, M. Anderson, G. Alarcon, J. J. Seoane, R. Selway, C. D. Binnie, *et al.*, "Responses to single pulse electrical stimulation identify epileptogenesis in the human brain in vivo," *Brain*, vol. 125, pp. 1709-18, Aug 2002.

[17] J. Engel, Jr., "Mesial temporal lobe epilepsy: what have we learned?," *Neuroscientist*, vol. 7, pp. 340-52, Aug 2001.

[18] F. Semah, M. C. Picot, C. Adam, D. Broglin, A. Arzimanoglou, B. Bazin, *et al.*, "Is the underlying cause of epilepsy a major prognostic factor for recurrence?," *Neurology*, vol. 51, pp. 1256-62, Nov 1998.

[19] M. Pfander, S. Arnold, A. Henkel, S. Weil, K. J. Werhahn, I. Eisensehr, *et al.*, "Clinical features and EEG findings differentiating mesial from neocortical temporal lobe epilepsy," *Epileptic Disord*, vol. 4, pp. 189-95, Sep 2002.

DOI:10.15774/PPKE.ITK.2016.004

[20] J. Engel, T. A. Pedley, and J. Aicardi, *Epilepsy: A Comprehensive Textbook*: Lippincott Williams & Wilkins, 2007.

[21] J. Janszky, I. Janszky, R. Schulz, M. Hoppe, F. Behne, H. W. Pannek, *et al.*, "Temporal lobe epilepsy with hippocampal sclerosis: predictors for long-term surgical outcome," *Brain,* vol. 128, pp. 395-404, Feb 2005.

[22] A. Kelemen, G. Rasonyi, A. Szucs, D. Fabo, and P. Halasz, "Predictive factors for the results of surgical treatment in temporal lobe epilepsy," *Ideggyogy Sz,* vol. 59, pp. 353-9, Sep 20 2006.

[23] A. M. McIntosh, S. J. Wilson, and S. F. Berkovic, "Seizure outcome after temporal lobectomy: current research practice and findings," *Epilepsia,* vol. 42, pp. 1288-307, Oct 2001.

[24] D. D. Spencer and S. S. Spencer, "Surgery for epilepsy," *Neurol Clin,* vol. 3, pp. 313-30, May 1985.

[25] H. G. Wieser, M. Ortega, A. Friedman, and Y. Yonekawa, "Long-term seizure outcomes following amygdalohippocampectomy," *J Neurosurg,* vol. 98, pp. 751-63, Apr 2003.

[26] M. G. Yasargil, H. G. Wieser, A. Valavanis, K. von Ammon, and P. Roth, "Surgery and results of selective amygdala-hippocampectomy in one hundred patients with nonlesional limbic epilepsy," *Neurosurg Clin N Am,* vol. 4, pp. 243-61, Apr 1993.

[27] P. Halasz, J. Vajda, and S. Czirjak, "[Surgical treatment of epilepsy]," *Ideggyogy Sz,* vol. 57, pp. 189-205, May 20 2004.

[28] C. Helmstaedter, "Neuropsychological aspects of epilepsy surgery," *Epilepsy Behav,* vol. 5 Suppl 1, pp. S45-55, Feb 2004.

[29] I. Blümcke, H. Beck, A. A. Lie, and O. D. Wiestler, "Molecular neuropathology of human mesial temporal lobe epilepsy," *Epilepsy Research,* vol. 36, pp. 205-223, 9// 1999.

[30] G. Buzsaki and E. I. Moser, "Memory, navigation and theta rhythm in the hippocampal-entorhinal system," *Nat Neurosci,* vol. 16, pp. 130-8, Feb 2013.

[31] M. S. Fanselow and H. W. Dong, "Are the dorsal and ventral hippocampus functionally distinct structures?," *Neuron,* vol. 65, pp. 7-19, Jan 14 2010.

[32] H. H. Pothuizen, W. N. Zhang, A. L. Jongen-Relo, J. Feldon, and B. K. Yee, "Dissociation of function between the dorsal and the ventral hippocampus in spatial learning abilities of the rat: a within-subject, within-task comparison of reference and working spatial memory," *Eur J Neurosci,* vol. 19, pp. 705-12, Feb 2004.

[33] P. Gloor, V. Salanova, A. Olivier, and L. F. Quesney, "The human dorsal hippocampal commissure," *An anatomically identifiable and functional pathway,* vol. 116, pp. 1249-1273, 1993-10-01 00:00:00 1993.

[34] I. Blumcke, M. Thom, E. Aronica, D. D. Armstrong, F. Bartolomei, A. Bernasconi, *et al.*, "International consensus classification of hippocampal sclerosis in temporal lobe epilepsy: a Task Force report from the ILAE Commission on Diagnostic Methods," *Epilepsia,* vol. 54, pp. 1315-29, Jul 2013.

[35] H. M. Duvernoy, F. Cattin, and P. Risold, *The Human Hippocampus*: Springer-Verlag Berlin Heidelberg, 2013.

[36] T. F. Freund and M. Antal, "GABA-containing neurons in the septum control inhibitory interneurons in the hippocampus," *Nature,* vol. 336, pp. 170-3, Nov 10 1988.

[37] R. Benini and M. Avoli, "Rat subicular networks gate hippocampal output activity in an in vitro model of limbic seizures," *J Physiol,* vol. 566, pp. 885-900, Aug 1 2005.

[38] L. Menendez de la Prida, "Functional features of the rat subicular microcircuits studied in vitro," *Behav Brain Res,* vol. 174, pp. 198-205, Nov 11 2006.

[39] P. A. Naber and M. P. Witter, "Subicular efferents are organized mostly as parallel projections: a double-labeling, retrograde-tracing study in the rat," *J Comp Neurol,* vol. 393, pp. 284-97, Apr 13 1998.

[40] S. O'Mara, "Controlling hippocampal output: the central role of subiculum in hippocampal information processing," *Behav Brain Res,* vol. 174, pp. 304-12, Nov 11 2006.

DOI:10.15774/PPKE.ITK.2016.004

[41] D. L. Rosene and G. W. Van Hoesen, "Hippocampal efferents reach widespread areas of cerebral cortex and amygdala in the rhesus monkey," *Science,* vol. 198, pp. 315-7, Oct 21 1977.
[42] G. W. Van Hoesen, D. L. Rosene, and M. M. Mesulam, "Subicular input from temporal cortex in the rhesus monkey," *Science,* vol. 205, pp. 608-10, Aug 10 1979.
[43] M. P. Witter and H. J. Groenewegen, "The subiculum: cytoarchitectonically a simple structure, but hodologically complex," *Prog Brain Res,* vol. 83, pp. 47-58, 1990.
[44] P. A. Naber, F. H. Lopes da Silva, and M. P. Witter, "Reciprocal connections between the entorhinal cortex and hippocampal fields CA1 and the subiculum are in register with the projections from CA1 to the subiculum," *Hippocampus,* vol. 11, pp. 99-104, 2001.
[45] E. Harris and M. Stewart, "Intrinsic connectivity of the rat subiculum: II. Properties of synchronous spontaneous activity and a demonstration of multiple generator regions," *J Comp Neurol,* vol. 435, pp. 506-18, Jul 9 2001.
[46] E. Harris and M. Stewart, "Propagation of synchronous epileptiform events from subiculum backward into area CA1 of rat brain slices," *Brain Res,* vol. 895, pp. 41-9, Mar 23 2001.
[47] E. Harris, M. P. Witter, G. Weinstein, and M. Stewart, "Intrinsic connectivity of the rat subiculum: I. Dendritic morphology and patterns of axonal arborization by pyramidal neurons," *J Comp Neurol,* vol. 435, pp. 490-505, Jul 9 2001.
[48] M. P. Witter, "Connections of the subiculum of the rat: topography in relation to columnar and laminar organization," *Behav Brain Res,* vol. 174, pp. 251-64, Nov 11 2006.
[49] F. Kloosterman, T. van Haeften, and F. H. Lopes da Silva, "Two reentrant pathways in the hippocampal-entorhinal system," *Hippocampus,* vol. 14, pp. 1026-39, 2004.
[50] A. Knopp, A. Kivi, C. Wozny, U. Heinemann, and J. Behr, "Cellular and network properties of the subiculum in the pilocarpine model of temporal lobe epilepsy," *J Comp Neurol,* vol. 483, pp. 476-88, Mar 21 2005.
[51] J. A. Corsellis, "The incidence of Ammon's horn sclerosis," *Brain,* vol. 80, pp. 193-208, Jun 1957.
[52] T. L. Babb, "Synaptic reorganizations in human and rat hippocampal epilepsy," *Adv Neurol,* vol. 79, pp. 763-79, 1999.
[53] Z. Magloczky and T. F. Freund, "Impaired and repaired inhibitory circuits in the epileptic human hippocampus," *Trends Neurosci,* vol. 28, pp. 334-40, Jun 2005.
[54] T. Sutula, G. Cascino, J. Cavazos, I. Parada, and L. Ramirez, "Mossy fiber synaptic reorganization in the epileptic human temporal lobe," *Ann Neurol,* vol. 26, pp. 321-30, Sep 1989.
[55] L. Wittner, L. Eross, S. Czirjak, P. Halasz, T. F. Freund, and Z. Magloczky, "Surviving CA1 pyramidal cells receive intact perisomatic inhibitory input in the human epileptic hippocampus," *Brain,* vol. 128, pp. 138-52, Jan 2005.
[56] L. Wittner, L. Eross, Z. Szabo, S. Toth, S. Czirjak, P. Halasz, *et al.*, "Synaptic reorganization of calbindin-positive neurons in the human hippocampal CA1 region in temporal lobe epilepsy," *Neuroscience,* vol. 115, pp. 961-78, 2002.
[57] J. E. Cavazos, S. M. Jones, and D. J. Cross, "Sprouting and synaptic reorganization in the subiculum and CA1 region of the hippocampus in acute and chronic models of partial-onset epilepsy," *Neuroscience,* vol. 126, pp. 677-88, 2004.
[58] P. D. Fisher, E. F. Sperber, and S. L. Moshe, "Hippocampal sclerosis revisited," *Brain Dev,* vol. 20, pp. 563-73, Dec 1998.
[59] I. Cohen, V. Navarro, S. Clemenceau, M. Baulac, and R. Miles, "On the origin of interictal activity in human temporal lobe epilepsy in vitro," *Science,* vol. 298, pp. 1418-21, Nov 15 2002.
[60] G. Huberfeld, L. Wittner, S. Clemenceau, M. Baulac, K. Kaila, R. Miles, *et al.*, "Perturbed chloride homeostasis and GABAergic signaling in human temporal lobe epilepsy," *J Neurosci,* vol. 27, pp. 9866-73, Sep 12 2007.
[61] J. Jackson, R. Goutagny, and S. Williams, "Fast and slow gamma rhythms are intrinsically and independently generated in the subiculum," *J Neurosci,* vol. 31, pp. 12104-17, Aug 24 2011.

DOI:10.15774/PPKE.ITK.2016.004

[62] C. Wozny, A. Kivi, T. N. Lehmann, C. Dehnicke, U. Heinemann, and J. Behr, "Comment on "On the origin of interictal activity in human temporal lobe epilepsy in vitro"," *Science,* vol. 301, p. 463; author reply 463, Jul 25 2003.

[63] C. Wozny, A. Knopp, T. N. Lehmann, U. Heinemann, and J. Behr, "The subiculum: a potential site of ictogenesis in human temporal lobe epilepsy," *Epilepsia,* vol. 46 Suppl 5, pp. 17-21, 2005.

[64] N. L. Cappaert, W. J. Wadman, and M. P. Witter, "Spatiotemporal analyses of interactions between entorhinal and CA1 projections to the subiculum in rat brain slices," *Hippocampus,* vol. 17, pp. 909-21, 2007.

[65] J. Gigg, D. M. Finch, and S. M. O'Mara, "Responses of rat subicular neurons to convergent stimulation of lateral entorhinal cortex and CA1 in vivo," *Brain Res,* vol. 884, pp. 35-50, Nov 24 2000.

[66] G. Buzsáki, "Theta Oscillations in the Hippocampus," *Neuron,* vol. 33, pp. 325-340, 2002.

[67] E. Grastyan, K. Lissak, I. Madarasz, and H. Donhoffer, "Hippocampal electrical activity during the development of conditioned reflexes," *Electroencephalogr Clin Neurophysiol,* vol. 11, pp. 409-30, Aug 1959.

[68] Z. Borhegyi and T. F. Freund, "Dual projection from the medial septum to the supramammillary nucleus in the rat," *Brain Res Bull,* vol. 46, pp. 453-9, Jul 15 1998.

[69] D. E. Arnolds, F. H. Lopes da Silva, J. W. Aitink, A. Kamp, and P. Boeijinga, "The spectral properties of hippocampal EEG related to behaviour in man," *Electroencephalogr Clin Neurophysiol,* vol. 50, pp. 324-8, Nov 1980.

[70] M. J. Kahana, R. Sekuler, J. B. Caplan, M. Kirschen, and J. R. Madsen, "Human theta oscillations exhibit task dependence during virtual maze navigation," *Nature,* vol. 399, pp. 781-4, Jun 24 1999.

[71] A. Kamondi, L. Acsady, and G. Buzsaki, "Dendritic spikes are enhanced by cooperative network activity in the intact hippocampus," *J Neurosci,* vol. 18, pp. 3919-28, May 15 1998.

[72] A. Kamondi, L. Acsady, X. J. Wang, and G. Buzsaki, "Theta oscillations in somata and dendrites of hippocampal pyramidal cells in vivo: activity-dependent phase-precession of action potentials," *Hippocampus,* vol. 8, pp. 244-61, 1998.

[73] I. Soltesz and M. Deschenes, "Low- and high-frequency membrane potential oscillations during theta activity in CA1 and CA3 pyramidal neurons of the rat hippocampus under ketamine-xylazine anesthesia," *J Neurophysiol,* vol. 70, pp. 97-116, Jul 1993.

[74] A. B. Tort, R. Scheffer-Teixeira, B. C. Souza, A. Draguhn, and J. Brankack, "Theta-associated high-frequency oscillations (110-160Hz) in the hippocampus and neocortex," *Prog Neurobiol,* vol. 100, pp. 1-14, Jan 2013.

[75] F. Moroni, L. Nobili, G. Iaria, I. Sartori, C. Marzano, D. Tempesta, *et al.*, "Hippocampal slow EEG frequencies during NREM sleep are involved in spatial memory consolidation in humans," *Hippocampus,* vol. 24, pp. 1157-1168, 2014.

[76] Z. Clemens, C. Borbély, B. Weiss, L. Eross, A. Szucs, A. Kelemen, *et al.*, "Increased mesiotemporal delta activity characterizes virtual navigation in humans," *Neuroscience Research,* vol. 76, pp. 67-75, 2013.

[77] Z. Clemens, B. Weiss, A. Szucs, L. Eross, G. Rásonyi, and P. Halász, "Phase coupling between rhythmic slow activity and gamma characterizes mesiotemporal rapid-eye-movement sleep in humans," *Neuroscience,* vol. 163, pp. 388-396, 2009.

[78] R. Bódizs, M. Békésy, A. Szűcs, P. Barsi, and P. Halász, "Sleep-Dependent Hippocampal Slow Activity Correlates with Waking Memory Performance in Humans," *Neurobiology of Learning and Memory,* vol. 78, pp. 441-457, 9// 2002.

[79] J. Jacobs, "Hippocampal theta oscillations are slower in humans than in rodents: implications for models of spatial navigation and memory," *Philosophical Transactions of the Royal Society of London B: Biological Sciences,* vol. 369, 2014-02-05 00:00:00 2014.

DOI:10.15774/PPKE.ITK.2016.004

[80] R. Bódizs, S. Kántor, G. Szabó, A. Szûcs, L. Erõss, and P. Halász, "Rhythmic hippocampal slow oscillation characterizes REM sleep in humans," *Hippocampus,* vol. 11, pp. 747-753, 2001.

[81] A. J. Watrous, D. J. Lee, A. Izadi, G. G. Gurkoff, K. Shahlaie, and A. D. Ekstrom, "A comparative study of human and rat hippocampal low-frequency oscillations during spatial navigation," *Hippocampus,* vol. 23, pp. 656-661, 2013.

[82] N. Axmacher, M. M. Henseler, O. Jensen, I. Weinreich, C. E. Elger, and J. Fell, "Cross-frequency coupling supports multi-item working memory in the human hippocampus," *Proceedings of the National Academy of Sciences,* vol. 107, pp. 3228-3233, February 16, 2010 2010.

[83] G. Buzsaki, Z. Horvath, R. Urioste, J. Hetke, and K. Wise, "High-frequency network oscillation in the hippocampus," *Science,* vol. 256, pp. 1025-7, May 15 1992.

[84] A. Draguhn, R. D. Traub, A. Bibbig, and D. Schmitz, "Ripple (approximately 200-Hz) oscillations in temporal structures," *J Clin Neurophysiol,* vol. 17, pp. 361-76, Jul 2000.

[85] R. J. Staba, C. L. Wilson, A. Bragin, D. Jhung, I. Fried, and J. Engel, Jr., "High-frequency oscillations recorded in human medial temporal lobe during sleep," *Ann Neurol,* vol. 56, pp. 108-15, Jul 2004.

[86] E. Urrestarazu, J. D. Jirsch, P. LeVan, J. Hall, M. Avoli, F. Dubeau, *et al.*, "High-frequency intracerebral EEG activity (100-500 Hz) following interictal spikes," *Epilepsia,* vol. 47, pp. 1465-76, Sep 2006.

[87] Z. Clemens, M. Molle, L. Eross, P. Barsi, P. Halasz, and J. Born, "Temporal coupling of parahippocampal ripples, sleep spindles and slow oscillations in humans," *Brain,* vol. 130, pp. 2868-78, Nov 2007.

[88] R. J. Staba, C. L. Wilson, A. Bragin, I. Fried, and J. Engel, Jr., "Quantitative analysis of high-frequency oscillations (80-500 Hz) recorded in human epileptic hippocampus and entorhinal cortex," *J Neurophysiol,* vol. 88, pp. 1743-52, Oct 2002.

[89] A. Bragin, C. L. Wilson, J. Almajano, I. Mody, and J. Engel, Jr., "High-frequency oscillations after status epilepticus: epileptogenesis and seizure genesis," *Epilepsia,* vol. 45, pp. 1017-23, Sep 2004.

[90] S. Rampp and H. Stefan, "Fast activity as a surrogate marker of epileptic network function?," *Clin Neurophysiol,* vol. 117, pp. 2111-7, Oct 2006.

[91] M. Le Van Quyen, F. Amor, and D. Rudrauf, "Exploring the dynamics of collective synchronizations in large ensembles of brain signals," *J Physiol Paris,* vol. 100, pp. 194-200, Oct 2006.

[92] A. Bragin, I. Mody, C. L. Wilson, and J. Engel, Jr., "Local generation of fast ripples in epileptic brain," *J Neurosci,* vol. 22, pp. 2012-21, Mar 1 2002.

[93] F. Grenier, I. Timofeev, and M. Steriade, "Neocortical very fast oscillations (ripples, 80-200 Hz) during seizures: intracellular correlates," *J Neurophysiol,* vol. 89, pp. 841-52, Feb 2003.

[94] G. A. Worrell, L. Parish, S. D. Cranstoun, R. Jonas, G. Baltuch, and B. Litt, "High-frequency oscillations and seizure generation in neocortical epilepsy," *Brain,* vol. 127, pp. 1496-506, Jul 2004.

[95] A. Bragin, J. Engel, C. L. Wilson, I. Fried, and G. W. Mathern, "Hippocampal and Entorhinal Cortex High-Frequency Oscillations (100–500 Hz) in Human Epileptic Brain and in Kainic Acid-Treated Rats with Chronic Seizures," *Epilepsia,* vol. 40, pp. 127-137, 1999.

[96] M. Le Van Quyen, A. Bragin, R. Staba, B. Crépon, C. L. Wilson, and J. Engel, "Cell Type-Specific Firing during Ripple Oscillations in the Hippocampal Formation of Humans," *The Journal of Neuroscience,* vol. 28, pp. 6104-6110, June 11, 2008 2008.

[97] K. J. Staley, "Neurons skip a beat during fast ripples," *Neuron,* vol. 55, pp. 828-30, Sep 20 2007.

[98] L. Menendez de la Prida and A. J. Trevelyan, "Cellular mechanisms of high frequency oscillations in epilepsy: on the diverse sources of pathological activities," *Epilepsy Res,* vol. 97, pp. 308-17, Dec 2011.

DOI:10.15774/PPKE.ITK.2016.004

[99] B. Diehl and H. O. Luders, "Temporal lobe epilepsy: when are invasive recordings needed?," *Epilepsia,* vol. 41 Suppl 3, pp. S61-74, 2000.
[100] H. Jasper, B. Pertuisset, and H. Flanigin, "EEG and cortical electrograms in patients with temporal lobe seizures," *AMA Arch Neurol Psychiatry,* vol. 65, pp. 272-90, Mar 1951.
[101] D. F. Rose, S. Sato, P. D. Smith, R. J. Porter, W. H. Theodore, W. Friauf, *et al.*, "Localization of magnetic interictal discharges in temporal lobe epilepsy," *Ann Neurol,* vol. 22, pp. 348-54, Sep 1987.
[102] V. Vignaendra, R. L. Matthews, and G. E. Chatrian, "Positive occipital sharp transients of sleep: relationships to nocturnal sleep cycle in man," *Electroencephalogr Clin Neurophysiol,* vol. 37, pp. 239-46, Sep 1974.
[103] H. G. Wieser, "ILAE Commission Report. Mesial temporal lobe epilepsy with hippocampal sclerosis," *Epilepsia,* vol. 45, pp. 695-714, Jun 2004.
[104] M. de Curtis and G. Avanzini, "Interictal spikes in focal epileptogenesis," *Prog Neurobiol,* vol. 63, pp. 541-67, Apr 2001.
[105] A. A. Ward, Jr. and R. P. Schmidt, "Some properties of single epileptic neurons," *Arch Neurol,* vol. 5, pp. 308-13, Sep 1961.
[106] T. L. Babb, E. Carr, and P. H. Crandall, "Analysis of extracellular firing patterns of deep temporal lobe structures in man," *Electroencephalogr Clin Neurophysiol,* vol. 34, pp. 247-57, Mar 1973.
[107] F. Bartolomei, F. Wendling, J. J. Bellanger, J. Regis, and P. Chauvel, "Neural networks involving the medial temporal structures in temporal lobe epilepsy," *Clin Neurophysiol,* vol. 112, pp. 1746-60, Sep 2001.
[108] G. Alarcon, J. J. Garcia Seoane, C. D. Binnie, M. C. Martin Miguel, J. Juler, C. E. Polkey, *et al.*, "Origin and propagation of interictal discharges in the acute electrocorticogram. Implications for pathophysiology and surgical treatment of temporal lobe epilepsy," *Brain,* vol. 120 (Pt 12), pp. 2259-82, Dec 1997.
[109] H. G. Wieser, "Temporal lobe epilepsy, sleep and arousal: stereo-EEG findings," *Epilepsy Res Suppl,* vol. 2, pp. 97-119, 1991.
[110] Z. Clemens, J. Janszky, A. Szucs, M. Bekesy, B. Clemens, and P. Halasz, "Interictal epileptic spiking during sleep and wakefulness in mesial temporal lobe epilepsy: a comparative study of scalp and foramen ovale electrodes," *Epilepsia,* vol. 44, pp. 186-92, Feb 2003.
[111] H. H. Lange, J. P. Lieb, J. Engel, Jr., and P. H. Crandall, "Temporo-spatial patterns of pre-ictal spike activity in human temporal lobe epilepsy," *Electroencephalogr Clin Neurophysiol,* vol. 56, pp. 543-55, Dec 1983.
[112] M. Sammaritano, G. L. Gigli, and J. Gotman, "Interictal spiking during wakefulness and sleep and the localization of foci in temporal lobe epilepsy," *Neurology,* vol. 41, pp. 290-7, Feb 1991.
[113] I. Khalilov, M. Le Van Quyen, H. Gozlan, and Y. Ben-Ari, "Epileptogenic actions of GABA and fast oscillations in the developing hippocampus," *Neuron,* vol. 48, pp. 787-96, Dec 8 2005.
[114] M. A. van 't Klooster, M. Zijlmans, F. S. Leijten, C. H. Ferrier, M. J. van Putten, and G. J. Huiskamp, "Time-frequency analysis of single pulse electrical stimulation to assist delineation of epileptogenic cortex," *Brain,* vol. 134, pp. 2855-66, Oct 2011.
[115] M. Zijlmans, P. Jiruska, R. Zelmann, F. S. Leijten, J. G. Jefferys, and J. Gotman, "High-frequency oscillations as a new biomarker in epilepsy," *Ann Neurol,* vol. 71, pp. 169-78, Feb 2012.
[116] J. Jacobs, M. Zijlmans, R. Zelmann, C. E. Chatillon, J. Hall, A. Olivier, *et al.*, "High-frequency electroencephalographic oscillations correlate with outcome of epilepsy surgery," *Ann Neurol,* vol. 67, pp. 209-20, Feb 2010.
[117] J. A. Blanco, M. Stead, A. Krieger, W. Stacey, D. Maus, E. Marsh, *et al.*, "Data mining neocortical high-frequency oscillations in epilepsy and controls," *Brain,* vol. 134, pp. 2948-59, Oct 2011.

DOI:10.15774/PPKE.ITK.2016.004

[118] M. Pail, J. Halamek, P. Daniel, R. Kuba, I. Tyrlikova, J. Chrastina, *et al.*, "Intracerebrally recorded high frequency oscillations: simple visual assessment versus automated detection," *Clin Neurophysiol,* vol. 124, pp. 1935-42, Oct 2013.

[119] G. A. Worrell, A. B. Gardner, S. M. Stead, S. Hu, S. Goerss, G. J. Cascino, *et al.*, "High-frequency oscillations in human temporal lobe: simultaneous microwire and clinical macroelectrode recordings," *Brain,* vol. 131, pp. 928-37, Apr 2008.

[120] T. Akiyama, H. Otsubo, A. Ochi, E. Z. Galicia, S. K. Weiss, E. J. Donner, *et al.*, "Topographic movie of ictal high-frequency oscillations on the brain surface using subdural EEG in neocortical epilepsy," *Epilepsia,* vol. 47, pp. 1953-7, Nov 2006.

[121] M. Zijlmans, J. Jacobs, R. Zelmann, F. Dubeau, and J. Gotman, "High-frequency oscillations mirror disease activity in patients with epilepsy," *Neurology,* vol. 72, pp. 979-86, Mar 17 2009.

[122] T. Akiyama, B. McCoy, C. Y. Go, A. Ochi, I. M. Elliott, M. Akiyama, *et al.*, "Focal resection of fast ripples on extraoperative intracranial EEG improves seizure outcome in pediatric epilepsy," *Epilepsia,* vol. 52, pp. 1802-11, Oct 2011.

[123] C. Haegelen, P. Perucca, C. E. Chatillon, L. Andrade-Valenca, R. Zelmann, J. Jacobs, *et al.*, "High-frequency oscillations, extent of surgical resection, and surgical outcome in drug-resistant focal epilepsy," *Epilepsia,* vol. 54, pp. 848-57, May 2013.

[124] A. Bragin, C. L. Wilson, R. J. Staba, M. Reddick, I. Fried, and J. Engel, Jr., "Interictal high-frequency oscillations (80-500 Hz) in the human epileptic brain: entorhinal cortex," *Ann Neurol,* vol. 52, pp. 407-15, Oct 2002.

[125] R. Zelmann, J. M. Lina, A. Schulze-Bonhage, J. Gotman, and J. Jacobs, "Scalp EEG is not a blur: it can see high frequency oscillations although their generators are small," *Brain Topogr,* vol. 27, pp. 683-704, Sep 2014.

[126] E. Urrestarazu, R. Chander, F. Dubeau, and J. Gotman, "Interictal high-frequency oscillations (100-500 Hz) in the intracerebral EEG of epileptic patients," *Brain,* vol. 130, pp. 2354-66, Sep 2007.

[127] N. V. Thakor and S. Tong, "Advances in quantitative electroencephalogram analysis methods," *Annu Rev Biomed Eng,* vol. 6, pp. 453-95, 2004.

[128] A. B. Gardner, G. A. Worrell, E. Marsh, D. Dlugos, and B. Litt, "Human and Automated Detection of High-Frequency Oscillations in Clinical Intracranial EEG Recordings," *Clinical neurophysiology : official journal of the International Federation of Clinical Neurophysiology,* vol. 118, pp. 1134-1143, 03/23 2007.

[129] B. Crepon, V. Navarro, D. Hasboun, S. Clemenceau, J. Martinerie, M. Baulac, *et al.*, "Mapping interictal oscillations greater than 200 Hz recorded with intracranial macroelectrodes in human epilepsy," *Brain,* vol. 133, pp. 33-45, Jan 2010.

[130] R. Zelmann, F. Mari, J. Jacobs, M. Zijlmans, R. Chander, and J. Gotman, "Automatic detector of high frequency oscillations for human recordings with macroelectrodes," *Conf Proc IEEE Eng Med Biol Soc,* vol. 2010, pp. 2329-33, 2010.

[131] R. Chander, "Algorithms to Detect High Frequency Oscillations in Human Intracerebral EEG," Master of Engineering Thesis, Department of Biomedical Engineering, McGill University, Montreal, 2007.

[132] O. A. Rosso, S. Blanco, J. Yordanova, V. Kolev, A. Figliola, M. Schurmann, *et al.*, "Wavelet entropy: a new tool for analysis of short duration brain electrical signals," *J Neurosci Methods,* vol. 105, pp. 65-75, Jan 30 2001.

[133] J. A. Blanco, M. Stead, A. Krieger, J. Viventi, W. R. Marsh, K. H. Lee, *et al.*, "Unsupervised classification of high-frequency oscillations in human neocortical epilepsy and control patients," *J Neurophysiol,* vol. 104, pp. 2900-12, Nov 2010.

[134] M. Dumpelmann, J. Jacobs, K. Kerber, and A. Schulze-Bonhage, "Automatic 80-250Hz "ripple" high frequency oscillation detection in invasive subdural grid and strip recordings in epilepsy by a radial basis function neural network," *Clin Neurophysiol,* vol. 123, pp. 1721-31, Sep 2012.

[135] J. R. Cho, E. Y. Joo, D. L. Koo, S. C. Hong, and S. B. Hong, "Clinical utility of interictal high-frequency oscillations recorded with subdural macroelectrodes in partial epilepsy," *J Clin Neurol,* vol. 8, pp. 22-34, Mar 2012.

DOI:10.15774/PPKE.ITK.2016.004

[136] X. Tang, L. Xia, Y. Liao, W. Liu, Y. Peng, T. Gao, *et al.*, "New approach to epileptic diagnosis using visibility graph of high-frequency signal," *Clin EEG Neurosci,* vol. 44, pp. 150-6, Apr 2013.

[137] A. Lopez-Cuevas, B. Castillo-Toledo, L. Medina-Ceja, C. Ventura-Mejia, and K. Pardo-Pena, "An algorithm for on-line detection of high frequency oscillations related to epilepsy," *Comput Methods Programs Biomed,* vol. 110, pp. 354-60, Jun 2013.

[138] G. Birot, A. Kachenoura, L. Albera, C. Benar, and F. Wendling, "Automatic detection of fast ripples," *J Neurosci Methods,* vol. 213, pp. 236-49, Mar 15 2013.

[139] S. V. Gliske, Z. T. Irwin, K. A. Davis, K. Sahaya, C. Chestek, and W. C. Stacey, "Universal automated high frequency oscillation detector for real-time, long term EEG," *Clin Neurophysiol,* Jul 22 2015.

[140] M. Brazdil, J. Cimbalnik, R. Roman, D. J. Shaw, M. M. Stead, P. Daniel, *et al.*, "Impact of cognitive stimulation on ripples within human epileptic and non-epileptic hippocampus," *BMC Neurosci,* vol. 16, p. 47, 2015.

[141] M. Amiri, J. M. Lina, F. Pizzo, and J. Gotman, "High Frequency Oscillations and spikes: Separating real HFOs from false oscillations," *Clin Neurophysiol,* Jun 3 2015.

[142] A. Sethi and C. Kemere, "Real time algorithms for sharp wave ripple detection," *Conf Proc IEEE Eng Med Biol Soc,* vol. 2014, pp. 2637-40, 2014.

[143] D. P. Nguyen, F. Kloosterman, R. Barbieri, E. N. Brown, and M. A. Wilson, "Characterizing the dynamic frequency structure of fast oscillations in the rodent hippocampus," *Front Integr Neurosci,* vol. 3, p. 11, 2009.

[144] S. R. Benbadis, W. C. LaFrance, Jr., G. D. Papandonatos, K. Korabathina, K. Lin, and H. C. Kraemer, "Interrater reliability of EEG-video monitoring," *Neurology,* vol. 73, pp. 843-6, Sep 15 2009.

[145] G. A. Worrell, K. Jerbi, K. Kobayashi, J. M. Lina, R. Zelmann, and M. Le Van Quyen, "Recording and analysis techniques for high-frequency oscillations," *Prog Neurobiol,* vol. 98, pp. 265-78, Sep 2012.

[146] C. E. Chatillon, R. Zelmann, J. A. Hall, A. Olivier, F. Dubeau, and J. Gotman, "Influence of contact size on the detection of HFOs in human intracerebral EEG recordings," *Clin Neurophysiol,* vol. 124, pp. 1541-6, Aug 2013.

[147] L. Menendez de la Prida, R. J. Staba, and J. A. Dian, "Conundrums of high-frequency oscillations (80-800 Hz) in the epileptic brain," *J Clin Neurophysiol,* vol. 32, pp. 207-19, Jun 2015.

[148] M. J. Hamberger, "Cortical language mapping in epilepsy: a critical review," *Neuropsychol Rev,* vol. 17, pp. 477-89, Dec 2007.

[149] G. S. Brindley and W. S. Lewin, "The sensations produced by electrical stimulation of the visual cortex," *J Physiol,* vol. 196, pp. 479-93, May 1968.

[150] T. Rasmussen and W. Penfield, "The human sensorimotor cortex as studied by electrical stimulation," *Fed Proc,* vol. 6, p. 184, 1947.

[151] G. S. Brindley and W. S. Lewin, "The visual sensations produced by electrical stimulation of the medial occipital cortex," *J Physiol,* vol. 194, pp. 54-5p, Feb 1968.

[152] G. A. Ojemann, "Individual variability in cortical localization of language," *J Neurosurg,* vol. 50, pp. 164-9, Feb 1979.

[153] R. P. Lesser, H. Luders, G. Klem, D. S. Dinner, H. H. Morris, J. F. Hahn, *et al.*, "Extraoperative cortical functional localization in patients with epilepsy," *J Clin Neurophysiol,* vol. 4, pp. 27-53, Jan 1987.

[154] B. Gordon, R. P. Lesser, N. E. Rance, J. Hart, Jr., R. Webber, S. Uematsu, *et al.*, "Parameters for direct cortical electrical stimulation in the human: histopathologic confirmation," *Electroencephalogr Clin Neurophysiol,* vol. 75, pp. 371-7, May 1990.

[155] E. Bellistri, I. Sartori, V. Pelliccia, S. Francione, F. Cardinale, M. de Curtis, *et al.*, "Fast Activity Evoked by Intracranial 50 Hz Electrical Stimulation as a Marker of the Epileptogenic Zone," *Int J Neural Syst,* vol. 25, p. 1550022, Aug 2015.

[156] R. Matsumoto, D. R. Nair, E. LaPresto, I. Najm, W. Bingaman, H. Shibasaki, *et al.*, "Functional connectivity in the human language system: a cortico-cortical evoked potential study," *Brain,* vol. 127, pp. 2316-30, Oct 2004.

DOI:10.15774/PPKE.ITK.2016.004

[157] R. Matsumoto, D. R. Nair, E. LaPresto, W. Bingaman, H. Shibasaki, and H. O. Luders, "Functional connectivity in human cortical motor system: a cortico-cortical evoked potential study," *Brain,* vol. 130, pp. 181-97, Jan 2007.

[158] H. Catenoix, M. Magnin, M. Guenot, J. Isnard, F. Mauguiere, and P. Ryvlin, "Hippocampal-orbitofrontal connectivity in human: an electrical stimulation study," *Clin Neurophysiol,* vol. 116, pp. 1779-84, Aug 2005.

[159] H. Catenoix, M. Magnin, F. Mauguiere, and P. Ryvlin, "Evoked potential study of hippocampal efferent projections in the human brain," *Clin Neurophysiol,* vol. 122, pp. 2488-97, Dec 2011.

[160] D. Boido, D. Kapetis, V. Gnatkovsky, C. Pastori, B. Galbardi, I. Sartori, *et al.*, "Stimulus-evoked potentials contribute to map the epileptogenic zone during stereo-EEG presurgical monitoring," *Hum Brain Mapp,* vol. 35, pp. 4267-81, Sep 2014.

[161] O. David, A. S. Job, L. De Palma, D. Hoffmann, L. Minotti, and P. Kahane, "Probabilistic functional tractography of the human cortex," *Neuroimage,* vol. 80, pp. 307-17, Oct 15 2013.

[162] R. Enatsu, Z. Piao, T. O'Connor, K. Horning, J. Mosher, R. Burgess, *et al.*, "Cortical excitability varies upon ictal onset patterns in neocortical epilepsy: a cortico-cortical evoked potential study," *Clin Neurophysiol,* vol. 123, pp. 252-60, Feb 2012.

[163] R. Matsumoto, D. R. Nair, A. Ikeda, T. Fumuro, E. Lapresto, N. Mikuni, *et al.*, "Parieto-frontal network in humans studied by cortico-cortical evoked potential," *Hum Brain Mapp,* vol. 33, pp. 2856-72, Dec 2012.

[164] M. E. Lacruz, J. J. Garcia Seoane, A. Valentin, R. Selway, and G. Alarcon, "Frontal and temporal functional connections of the living human brain," *Eur J Neurosci,* vol. 26, pp. 1357-70, Sep 2007.

[165] Y. Yamao, R. Matsumoto, T. Kunieda, Y. Arakawa, K. Kobayashi, K. Usami, *et al.*, "Intraoperative dorsal language network mapping by using single-pulse electrical stimulation," *Hum Brain Mapp,* vol. 35, pp. 4345-61, Sep 2014.

[166] O. D. Creutzfeldt, S. Watanabe, and H. D. Lux, "Relations between EEG phenomena and potentials of single cortical cells. I. Evoked responses after thalamic and epicortical stimulation," *Electroencephalography and Clinical Neurophysiology,* vol. 20, pp. 1-18, 1// 1966.

[167] S. Goldring, G. Harding, and E. Gregorie, "Distinctive electrophysiological characteristics of functionally discrete brain areas: a tenable approach to functional localization," *Journal of Neurosurgery,* vol. 80, pp. 701-709, 1994.

[168] D. P. Purpura, J. L. Pool, J. Ransohoff, M. J. Frumin, and E. M. Housepian, "Observations on evoked dendritic potentials of human cortex," *Electroencephalography and Clinical Neurophysiology,* vol. 9, pp. 453-459, 1957/08/01 1957.

[169] L. Wittner, G. Huberfeld, S. Clémenceau, L. Erőss, E. Dezamis, L. Entz, *et al.*, *The epileptic human hippocampal cornu ammonis 2 region generates spontaneous interictal-like activity in vitro* vol. 132, 2009.

[170] S. S. Cash, E. Halgren, N. Dehghani, A. O. Rossetti, T. Thesen, C. Wang, *et al.*, "The human K-complex represents an isolated cortical down-state," *Science,* vol. 324, pp. 1084-7, May 22 2009.

[171] M. Steriade and I. Timofeev, "Neuronal Plasticity in Thalamocortical Networks during Sleep and Waking Oscillations," *Neuron,* vol. 37, pp. 563-576, 2/20/ 2003.

[172] R. Csercsa, B. Dombovari, D. Fabo, L. Wittner, L. Eross, L. Entz, *et al.*, "Laminar analysis of slow wave activity in humans," *Brain,* vol. 133, pp. 2814-29, Sep 2010.

[173] B. Hangya, Z. Borhegyi, N. Szilagyi, T. F. Freund, and V. Varga, "GABAergic neurons of the medial septum lead the hippocampal network during theta activity," *J Neurosci,* vol. 29, pp. 8094-102, Jun 24 2009.

[174] N. K. Logothetis, M. Augath, Y. Murayama, A. Rauch, F. Sultan, J. Goense, *et al.*, "The effects of electrical microstimulation on cortical signal propagation," *Nat Neurosci,* vol. 13, pp. 1283-91, Oct 2010.

[175] D. S. Rosenberg, F. Mauguière, H. Catenoix, I. Faillenot, and M. Magnin, "Reciprocal Thalamocortical Connectivity of the Medial Pulvinar: A Depth Stimulation and Evoked

DOI:10.15774/PPKE.ITK.2016.004

Potential Study in Human Brain," *Cerebral Cortex,* vol. 19, pp. 1462-1473, June 1, 2009 2009.

[176] C. J. Keller, S. Bickel, L. Entz, I. Ulbert, M. P. Milham, C. Kelly, *et al.*, "Intrinsic functional architecture predicts electrically evoked responses in the human brain," *Proc Natl Acad Sci U S A,* vol. 108, pp. 10308-13, Jun 21 2011.

[177] R. Enatsu, R. Matsumoto, Z. Piao, T. O'Connor, K. Horning, R. C. Burgess, *et al.*, "Cortical negative motor network in comparison with sensorimotor network: a cortico-cortical evoked potential study," *Cortex,* vol. 49, pp. 2080-96, Sep 2013.

[178] M. Iwasaki, R. Enatsu, R. Matsumoto, E. Novak, B. Thankappen, Z. Piao, *et al.*, "Accentuated cortico-cortical evoked potentials in neocortical epilepsy in areas of ictal onset," *Epileptic Disord,* vol. 12, pp. 292-302, Dec 2010.

[179] D. Flanagan, A. Valentin, J. J. Garcia Seoane, G. Alarcon, and S. G. Boyd, "Single-pulse electrical stimulation helps to identify epileptogenic cortex in children," *Epilepsia,* vol. 50, pp. 1793-803, Jul 2009.

[180] E. Bullmore and O. Sporns, "Complex brain networks: graph theoretical analysis of structural and functional systems," *Nat Rev Neurosci,* vol. 10, pp. 186-98, Mar 2009.

[181] D. S. Bassett, E. Bullmore, B. A. Verchinski, V. S. Mattay, D. R. Weinberger, and A. Meyer-Lindenberg, "Hierarchical organization of human cortical networks in health and schizophrenia," *J Neurosci,* vol. 28, pp. 9239-48, Sep 10 2008.

[182] R. L. Buckner, J. Sepulcre, T. Talukdar, F. M. Krienen, H. Liu, T. Hedden, *et al.*, "Cortical hubs revealed by intrinsic functional connectivity: mapping, assessment of stability, and relation to Alzheimer's disease," *J Neurosci,* vol. 29, pp. 1860-73, Feb 11 2009.

[183] C. J. Honey, O. Sporns, L. Cammoun, X. Gigandet, J. P. Thiran, R. Meuli, *et al.*, "Predicting human resting-state functional connectivity from structural connectivity," *Proc Natl Acad Sci U S A,* vol. 106, pp. 2035-40, Feb 10 2009.

[184] D. J. Felleman and D. C. Van Essen, "Distributed hierarchical processing in the primate cerebral cortex," *Cereb Cortex,* vol. 1, pp. 1-47, Jan-Feb 1991.

[185] A. Burkhalter and K. L. Bernardo, "Organization of corticocortical connections in human visual cortex," *Proc Natl Acad Sci U S A,* vol. 86, pp. 1071-5, Feb 1989.

[186] H. Oya, P. W. Poon, J. F. Brugge, R. A. Reale, H. Kawasaki, I. O. Volkov, *et al.*, "Functional connections between auditory cortical fields in humans revealed by Granger causality analysis of intra-cranial evoked potentials to sounds: comparison of two methods," *Biosystems,* vol. 89, pp. 198-207, May-Jun 2007.

[187] C. Yan and Y. He, "Driving and driven architectures of directed small-world human brain functional networks," *PLoS One,* vol. 6, p. e23460, 2011.

[188] J. F. Smith, A. Pillai, K. Chen, and B. Horwitz, "Effective Connectivity Modeling for fMRI: Six Issues and Possible Solutions Using Linear Dynamic Systems," *Front Syst Neurosci,* vol. 5, p. 104, 2011.

[189] L. Entz, E. Toth, C. J. Keller, S. Bickel, D. M. Groppe, D. Fabo, *et al.*, "Evoked effective connectivity of the human neocortex," *Hum Brain Mapp,* vol. 35, pp. 5736-53, Dec 2014.

[190] L. Eross, A. G. Bago, L. Entz, D. Fabo, P. Halasz, A. Balogh, *et al.*, "Neuronavigation and fluoroscopy-assisted subdural strip electrode positioning: a simple method to increase intraoperative accuracy of strip localization in epilepsy surgery," *J Neurosurg,* vol. 110, pp. 327-31, Feb 2009.

[191] I. Ulbert, E. Halgren, G. Heit, and G. Karmos, "Multiple microelectrode-recording system for human intracortical applications," *J Neurosci Methods,* vol. 106, pp. 69-79, Mar 30 2001.

[192] I. Ulbert, G. Heit, J. Madsen, G. Karmos, and E. Halgren, "Laminar analysis of human neocortical interictal spike generation and propagation: current source density and multiunit analysis in vivo," *Epilepsia,* vol. 45 Suppl 4, pp. 48-56, 2004.

[193] O. Darbin, L. Newton, and T. Wichmann, "A new probe to monitor the effects of drugs on local field potentials," *Journal of Neuroscience Methods,* vol. 155, pp. 291-295, 9/15/ 2006.

DOI:10.15774/PPKE.ITK.2016.004

[194] A. R. Dykstra, A. M. Chan, B. T. Quinn, R. Zepeda, C. J. Keller, J. Cormier, *et al.*, "Individualized localization and cortical surface-based registration of intracranial electrodes," *Neuroimage,* vol. 59, pp. 3563-70, Feb 15 2012.

[195] A. M. Dale, B. Fischl, and M. I. Sereno, "Cortical surface-based analysis. I. Segmentation and surface reconstruction," *Neuroimage,* vol. 9, pp. 179-94, Feb 1999.

[196] A. Pfadt and D. J. Wheeler, "Using statistical process control to make data-based clinical decisions," *J Appl Behav Anal,* vol. 28, pp. 349-70, Fall 1995.

[197] C. J. Keller, C. J. Honey, L. Entz, S. Bickel, D. M. Groppe, E. Toth, *et al.*, "Corticocortical evoked potentials reveal projectors and integrators in human brain networks," *J Neurosci,* vol. 34, pp. 9152-63, Jul 2 2014.

[198] D. S. Bassett, B. G. Nelson, B. A. Mueller, J. Camchong, and K. O. Lim, "Altered resting state complexity in schizophrenia," *Neuroimage,* vol. 59, pp. 2196-207, Feb 1 2012.

[199] J. H. Wang, X. N. Zuo, S. Gohel, M. P. Milham, B. B. Biswal, and Y. He, "Graph theoretical analysis of functional brain networks: test-retest evaluation on short- and long-term resting-state functional MRI data," *PLoS One,* vol. 6, p. e21976, 2011.

[200] M. Rubinov and O. Sporns, "Complex network measures of brain connectivity: Uses and interpretations," *NeuroImage,* vol. 52, pp. 1059-1069, 9// 2010.

[201] J. Jacobs, P. LeVan, R. Chander, J. Hall, F. Dubeau, and J. Gotman, "Interictal high-frequency oscillations (80-500 Hz) are an indicator of seizure onset areas independent of spikes in the human epileptic brain," *Epilepsia,* vol. 49, pp. 1893-907, Nov 2008.

[202] G. Heit, I. I. Ulbert, E. Halgren, G. Karmos, and L. Shuer, "Current source density analysis of synaptic generators of human interictal spike," *Stereotact Funct Neurosurg,* vol. 73, p. 116, 1999.

[203] D. Fabo, Z. Magloczky, L. Wittner, A. Pek, L. Eross, S. Czirjak, *et al.*, "Properties of in vivo interictal spike generation in the human subiculum," *Brain,* vol. 131, pp. 485-99, Feb 2008.

[204] I. Ulbert, Z. Magloczky, L. Eross, S. Czirjak, J. Vajda, L. Bognar, *et al.*, "In vivo laminar electrophysiology co-registered with histology in the hippocampus of patients with temporal lobe epilepsy," *Exp Neurol,* vol. 187, pp. 310-8, Jun 2004.

[205] G. Liu, H. Guo, C. Guo, S. Zhao, D. Gong, and Y. Zhao, "Involvement of IRE1α signaling in the hippocampus in patients with mesial temporal lobe epilepsy.," *Brain Res Bull,* Oct 2010.

[206] W. W. Dawson and H. W. Doddington, "Phase distortion of biological signals: Extraction of signal from noise without phase error," *Electroencephalography and Clinical Neurophysiology,* vol. 34, pp. 207-211, 1973/02/01 1973.

[207] A. Winkler, M. Mayer, S. Schnaitmann, M. Ombay, B. Mathias, E. Schmutzhard, *et al.*, "Belief systems of epilepsy and attitudes toward people living with epilepsy in a rural community of northern Tanzania.," *Epilepsy Behav,* Oct 2010.

[208] A. Bragin, J. Engel, Jr., and R. J. Staba, "High-frequency oscillations in epileptic brain," *Curr Opin Neurol,* vol. 23, pp. 151-6, Apr 2010.

[209] S. Makeig, "Auditory event-related dynamics of the EEG spectrum and effects of exposure to tones," *Electroencephalography and Clinical Neurophysiology,* vol. 86, pp. 283-293, 1993/04/01 1993.

[210] A. B. L. Tort, R. Komorowski, H. Eichenbaum, and N. Kopell, "Measuring Phase-Amplitude Coupling Between Neuronal Oscillations of Different Frequencies," *Journal of Neurophysiology,* vol. 104, pp. 1195-1210, 2010-08-01 00:00:00 2010.

[211] I. Daubechies, "The wavelet transform time-frequency localization and signal analysis," *IEEE Transactions on Information Theory,* vol. Vol. 36, pp. 961-1004, 1990.

[212] C. Torrence and G. Compo, "A practical guide to wavelet analysis," *Bulletin of the American Meteorological Society,* vol. Vol. 79, 1998.

[213] R. Zelmann, M. Zijlmans, J. Jacobs, C. E. Chatillon, and J. Gotman, "Improving the identification of High Frequency Oscillations," *Clin Neurophysiol,* vol. 120, pp. 1457-64, Aug 2009.

DOI:10.15774/PPKE.ITK.2016.004

[214] A. P. Bagshaw, J. Jacobs, P. LeVan, F. Dubeau, and J. Gotman, "Effect of sleep stage on interictal high-frequency oscillations recorded from depth macroelectrodes in patients with focal epilepsy," *Epilepsia,* vol. 50, pp. 617-628, 2009.

[215] A. Bragin, J. Engel, Jr., C. L. Wilson, I. Fried, and G. Buzsaki, "High-frequency oscillations in human brain," *Hippocampus,* vol. 9, pp. 137-42, 1999.

[216] J. Jacobs, C. Vogt, P. LeVan, R. Zelmann, J. Gotman, and K. Kobayashi, "The identification of distinct high-frequency oscillations during spikes delineates the seizure onset zone better than high-frequency spectral power changes," *Clin Neurophysiol,* Apr 17 2015.

[217] J. Rafiee, M. A. Rafiee, N. Prause, and M. P. Schoen, "Wavelet basis functions in biomedical signal processing," *Expert Systems with Applications,* vol. 38, pp. 6190-6201, 5// 2011.

[218] M. Nielsen, E. N. Kamavuako, M. M. Andersen, M. F. Lucas, and D. Farina, "Optimal wavelets for biomedical signal compression," *Med Biol Eng Comput,* vol. 44, pp. 561-8, Jul 2006.

[219] E. W. Schomburg, A. Fernandez-Ruiz, K. Mizuseki, A. Berenyi, C. A. Anastassiou, C. Koch, *et al.,* "Theta phase segregation of input-specific gamma patterns in entorhinal-hippocampal networks," *Neuron,* vol. 84, pp. 470-85, Oct 22 2014.

[220] M. A. Belluscio, K. Mizuseki, R. Schmidt, R. Kempter, and G. Buzsaki, "Cross-frequency phase-phase coupling between theta and gamma oscillations in the hippocampus," *J Neurosci,* vol. 32, pp. 423-35, Jan 11 2012.

[221] J. Csicsvari, H. Hirase, A. Czurko, A. Mamiya, and G. Buzsaki, "Fast network oscillations in the hippocampal CA1 region of the behaving rat," *J Neurosci,* vol. 19, p. Rc20, Aug 15 1999.

[222] E. Toth, D. Fabo, Z. Magloczky, L. Eross, A. Solyom, S. Czirjak, *et al.,* "Spontaneous ripples in the human hippocampal formation," presented at the ILEA, Budapest, 2009.

[223] H. G. Wieser and K. Schindler, *Classification of seizure outcome following epilepsy surgery, in: Textbook of Epilepsy Surgery* Informa Healthcare, 2008.